Experimental Investigation on

Passive Earth Pressure on Walls Retaining Collapsible Soil

Anamaria Mihaela Poterasu

A thesis in

The Department of Building, Civil and

Environmental Engineering

Presented in Partial Fulfillment of the requirements

for the Degree of Master of Applied Science (Civil Engineering) at

Concordia University

Montreal, Quebec, Canada

September 2013

CONCORDIA UNIVERSITY

SCHOOL OF GRADUATE STUDIES

This is to certify that the thesis prepared

By: **Anamaria Mihaela Poterasu**

Entitled: **Experimental Investigation on Passive Earth Pressure on Walls Retaining Collapsible Soil**

and submitted in partial fulfillment of the requirements for the degree of

MASTER OF APPLIED SCIENCE (Civil Engineering)

complies with the regulations of the University and meets the accepted standards with respect to originality and quality.

Signed by the final examining committee:

Dr. M. Nokken	Chair
Dr. L. Amador	Examiner
Dr. G. Gouw	Examiner
Dr. Adel M. Hanna	Supervisor

Approved by _____

Chair of Department or Graduate Program Director

_____

Dean of Faculty

Date _____

ABSTRACT

Experimental investigation of the passive earth pressure on retaining wall when the backfill is collapsible soil

Anamaria Mihaela Poterasu

Collapsible soil is one of the problematic soils in geotechnical engineering. They are known for their strength when they are dry and their sudden and excessive loss of volume when they are inundated.

The present study presents the results of experimental investigations on passive earth pressure acting on walls retaining dry and wet collapsible soils. The objective of these investigations was to study the effect of inundation due to the rise of the ground water table on the earth pressure. Lab Tests were carried out on a prototype set-up which was developed to simulate the movement of a retaining wall towards the collapsible backfill, meaning the passive pressure state. The experiments were conducted on collapsible soil with various collapse potentials to study this variation effect on the results.

The results of the experimental investigation were used to validate the results of the numerical model developed in this investigation. The numerical model was used to generate results for a wide range of parameters, which believe to govern this complex soil.

ACKNOWLEDGMENTS

I would like to express my sincere gratitude to Professor Dr. Adel M. Hanna for his constant interest, talented support and supervision on the development of this research thesis. I want to express my heartfelt gratitude for the patience he showed when I was a novice researcher. Specially, I am thankful for the freedom he has provided me in deciding my goals and experimenting with the approaches towards achieving them. He has taught me and demonstrated what it means to be a professor and a mentor.

I would like to thank the technicians and staff of the department of Building, Civil and Environmental Engineering for their help, especially Mark Ellie that help with the construction of the experimental set-up.

Finally I would like to thank my parents and my sister that have supported me from a distance and gave me the strength to succeed in pursuing my goals. I offer my eternal gratitude to grandfather Ion Dobrescu that guided me from heaven and without whom I would not been able to begin my journey on this path.

TABLE OF CONTENTS

LIST OF FIGURES

LIST OF TABLES

LIST OF SYMBOLS

Symbol

C_c	=	Coefficient of curvature
C_u	=	Uniformity coefficient
w_c	=	Initial moist content
γ	=	Unit weight
γ_d	=	Dry unit weight
$\gamma_{d\ max}$	=	Maximum dry unit weight
w_{opt}	=	Optimum water content
G_s	=	Specific gravity
e	=	Void ratio
S	=	Degree of saturation
w_l	=	Liquid limit
w_p	=	Plastic limit
PI	=	Plasticity index
C_p	=	Collapse potential
P_h	=	Horizontal component if the passive earth pressure
P_p	=	Total passive earth pressure acting at an angle δ with the horizontal
d	=	Width of the wall
h	=	Height of the wall
k_p	=	Coefficient of passive earth pressure
$\emptyset$	=	Angle of internal friction
c'	=	Soil cohesion

e_L	=	Natural void ratio
e_0	=	Void ratio at liquid limit
γ_{0d}	=	In situ dry density
γ_{Ld}	=	Dry density of the soil at liquid limit
e_n	=	Void ratio before flooding at vertical pressure
e_m	=	Void ratio at the end of collapse at the same pressure
Δe_c	=	Change in void ratio upon wetting
e_0	=	Initial void ratio
ΔH_0	=	Change in the height upon wetting
H_c	=	Initial height
σ'_p , $\sigma'_{h,0}$	=	Horizontal effective stress
σ'_0 , $\sigma'_{v,0}$	=	The vertical effective principal stress
u	=	Pour water pressure
γ_w	=	Unit weight of water
k_0	=	Coefficient of at rest earth pressure
E	=	Modulus of elasticity
Ψ	=	Dilatancy
γ_{usat}	=	Unsaturated unit weight
γ_{sat}	=	Saturated unit weight
ν	=	Poisson's ratio

CHAPTER 1

INTRODUCTION

1.1 General

Retaining walls are structures for which the main load is represented by the earth pressure. The aim of these structures is to support the side of an excavation or a fill or to support the pressure of water in the case of cofferdams.

Retaining walls are permanent retaining structures that support the soil placed behind them. The design of a retaining wall depends on its type, movement and also on the properties of the soil backfill.

In the literature, several theoretical and experimental studies have been presented. However, these attempts have been limited for cases of backfills of normally and overconsolidated sands or clay. None of the cases considered the presence of collapsible soil as the backfill of the retaining wall which arises as a challenge in geotechnical engineering according to difficulties engineers face when dealing with this problematic soil.

1.2 Research Objectives

The objective of this research was to study the effect of soil collapse on the passive earth pressure developed behind a retaining structure. For this purpose, a prototype experimental set-up was developed to measure the wall movement after the collapse of the soil caused by inundation. The retaining wall used in the experimental investigation was a frictionless wall. For this type of retaining wall the friction between the soil and the wall is neglected.

The results from the experimental investigation were used to validate the numerical model constructed. The finite element models were constructed for different soil mixtures that presented various collapse potentials. In order to observe the change in pressure after collapse, the coefficient of passive earth pressure was calculated for all of the mixtures.

The scope of this research was to investigate the decrease in passive earth pressure after collapse of the soil. This loss in passive resistance of the soil after inundation may cause severe problems to the retaining walls. Hence special considerations must be taken when designing structures retaining collapsible soils. For this purpose a formula was developed to predict the coefficient of passive earth pressure after collapse function of the collapse potential of the soil. The formula can be used for collapse potentials that are between 4.2% and 14%. This range covers a wide variety of collapsible soils that can cause different problems for the retaining walls.

CHAPTER 2

LITERATURE REVIEW

2.1 General

With the civilization rapidly increasing the construction domain has adapted and many metropolitan and large structures have been erected in areas of collapsible soils. The human activities require the use of water for industrialization, agriculture and domestic purposes which can cause damage to structures founded on collapsible soils.

Collapsible soils are known as problematic soils, which possess considerable strength when dry and lose their strength when inundated experiencing excessive settlements.

The soil response to inundation (i.e. landslides or significant soil settlements) could not be predicted beforehand. The irrecoverable volume reduction of collapsible soils takes place fast and sudden and no measurements can be taken to stop the problem once it initiates.

The passive earth pressure is the resisting force on which the design theories of structures is based. The calculation of the passive earth pressure for this type of problematic soils is still one of the challenges in the field of soil mechanics.

In this chapter, the literature will be reviewed under the following headings:

1. Literature pertinent to collapsible soils
2. Literature pertinent to passive earth pressure.

2.2 Literature Review Pertinent To Collapsible Soils

Collapsible soils are defined as “an unsaturated soil that goes through a radical rearrangement of particles and great loss of volume upon wetting with or without additional loading” (Bara, 1976).

(Dudley, 1970) suggested the term “collapse” to describe the volume reduction that causes the lowering of the ground surface. On the other hand, the additional settlement of the foundation due to the wetting of a partly saturated soil, normally without any increase of applied pressure, was termed as “collapse” by Jennings and Knight (Jennings, 1975).

Deposit mechanisms

Since collapsible soils are usually “loose”, they are generally created by deposition mechanisms that yield loose deposits.

The mechanisms that account for almost all naturally occurring collapsible soil deposits are debris flows and alluvial depositions, and also depositions of wind-blown materials. (Beckwith, 1995) (Derbyshire, 1995)

According to Jennings and Knight (1975), the soil deposits most likely to collapse are:

a) loose fills
b) altered windblown sands
c) hill wash of loose consistency
d) decomposed granite and other acid igneous rocks

Collapsible soils are generally characterized by their loose structure of bulky shaped grains; often silt to fine sand size with small amounts of clay. There may be only slight cementing agents such as calcium carbonate, salts and dried clay, with combinations being common.

Bell (1997) reported that the majority of naturally occurring collapsible soils are aeolian deposits. Aeolian deposits such as loess, dunes and other windblown deposits are encountered in different parts of the world. Clemence (1981) presented that loess covers about 17% of the United States, about 17% of Europe, 15% of Russia and Siberia, and large areas of China. Loess is also encountered in South America and Southern Africa.

Aeolian soils have a loose open, metastructure bonded by cementing agents, which upon wetting, become weak and may dissolve causing collapse. These soils are composed primarily of quartz along with feldspar and clay minerals. Bell (1997) reported that increasing the clay mineral content decreases the likelihood of collapse. Khelifa (2007) concluded that the soil is not susceptible to collapse if the clay content of the soil is greater than 30%.

Water deposits include alluvial fans, mud flows and flash flood deposits. These deposits are laid down by water in saturated state. They become hard and as they dry, they become less compressible with relatively low density. The structure is usually open and porous, and soil grains are bonded together by cementing agents during deposition. If these deposits are subsequently exposed to water accompanied with or without additional loading, they may collapse, thereby causing large settlements.

Residual soils cover a wide range of sizes, from clay size up to the gravel range. The collapsible structure is developed as a result of the leaching of the soluble and colloidal matter from the residual soil. This leaching of the soluble and fine materials results in a porous and unstable structure.

Types of bonds in collapsing soils

Practically the open and unstable (meta-stable) structure makes collapsible soil susceptible to immediate collapse during inundation. The basic concept is of an open structure, often of bulky shaped grains, held together by some bonding material of force.

Types of bonds:

a) Capillary tension which provides strength in partially saturated fine-grained cohesionless soils such as illustrated in Figure 2.1.a. (Clemence, 1981)

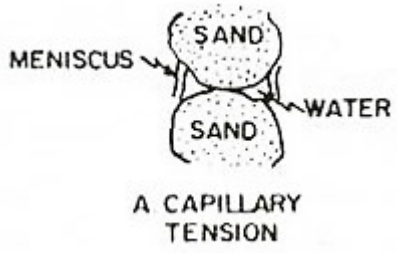

Fig.2.1.a Typical collapsible soil structures - Capillary tension (after Clemence and Finbarr, 1981)

The effect of the capillary stresses is to provide a tension force on soil grains, which provides considerable strength and stiffness for the soil mass, and is known as soil suction. (Vitton, 1997).

Capillary action within unsaturated soil matrix causes the development of negative pore water pressure as the moisture content exists within the micro-pores only, rather than the large macro-pores between the large flocs and/or coarse grains. Negative pore water pressure, with respect to atmospheric pressure, is termed as matric suction in unsaturated soil mechanics. Typically, the pore air pressure in collapsible soils is in atmospheric pressure condition. The higher the matric suction is, the higher the additional bond strength (due to capillary force.). Therefore, if the soil moisture content

remains constant at its initial (unsaturated) value, the original porous structure of collapsible soils can be maintained under heavy external loads.

The bond strength due to capillary action (matric suction) is available only when negative pore water pressure exists with the soil matrix. Inundation causes reduction in matric suction (or negative pore water pressure) due to the increase of water (or water pressure) in the pore. During inundation of any unsaturated soil, matric suction diminishes continually and becomes zero when the soil attained full saturation. As a result, collapsible soil experiences immediate volume reduction during inundation, as this bond strength is lost due to matric suction reduction.

b) In cases where the soil consists of sand with fine silt binder is illustrated in the Figure 2.1.b. It is assumed that simple capillary forces provide the silt-silt and silt-sand bonds in capillary voids (Barden, 1973)

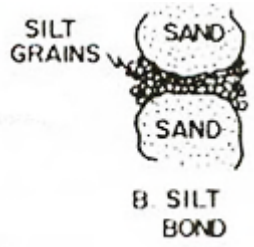

Fig.2.1.b Typical collapsible soil structures – Silt Bond (after Clemence and Finbarr, 1981)

c) The majority of collapsing soils involve the action of clay plates in the bonds between the bulky sand and silt grains. The structural arrangements will depend on the geologic origins and history of the soil as for example:

If the clay was formed in place by sedimentation it could form a parallel plate onion-skin effect around the quartz particles as illustrated in the Figure 2.1.c.

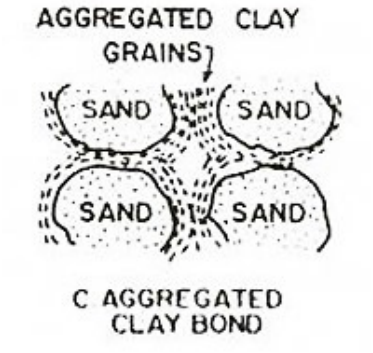

Fig.2.1.c Typical collapsible soil structures – Aggregated clay bond (after Clemence and Finbarr, 1981)

If the clay was originally in suspension in the pore water, then the gradual evaporation would cause the clay plates to retreat with the water into the menisci at the interparticle contacts. (Knight, 1960) indicates that under such conditions the clay would form a random flocculated structure as illustrated in the Fig.2.1.d.

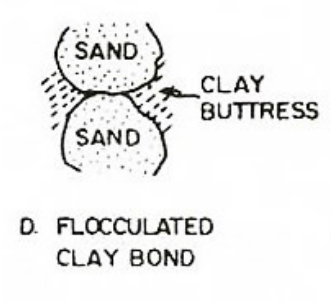

Fig.2.1.d Typical collapsible soil structures – Flocculated clay bond (after Clemence and Finbarr, 1981)

The addition of water in this case would cause the clay grains to separate and thus producing a loss of strength.

d) There are other cementing agents include silt bonds, clay bonds, and clay or calcium carbonate bridges as illustrated in Figures 2.1.e and 2.1.f.

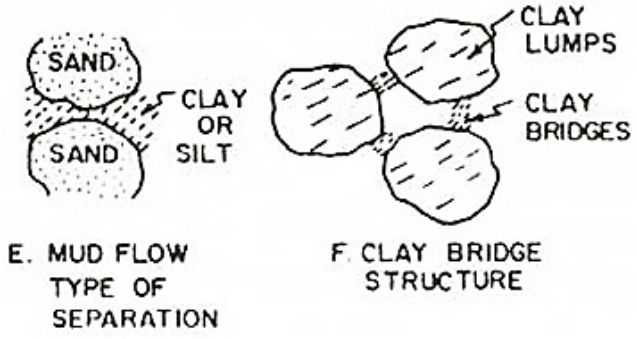

Fig.2.1.e, f Typical collapsible soil structures (after Clemence and Finbarr, 1981)

These materials restrain the bulky grains from rotating so that a more dense arrangement could be gained. Wetting destroys capillary bonds, softens clay bonds and bridges in an open structure. Increased saturation under an applied load can result in gradual settlement or a sudden collapse as the soil bonds are weakened.

It is seen that bonding between the bulky grains in the open structure of collapsing soils can involve either simple capillary suctions, clay buttresses or chemical cementing. In certain cases one type may dominate but in other cases there will be a complex interaction. However, whatever the physical basis of the bond strength, all types are weakened by the addition of water.

In the case of capillary suction the drop in strength will be immediate, in the case of clay buttresses rather slower, and in the case of chemical cementing it might be very slow (Barden, 1973).

Mechanism of collapse

The loose, bulky structural arrangement of the soil particles is a key element in the collapse mechanism.

(Casagrande, 1932) has demonstrated that a portion of the fine-grained fraction of the soil exists as bonding material for the larger grained particles. These bonds undergo local compression in the small gaps between adjacent grains resulting in the development of strength.

At natural moisture content, the structure of the soil is in equilibrium under the action of overburden pressures. As long as the soil remains dry, the structure remains highly voided without any large relative movement of the soil grains as shown in Figure 2.2 a.

When the soil is wetted and the critical moisture content is exceeded, the clay silt or salt binder that provide the cementation of the particles will soften, weaken and/or dissolve to some extent. Eventually these binders reach a stage where they no longer resist deformation forces and the structure collapses s shown in Figure 2.2.b.

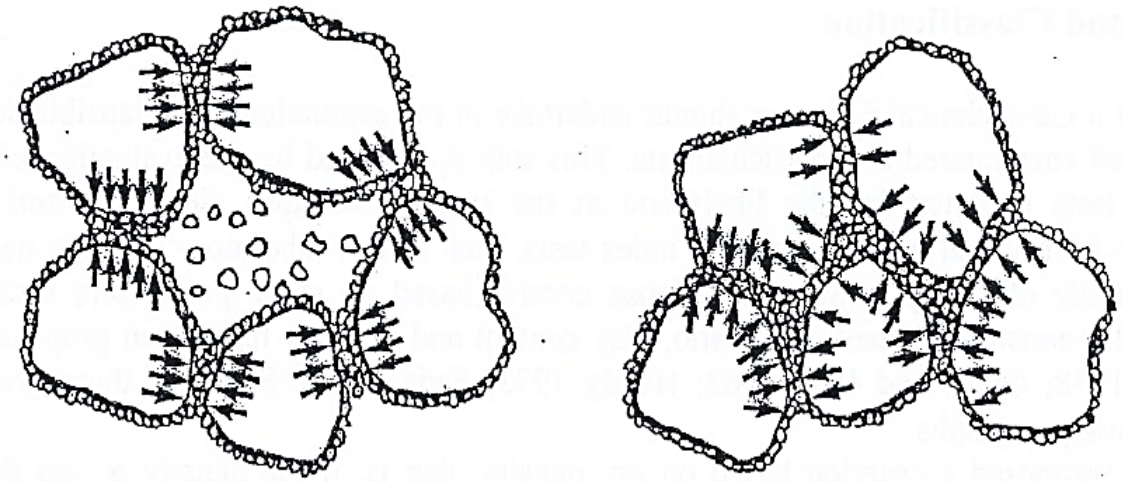

a. Loaded soil structure before inundation

b. Loaded soil structure after inundation

Figure 2.2. Loaded structure before and after inundation (after Casagrande 1932)

(Aitchinson, 1956) reported that for uniform spherical grains in an open cubical packing, the maximum added pressure due to capillary effect occurs at moisture content about 32%.

For the densest packing of uniform spherical grains, the maximum tension occurs at 10% moisture content. Investigations conducted with various collapsible soils showed that the peak effective stress values occur at moisture contents less that saturation and above 10% water content (Clemence and Finbarr 1981).

(Holtz, 1961) describes the collapse mechanism as the result of capillary pressures approaching zero and the degree of saturation increasing to 100%.

(Burland, 1965) described the collapse mechanism in terms of the stability at the interparticle contact points. Due to wetting the negative pore water pressure at the points decrease, causing grain slippage and distortion.

(Dudley, 1970) explained that as the soil dries below the shrinkage limit, the remaining water at the grains contact points is placed under tension. Thus the excess water pressure becomes negative and therefore, the actual effective stress becomes larger than the total stress applied by the load. This increases the apparent strength of the soil.

Mathewson (1981) believes that the soil structure in partly saturated soils is maintained by the surface tension of water held at the contacts of the grains and that the saturation of the soil fills the voids and reduces the surface tension to zero.

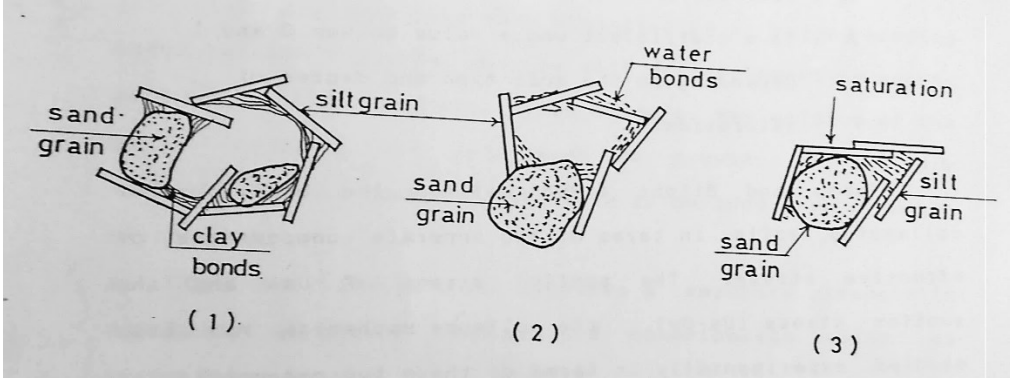

(1)Dry state (2) Partially saturated (3) After saturation

Figure 2.3. Mechanism of collapsing soil (after Mathewson, 1981)

In dry soils, the bonding agent is believed to be an oriented layer of clay minerals that was drawn into the fine pores as the soil dried out and that collapse occurs as the clay layer is re-suspended in the voids upon saturation as illustrated in Figure 2.3.

(Dudley, 1970), (Barden, 1973) and (Mitchell, 1993) explained the collapse phenomenon in terms of the cementing agents at the contact points of the soil grains. They identified four conditions required for the collapse to occur:

1. An open, partially unstable, partially saturated fabric.
2. A high enough total stress so that the structure is metastable.
3. A strong enough clay binder or other cementing agent to stabilize the structure when dry.
4. The addition of water to the soil which reduces the soil suctions (the negative pore water pressure) and thus produces collapse.

(Collins, 1978) explained that an open fabric, which is a prerequisite for collapse, may be comprised of:

a) clothed grain-grain contacts;
b) grain bridges or buttresses comprised of either clay or silt plus possibly cementations material such as iron oxide or carbonates
c) clay aggregates.

The rate of collapse depends on the type of bonding and this was indicated by (Tadepalli, 1992) who reported that the collapse phenomenon is primarily related to the reduction of the matric suction during inundation.

Identification of collapsible soils (simple methods)

a) Dispersion test

(Benites, 1968) proposed a laboratory dispersion test in which a two-gram soil is dropped at its natural water content, into a beaker of water and the time to disperse completely is recorded. For collapsible soils, dispersion time is less than 30 seconds. This test is may not be suitable for non-cohesive or granular collapsing soils.

b) Color test

(Arman, 1972), developed a color test, in which 100 grams of silt is placed in a 500 ml beaker containing 9 grams of sodium metahexaphosphate and 300ml of distilled water. The sample is allowed to settle overnight. A black color of the liquid indicates that the soil may be susceptible to collapse.

The disadvantage of this test is that it may be misleading for soil containing some mineral components which give the black color without being susceptible to collapse.

c) Visual identification test

(Jennings, 1975) described a very simple test called the “Sausage” test. A hand-size sample of the soil is broken into pieces, and each is trimmed until the two pieces are approximately equal in volume. One of the pieces of soil is then wetted and molded in the hand to form a damp ball. The volumes of the remaining dry piece and the damp ball are then compacted. If the wetted ball is obviously smaller, collapse potential may be suspected.

Prediction methods based the soil parameters

(Hanna, 2009) stated that the methods available in the literature can be divided into four categories:

1. Methods based on void ratio, density and water content relationship;
2. Methods based on water content and Atterberg limits relationship;
3. Methods based on density and Atterberg limits;
4. Methods based on particle size distribution of soils.

1. Methods based on void ratio, density and water content relationship

a) (Denisov, 1951) indicated that collapse will occur upon wetting if the naturally void ratio is smaller than the void ratio at liquid limit. He also proposed a coefficient of collapse as: $$K = \frac{e_L}{e_0}$$

where

e_L= natural void ratio and e_0= void ratio at liquid limit

He suggested the following value for the prediction of collapse:

K (value)	*Possibility of collapse*
0.5-0.75	highly collapsible
≥1.00	non collapsible

b) (Clevenger, 1956) stated that if:

- γ_{0d} <1.28 g/cm^3 , then the settlement produced will be large
- γ_{0d} >1.44 g/cm^3, then the settlement produced will be small

where γ_{0d} is the in situ dry density

c) (Gibbs, 1962)proposed the use of the natural dry density and liquid limit as criteria for predicting collapse. This method is based on the assumption that a soil which has sufficient voids to hold its liquid limit at saturation is susceptible to collapse upon wetting.

d) In Russian literature (Markin, 1969)considered that a soil is susceptible to collapse upon wetting if the in-situ degree of saturation (S) is less than 60% and

$$\frac{e_0 - e_L}{1+e_0} > -0.1$$

He stated as well that if:

$$\alpha = \frac{\gamma_{0d}}{\gamma_{Ld}}$$

α > 1.3	Prone to swelling
α < 1.1	Prone to collapse

where:

γ_{0d} = in situ dry density

γ_{Ld}= the dry density of the soil at liquid limit

e) (Bara, 1967) considered the soil to be collapsible when

$$\frac{\gamma_{0d}}{\gamma_{Ld}} < 1.0$$

where,

γ_{0d} = in situ dry density

γ_{Ld} = the dry density of the soil at liquid limit.

f) (Zur, 1973) stated other criteria to identify soil collapse.

$$\text{If } \frac{\gamma_{0d}}{\gamma_{Ld}} < 1.0 \quad \text{then the soil will collapse.}$$

In the above equation:

γ_{0d} = in situ dry density

γ_{Ld} = the dry density of the soil at liquid limit.

g) (Milivic, 1981) stated that the coefficient of collapse is expressed by

$$i = \frac{e_n - e_m}{1 + e_n}$$

where:

e_n = void ratio before flooding at vertical pressure

e_m = void ratio at the end of collapse at the same pressure

i = is greater for lower values of initial dry densities, and for lower values of initial water content, and higher values of wetting pressure.

2. Methods based on water content and Atterberg limits relationship

a) (Freda, 1964)proposed the following collapse index:

$$k_L = \frac{\frac{m}{S_r} - PL}{PI}$$

where:

m = natural moisture content

S_r = degree of saturation

PL = plastic limit

PI = plasticity index

He suggested that if the collapse index k_L >0.85 then is an indicative of a collapsible soil.

3. Methods based on density and Atterberg limits

a) (Bara, 1977) suggested that the estimate of the susceptibility of soil to collapse includes naturally dry density, natural moisture contents, liquid limit and the compared moisture content required for saturation at each natural density.

The soil is considered to collapse under three conditions:

- when the natural moisture is less than the liquid limit
- the liquid limit is less than the saturation moisture
- the less the density of the soil, the greater the amount of collapse

b) (Beckwith, 1979) suggested the use of typical index properties to identify collapsible soils. He suggested that collapsible soils might be indicated by a plasticity index value PI<10, a value of the unit weight γ_d<14.9 kN/m^3 and moisture content < 4% to 8%.

4. Methods based on particle size distribution of soils

a) (Jennings, 1975) introduced the concept of the critical value of degree of saturation (S_r), below which the collapse will occur.

The value depends on the grain size distribution:

Type of soil	*(S_r) critical*
Fine gravel (1-6mm)	6-10 %
Fine silty sands (150-2μ)	50-60 %
Clayey silts (150-0.2μ)	90-95 %

Table.2.1 Critical values of degree of saturation

Some of the existing methods in the literature have been summarized by T. Ayadat and A.M. Hanna (2011) in the following tables:

TABLE 1*a*. Existing criteria for soil collapse prediction

Expression	Reference	Remarks
$K=\frac{e_L}{e_0}$	Denisov [14]	K = 0.5 – 0.75 highly collapsing soils K = 1.0 non collapsible loams K = 1.5 – 2.0 non collapsible soils
$w_L\Big/\left(\frac{\gamma_w}{\gamma_d}-\frac{1}{G_s}\right)$	Gibbs and Bara [26]	< 1.0 collapse occur
$\alpha=(e_0-e_L)/(1+e_0)$	Markin [15]	α < - 0.3 prone to swelling α > - 0.1 and S_0 < 60% susceptible to collapse
$\alpha=(e_0-e_L)/(1+e_0)$	Minheev (1969)	S_0 < 0.6 and α > - 0.1 susceptible to collapse (this criterion is known as the new soviet building code)
$K_d=w_L-w_0/I_p$	Priklonskij [21]	K_d < 0 highly collapsing soils, K_d > 0.5 non collapsing soils, K_d > 1.0 swelling soils
$K_L=\left(\frac{w_0}{S_0}-w_p\right)\Big/I_p$	Feda [22]	For S_0 < 60% K_L > 0.85 collapsible soils
$R=\frac{w_s}{w_L}=\left(\frac{\gamma_w}{\gamma_d}-\frac{1}{G_s}\right)\Big/w_L$	Gibbs [25]	R ≥ 1% collapse susceptible This was also put into graph form
$\alpha=\gamma_{0_d}/\gamma_{L_d}$	Markin [15]	α > 1.3 prone to swelling α < 1.1 prone to collapse
$\gamma_{0_d}<1.28$ g/cm^3, $\gamma_{0_d}>1.44$ g/cm^3	Clevenger [11]	Settlement will be large, Settlement will be small
$R=5.5-3.82\log\frac{w_L}{w_p}-1.63\log w_p-1.24\log C_u-0.918\log P_{10}-0.303P_{200}+0.465\log\frac{D_{60}}{D_{40}}-0.45\log\frac{D_{90}}{D_{50}}$	Anderson [27]	

TABLE 1*b*. Existing criteria for soil collapse prediction (continued)

Expression	Reference	Remarks
$\delta(5,3)=0.166(S_0)^2+0.665I_p+0.078e_0-0.165S_0-0.85I_pS_0$	Krastilov [23]	
$\delta_{sp}=K(n_0-40)(30-w_0)$	Minkov et al.[17]	K = 0.02 for loess sand, K = 0.03 for sandy loess K = 0.05 for typical loess, K = 0.08 for clayey loess K = 0.09 for loess like clay
$I'_p=14.6\frac{S}{9}$	Salas et al. [18]	Gypsum soils of low I_P are in many respect similar to loess soils, although they exhibit greater collapse and compressibility
$n_0>40\%$	Feda [19]	Soil is susceptible to collapse
Lowa loess with clay < 0.002 mm contents	Handy [20]	< 16% high probability of collapse, 16 to 24 % probably collapsible , 24 to 32 % less than 50% probability > 32% usually safe from collapse
Cu ≤ 4% 4 < Cu < 12 Cu ≥ 12	Ayadat and Belouahri [28]	Safe from collapse Transition interval (collapse may occur) Soil is collapsible
Graphical method based on the work of Kenney and Lau (1985)	Ayadat et al. [2]	Collapse occur if the equivalent grain size curve of the soil is situated above or cut the line H = 1.3 F
I_p < 20, 15 < w_L < 35	Ayadat and Ouali (1999)	Collapse is susceptible
$CP=a(\gamma_d-15.27)+bw_0+17$ $a=-0.036C_u-1.379$ $b=0.0006C_u^2-0.089C_u+1.3$	Ayadat and Hanna [44]	CP < 1 collapse will not take place CP > 1 collapse is susceptible

Fig.2.4 After T. Ayadat and A.M. Hanna “Assessment Of Soil Collapse Prediction Methods” (2009)

In order to predict the susceptibility of the soil to collapse directly by knowing its bulk and soil constituents unit weight they proposed the following expression:

$$\gamma < 0.78\,\gamma_S$$

where: γ = bulk unit weight of soil

γ_S = specific soil unit weight.

This expression can be presented in form of a chart:

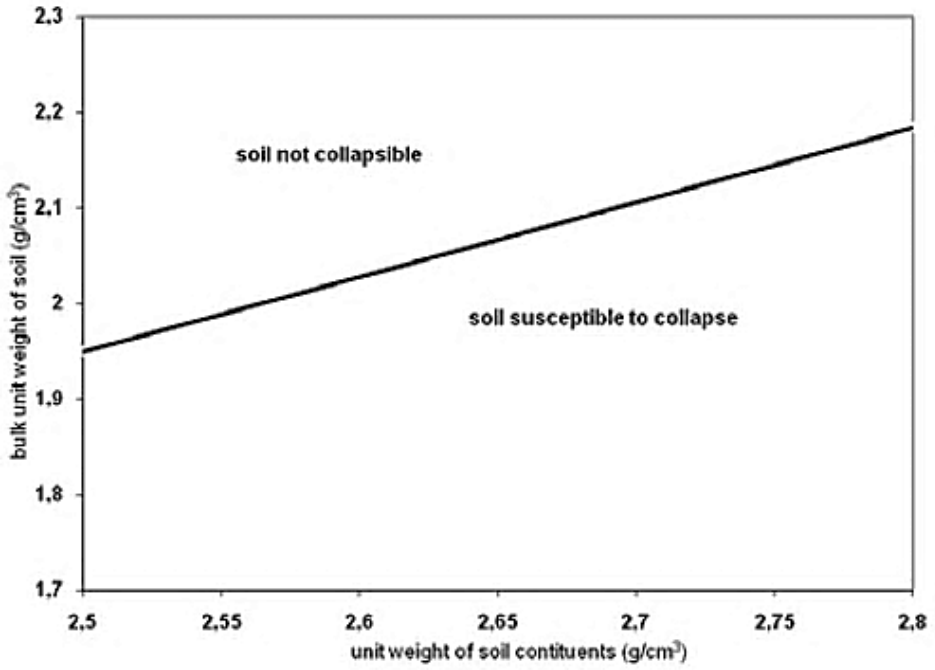

Figure 2.5. T. Ayadat and A.M. Hanna "Assessment Of Soil Collapse Prediction Methods" (2009)

Prediction methods based on Laboratory tests - Single Odometer Test

Developed by Knight in 1963, the test method consists of placing a soil sample at natural water content in an odometer (consolidometer), applying vertical stresses progressively until a predetermined pressure stress (usually of 200kPa) is reached. At the end of the loading the sample is flooded with water and left for 24 hours. The consolidation test is then continued to its maximum loading limit.

The collapse potential is defined as:

$$C_p = \frac{\Delta e_c}{1+e_0} \qquad \text{or} \qquad C_p = \frac{\Delta H_0}{H_c}$$

where:

Δe_c = change in void ratio upon wetting

e_0 = initial void ratio

ΔH_0 = change in the height upon wetting

H_c = initial height

Jennings and Knight (1975) have suggested the following values for collapse potential:

Collapse potential %	*Severity problem*
0-1	No problem
1-5	Moderate trouble
5-10	Trouble
10-20	Severe trouble
>20	Very severe trouble

Mitigation Methods

The appropriate method of choice depends on the depth of the collapsible soil, type of structure to be constructed and the cost and practicality of the method. Some of the mitigation methods are:

- Soil replacement. If the depth of the collapsible soil layer is shallow, it can be excavated and the structure can be supported directly on the exposed non-collapsible soil.
- Prewetting. Prewetting means flooding or wetting the soil which is expected to exhibit collapse upon saturation before the structure is build, so that collapse will be minimized after the structure is built. (Houston, 1977) (Bara, 1967)
- Controlled wetting. The method is similar to prewetting except that it is performed after the structure is in place. The quantities of water are approximated and added in increments. The same method can be used for buildings that exhibit tilt due to differential settlement.
- Moisture control. This method implies the prevention of water into the ground. Some of the measures that can be taken include: controlling water irrigation, placing landscaping in watertight planter boxes, placing pavement or buried geomembranes around the perimeter of the structure and placing effective surface and buried drainage systems.
- Compaction control. This is one of the most practical and effective methods of minimizing soil collapse. Compaction has been used for both shallow and deep collapsible soils.

- Chemical stabilization or grouting. The method develops cementation within the soil structure and thus it resists collapse when wetted. Penetration of chemical solution as sodium silicate and calcium chloride is generally costly and is used for small areas.
- Heat treatment. Burning gas and fuel oil in pressurized boreholes that are closely spaced will stabilize a column with a diameter of 1.5-2 meters.
- Differential settlement resistant foundations. It may be feasible to use spread footing if the collapsible soil deposit is thin. If the soil layer is thick, using deep foundations such as compaction piles to transfer the loads through the collapsible layers to the safe strata below.

2.3 Literature Review Pertinent to Passive Earth Pressure

General

Retaining structures, such as retaining walls and basement walls are encountered in foundation engineering, and they may support slopes of earth masses. The design of these structures requires the knowledge of the lateral forces that act between the earth and structure.

Since lateral forces applied to retaining structures are primarily directed so as to destabilize the structure (driving forces), determination of the magnitude and orientation of these forces are crucial to the development of a safe and economic design to resist those driving forces and also to incorporate an acceptable Factor of Safety into the overall design.

There are three cases of interaction between the wall and the soil:

1. The wall is moving away from the soil behind. The soil tends to expand or dilate. The action exerted by the soil on the wall is called **active earth pressure**. The resultant of the active earth pressure on the face of the wall is the active thrust P_a.
2. The wall is moving towards the soil behind which is compressed. For a certain displacement of the wall, a continuous failure surface develops, linking the base of the wall with the ground surface. The resistance opposed by the soil to the wall movement is called **passive earth pressure** or **passive resistance**. The resultant of the passive earth pressure on the face of the wall is the passive resistance $P_{p.}$
3. When the earth pressures on both sides of the wall are identical there is no movement and no possibility of developing neither active nor passive pressures. This case is the **at rest** condition and corresponds to the elastic equilibrium in the soil mass.

Passive lateral earth pressure – Coulomb's theory

The movement of a frictionless wall against the soil mass behind it produces an increase of the horizontal pressures acting on the wall and produces a compression of the soil. The basic assumptions for the earth pressure theories proposed by Coulomb are:

1) Soil is isotropic and homogeneous and has both internal friction and cohesion.

2) The rupture surface is a plane surface and the backfill surface is horizontal.

3) The friction resistance is distributed uniformly along the rupture surface and soil to-soil friction coefficient is $f = \tan \phi$.

4) The failure wedge is a rigid body undergoing translation.

5) Friction forces are developed between the wall and the soil.

6) Failure is a two-dimensional problem, namely a plane strain problem.

From all the planes that pass through the foot of the wall the one that has the smallest resistance must be found. This resistance is called passive resistance. The displacement needed for the passive condition is much larger than in the active state.

A trial failure plane BC is chosen (Figure 2.6a), at an angle α to the horizontal. The equilibrium of the soil wedge ABC is considered. The forces acting on the soil wedge and the force polygon is shown in the figure 2.6a.

The soil wedge ABC must be in equilibrium under the following forces:

- its own weight (W);
- the reaction (F) on the failure plane; at failure, when the shear strength of the soil has been fully mobilized, the direction of F is at an angleϕ' to the normal drawn to the plane BC. F being the resultant of the normal and shear forces on the failure plane;

- The reaction to the force, (P_p) between to soil and the wall. The reaction P_p acts at an angleδ' to the normal drawn to the face of the wall.

The triangle forces can be drawn as shown in figure 2.6b and the value of P_p determined.

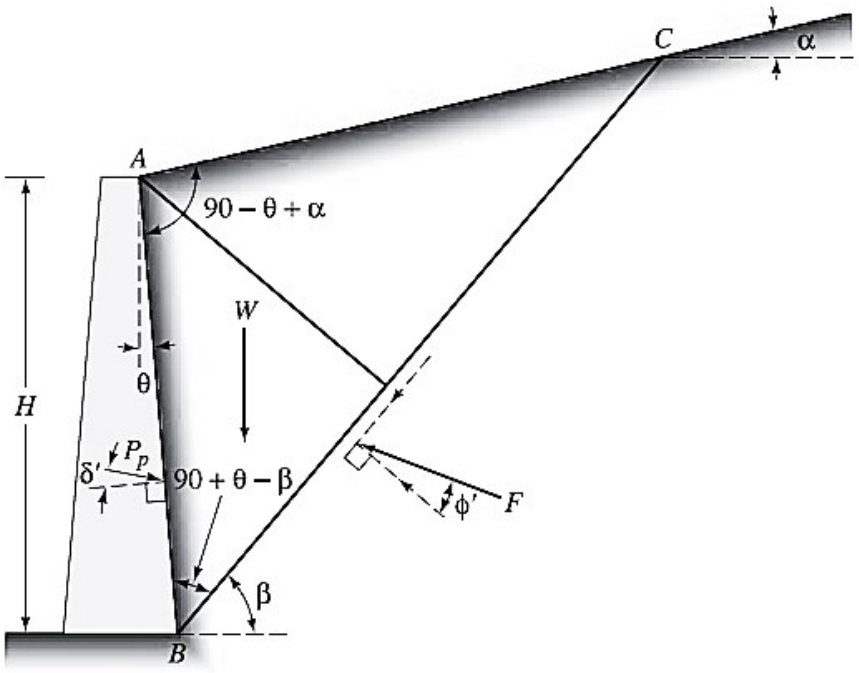

Figure 2.6 a Trial failure wedge (After Braja M. Das "Fundamentals of Geotechnical Engineering)

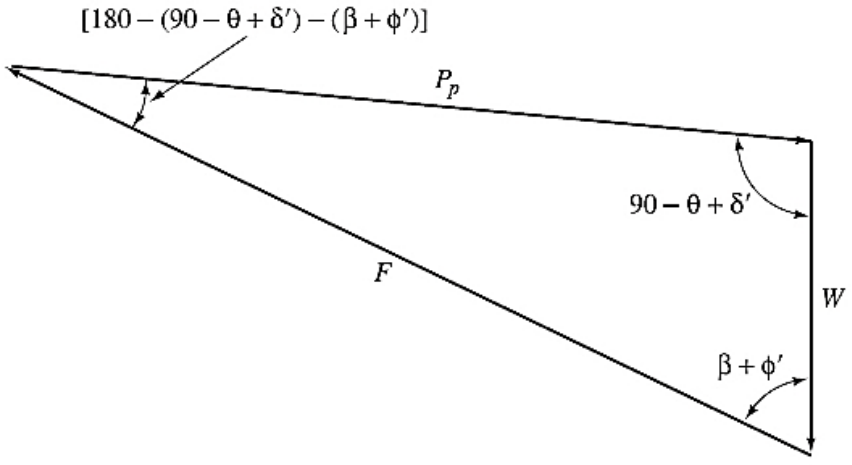

Figure 2.6 b Force polygon (After Braja M. Das "Fundamentals of Geotechnical Engineering)

From the force triangle the resulting Coulomb passive earth pressure is defines as:

$$P_p = \frac{1}{2} k_p \gamma H^2$$

Where k_p is Coulomb's active earth pressure coefficient and is given by:

$$k_p = \frac{cos^2(\emptyset' + \theta)}{cos^2\theta \, cos(\delta' - \theta)[1 - \sqrt{\frac{sin(\emptyset' - \delta') \sin(\emptyset' + \alpha)}{cos(\delta' - \theta) \cos(\alpha - \theta)}}]^2}$$

Passive lateral earth pressure – Rankine's theory

Rankine's passive state on a frictionless wall that extends to an infinite depth is illustrated in the figure below.

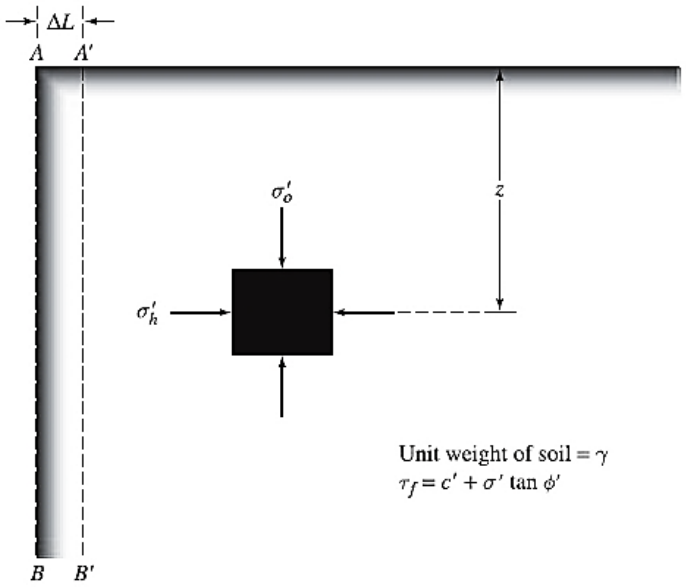

Figure 2.7 The vertical and horizontal effective principal stresses on a soil element at a depth z. After Braja M. Das "Fundamentals of Geotechnical Engineering

In Figure 2.8 the Mohr's circle "a" represents the initial stresses condition of the soil element. Mohr's circle "b" from the same figure represents the maximum stress condition of the soil element. This is achieved when the wall is gradually pushed into the soil mass and the effective principal stress σ'_h will increase to its failure value.

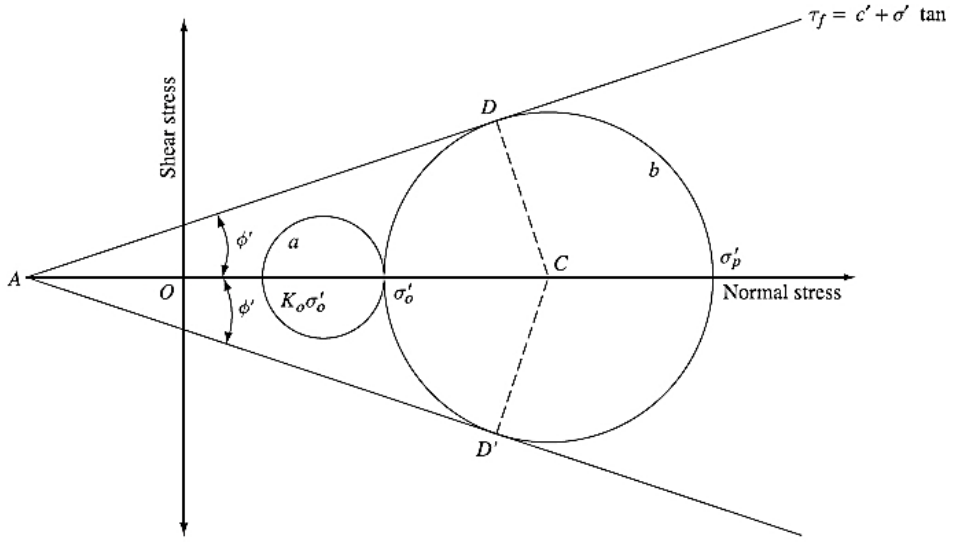

Figure 2.8 Mohr's circle for the passive limit state in case of cohesive soil
Braja M. Das "Fundamentals of Geotechnical Engineering"

The effective lateral earth pressure σ'_p which is the major principal stress is called Rankine's passive earth pressure.

For cohesive soil:

-The vertical effective principal stress is:

$$\sigma'_0 = \gamma\, z$$

-The horizontal effective principal stress is:

$$\sigma'_p = \gamma\, z\, tan^2\left(45^o + \frac{\emptyset}{2}\right) + 2c'\tan(45^o + \frac{\emptyset}{2})$$

-Rankine's passive earth pressure coefficient:

$$k_p = \frac{\sigma'_p}{\sigma'_0} = tan^2\left(45^o + \frac{\emptyset}{2}\right)$$

To the passive state corresponds two families of slip planes orientated at $45^o - \frac{\emptyset}{2}$ to the horizontal as indicated in the figure below.

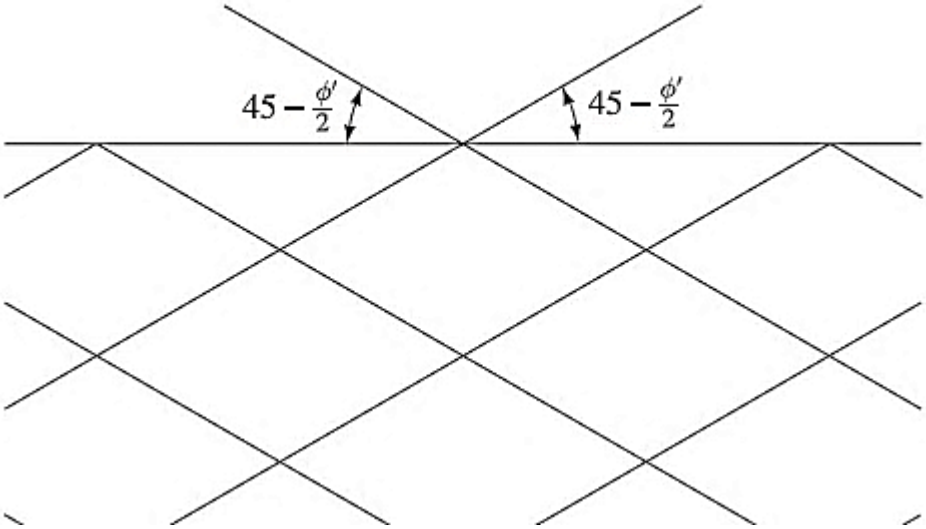

Figure 2.9 Failure plane of the wedge of soil in case of passive limit state
Braja M. Das “Fundamentals of Geotechnical Engineering “

Rankine's passive earth pressure distribution against retaining walls

a) Case for a cohesionless soil backfill with horizontal ground surface

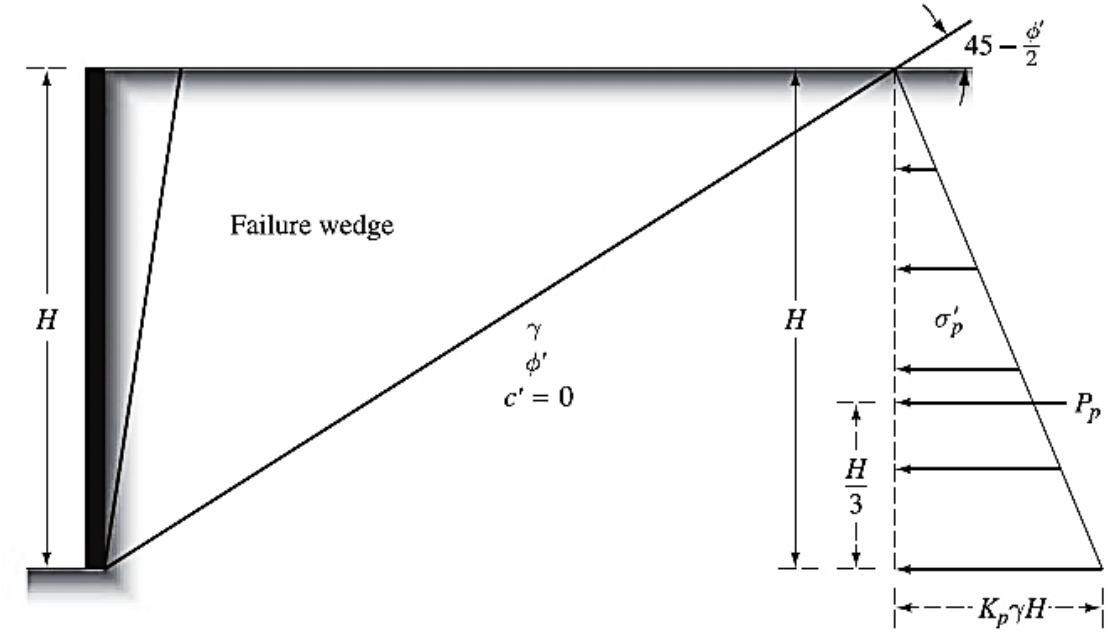

Figure 2.10 Pressure distribution against a retaining wall for cohesionless soil backfill with horizontal ground surface (After Braja M. Das "Fundamentals of Geotechnical Engineering)

The soil properties are known:

- Unit weight γ
- Angle of friction ∅
- Cohesionless soil : $c' = 0$

For Rankine's passive state, the earth pressure at any depth against the retaining wall can be given by the equation: $\sigma_p = \sigma'_p = \gamma\ z\ tan^2\left(45^o + \frac{\emptyset}{2}\right) = K_p\gamma\ z$

The stress increases linearly with depth so at the bottom of the wall it will become:

$$\sigma_p = K_p\gamma\ H$$

The total force, P_p, per unit length of the wall is equal to the area of the pressure diagram so:

$$P_p = \frac{1}{2}k_p\gamma\ H^2$$

b) Case for partially submerged cohesionless soil backfill that supports surcharge

a)

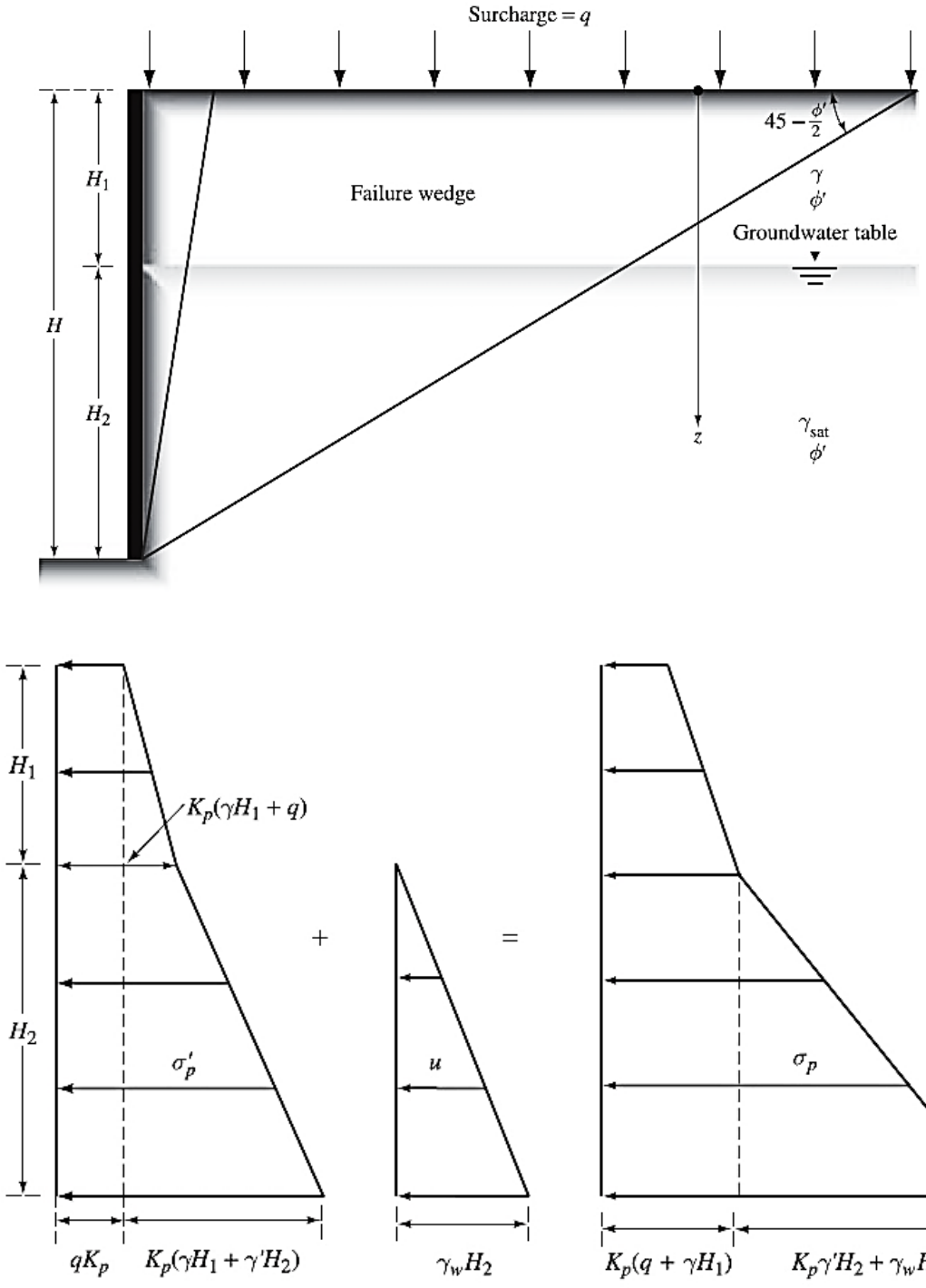

b) c) d)

Figure 2.11 Rankine's passive earth pressure distribution against a retaining wall with partially submerged cohesionless soil backfill supporting surcharge (After Braja M. Das "Fundamentals of Geotechnical Engineering)

The Figure 2.11 shows a frictionless retaining wall of height H and a backfill of cohesionless soil. The ground water table is located at a depth of H_1 below ground surface, and the backfill is supporting a surcharge pressure of q per unit area.

The effective passive earth pressure at any depth can be given by:

$$\sigma'_p = k_p \, \sigma'_0$$

Where:

σ'_0 = the vertical effective principal stress

σ'_p = the lateral effective principal stress

At $= 0$:

The vertical principal stress equals the surcharge: $\sigma_0 = \sigma'_0 = q$

The horizontal principal stress will be: $\sigma_p = \sigma'_p = k_p q$

The pore water pressure: $u = 0$

At $= H_1$:

The vertical principal stress equals the surcharge: $\sigma_0 = \sigma'_0 = (q + \gamma H_1)$

The horizontal principal stress will be: $\sigma_p = \sigma'_p = k_p(q + \gamma H_1)$

The pore water pressure: $u = 0$

At $= H$:

The vertical principal stress equals the surcharge: $\sigma_0 = \sigma'_0 = (q + \gamma H_1 + \gamma' H_2)$

The horizontal principal stress will be: $\sigma_p = \sigma'_p = k_p(q + \gamma H_1 + \gamma' H_2)$

The pore water pressure: $u = \gamma_w H_2$

The total lateral pressure (Figure 2.11 d), σ_a, diagram is the sum of the pressure diagrams shown in Figure 2.11 b and c. The total active force per unit length of the wall is the area of the total pressure diagram. Thus:

$$P_p = k_p qH + \frac{1}{2}k_p\gamma\, H_1^2 + k_p\gamma\, H_1 H_2 + \frac{1}{2}(k_p\gamma' + \gamma_w)H_2^2$$

c) Case for cohesive soil backfill with horizontal ground surface

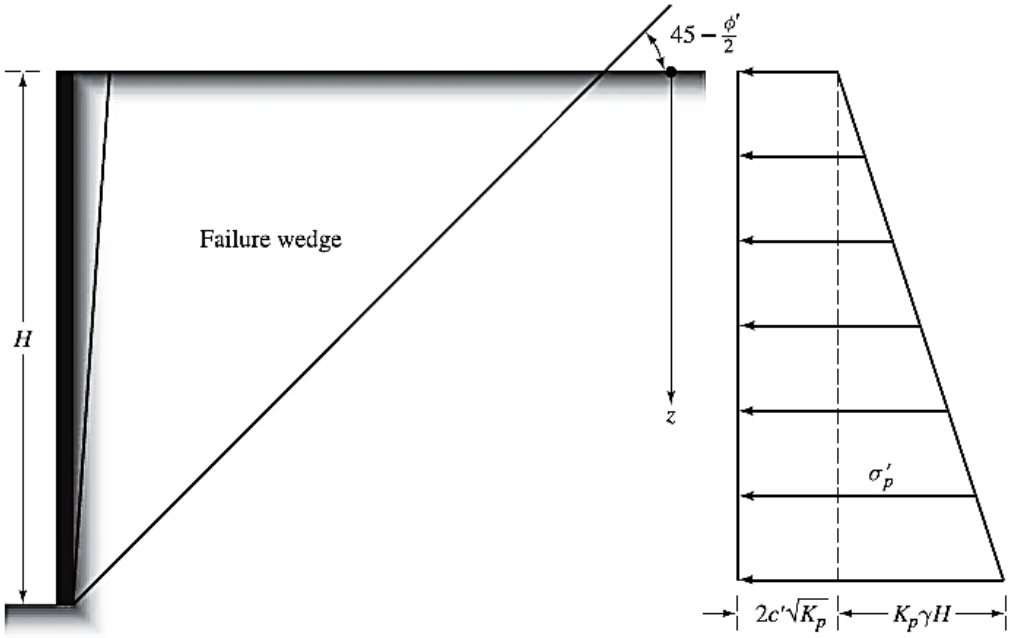

Figure 2.12 Rankine's passive earth pressure distribution against a retaining wall cohesive backfill. (After Braja M. Das "Fundamentals of Geotechnical Engineering)

The passive pressure against the wall at any depth below the ground surface can be expressed as: $\sigma'_p = \gamma\, zk_p + 2c'\sqrt{k_p}$

At $= 0$: $\sigma_p = \sigma'_p = 2c'\sqrt{k_p}$

At $= H$: $\sigma_p = \sigma'_p = \gamma\, Hk_p + 2c'\sqrt{k_p}$

The passive force per unit length of the wall can be found from the area of the pressure diagrams from Figure 2.12 as: $P_p = \frac{1}{2}k_p\gamma H^2 + 2c'H\sqrt{k_p}$

(Fellenius, 1927) assuming a circular rupture line was able to make a simple analysis for frictionless soil because the unknown stresses do not enter into the moment equation about the center of the circle.

(Caquot, 1948) presented a solution for the passive earth pressure acting on the face of a wall, showing that the mobilized value of the wall frictional angle δ depends on the type of the wall movement. They developed charts for the values of the passive earth pressure coefficient k_p using curved failure surface for granular soil (c=0) for the case of: $\phi = \delta$.

(Narain, 1969) investigated experimentally the determination of the rupture surface behind a retaining wall subjected to translation or rotation around its bottom or top for the case of loose or dense sand conditions. He reported that the magnitude of passive earth pressure reached the maximum values when the wall was rotated around its bottom and reached its minimum value when the wall was rotated about its top.

(James, 1970) studied the distribution of normal and shear stresses on a rough plane wall rotating about its toe into a mass of dry sand with a horizontal surface. They reported that the earth pressure reaches first its peak value near the top of the wall where the rupture surface is first observed. Furthermore, the magnitude of the passive earth pressures measured in the case of dense sand are much greater than those measured for loose sands.

(Kumar, 1997) developed charts based on an assumed failure surface consisted of a logarithmic spiral and a plane parts to determine the magnitudes of passive earth pressure coefficients. They found that the statically admissible inclination of the failure surface with the wall depends on the values of the angles of wall-soil (δ), angle of vertical inclination of the wall (ι) and the angle of shearing resistance (ϕ). They reported

that the angle of the failure surface with the horizontal would control the curvature of the failure surface.

They presented the passive earth pressure coefficient for the critical surface as:

$$k_p = \frac{P_p cos\delta}{\frac{\gamma D^2}{2}}$$

Where:

P_p = resultant of passive earth pressure resistance

D = Height of the wall

γ = unit weight of the soil

(Terzaghi, 1920) preformed measurement of horizontal passive earth pressure using a two inch high wall. Passive earth pressure coefficients were observed to be greater than 10 for dense sand after smaller wall movements, and well in the excess of the value of 2 for loose sand at a wall movement equal to 15% of its height. Based on his experiments, Terzaghi had noticed that the translational movement of a retaining wall greatly influences the horizontal passive earth pressure against the wall.

(Franzius, 1924) built a single wall 1m wide and 0.6 m high to determine the effects of wall friction on passive resistance. From these results, he concluded that the observed values were at least twice the values computed on the assumption of zero wall friction.

(Hansen, 1953) studied the rupture planes under different types of wall movement in a small scale model with a wall 15cmx15cm. he indicated differences in the shape and size of the rupture wedges under different wall displacements and with different wall frictions.

(Rowe, 1965) directly measured the passive earth pressure on a vertical wall movement by translation against a horizontal fill of dry sand. The test apparatus was constructed within part of a bin 14ftx9ft in a new 60 ton sand flume. The wall contact with

the sand is 6ft wide and 1.5ft and consisted on three separate sections each 2ft wide. The central sections housed three columns of six earth pressure cells. This elaborate equipment allowed a control of the wall direction and of the consequent rate of mobilization of wall friction. From the test results, Rowe and Peaker observed that the distribution of the pressure on the translating wall was essentially linear in all the tests at each stage of deformation up to failure. They also discovered that the angle of wall friction changed in relation to the rate of displacement. Their test results show that the passive earth coefficient k_p , the friction angle of the soil and the wall friction, increase initially with the increase of the wall's translational movements and kept constant after they reached the peak values.

CHAPTER 3

EXPERIMENTAL INVESTIGATION

3.1 General

An experimental setup was designed and built to simulate the condition of a retaining wall subjected to passive earth pressure. In order to model the passive pressure in the soil mass, the retaining wall was designed to be pushed into the soil. The horizontal forces applied on the retaining wall, as well as the horizontal displacements were measured.

The present investigation was performed using collapsible soil as backfill material. Then the soil was inundated from the bottom modeling the rise of the ground water table.

This chapter describes the design of the experimental setup and its components, the properties of the materials used and the laboratory preparation of the collapsible soil.

Figure 3.1 presents a sketch of the setup used in this investigation, which consists of a testing tank, loading device supported by a steel frame and elevated water tank with constant water head that supplies the water to the soil in the testing tank through the water distribution system.

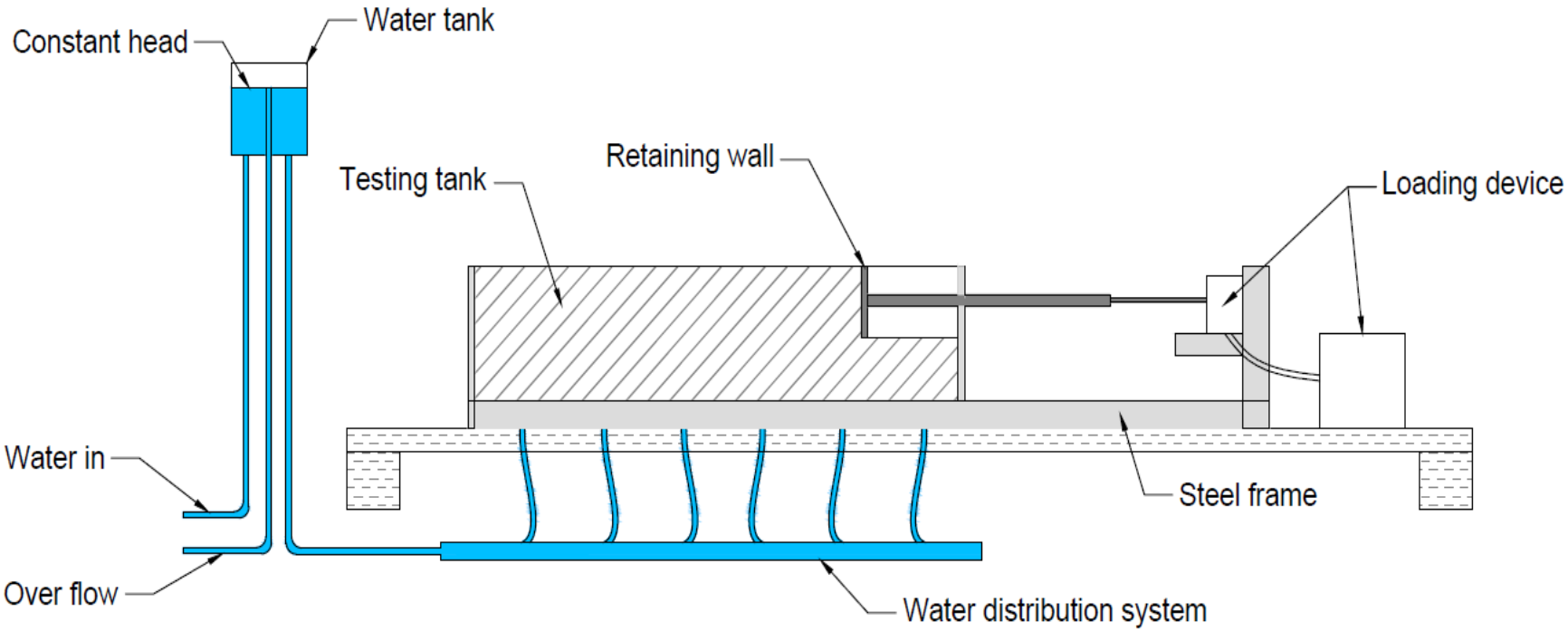

Fig.3.1 Sketch of experimental setup

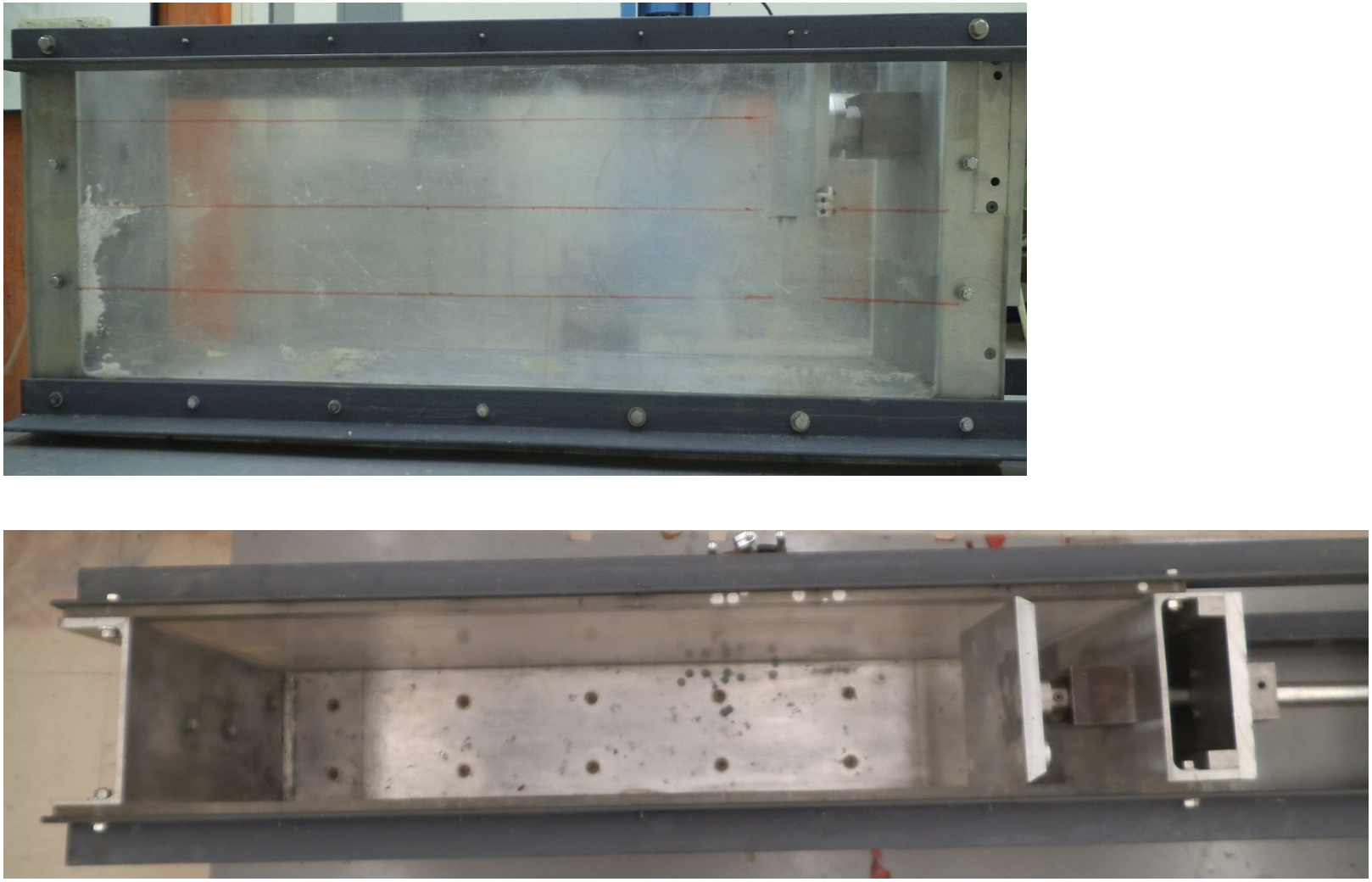

Fig.3.2a. Testing tank front and top view

3.2 Test setup

The experimental setup consisted of a testing tank, retaining wall, loading system and water distribution system.

- Testing tank

The inner dimensions of the tank are 1080 mm, 195 mm and 406 mm length, width and depth respectively. Figure 3.2a shows a top and side view of the testing tank used in the present investigation. The longitudinal sides are manufactured from 10 mm Plexiglas sheets which were transparent in order to observe the movement of the soil behind the wall and, accordingly, the failure mechanism. The lateral sides of the tank were aluminum alloy channels. The tank was laterally braced using steel angles to prevent the deflection of the tank during loading. The bracing system job was to support the loading system in order to ensure the horizontal direction of the loading system.

To simulate the rise of the ground water level, 12 thin- tubes were connected to the bottom of the tank. The tubes were receiving water from an elevated water tank and remained connected and open throughout the testing procedures.

- Retaining wall and loading system

A metal plate was placed on the upper part of the tank to simulate a retaining wall. The dimensions of the plate were 195mm x 215mm x 19 mm width, depth and thickness, respectively. The retaining wall was allowed to move horizontally, but no rotation was permitted. In order to simulate the plane strain condition in the sand mass, the width of the plate was kept the same as the width of the testing tank.

The plate was held vertically through a rod that passed through two sets of roller bearings Figure 3.2b. On the roller bearing that was inside the testing tank, a plastic seal was attached so that when soil was inundated, the water would not infiltrate into the bearing. Prior to testing the wall, the metal rod and the bearing were greased with thick

waterproof grease to prevent rust. The roller bearings allowed the loading rod that supports the retaining wall to have a horizontal movement but no rotation and no vertical displacements. The two roller bearings can be observed in Figure 3.2a and Figure 3.2 b.

On the exterior of the testing thank the metal rod was connected to the loading system through a loading cell that was used to measure the horizontal component of the total passive earth pressure. The end side of the steel rod was fileted to fit the load cell. The other side of the load cell was connected to a large diameter screw that was part of the loading machine. The horizontal alignment of this connection was properly measured and fixed in order to avoid any inclination of the applied force. The load cell connections are presented in Figure 3.4.

The wall movements were measured by an electrical sensor (Linear Variable Displacement Transducer LVDT). The LVDT was connected to the side of the testing tank and to the retaining wall. It was detached during inundation to avoid any water contact. After calibration the LVDT was connected to the Data acquisition system (D.A.S.) and the displacement was recorded in millimeters.

The loading system consisted of a gear box manufactured by Wykeham Farrance. The fixed gear box was used to generate horizontal force which in return produced a horizontal movement of the steel rod that was connected to the retaining wall. Figure 3.3 shows a picture of the gear box used. The forces generated by the gear box were measured by the Load Cell which was connected on one side to the horizontal retaining wall rod and on the other side to the horizontal rod of the gear box (Figure 3.4). After calibration the load cell was connected to the D.A.S. to register the force applied in Newton.

Fig.3.2b. Retaining wall

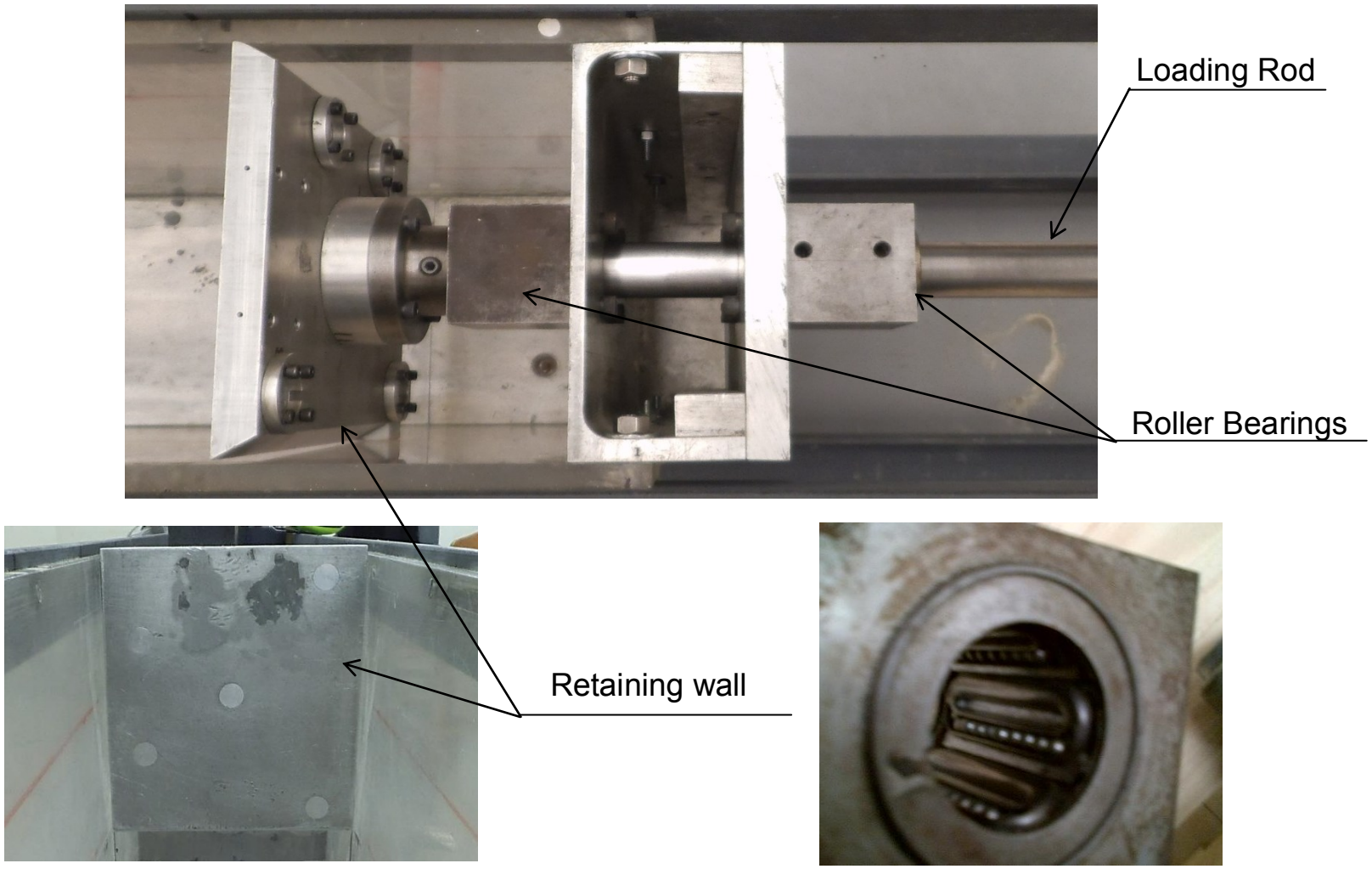

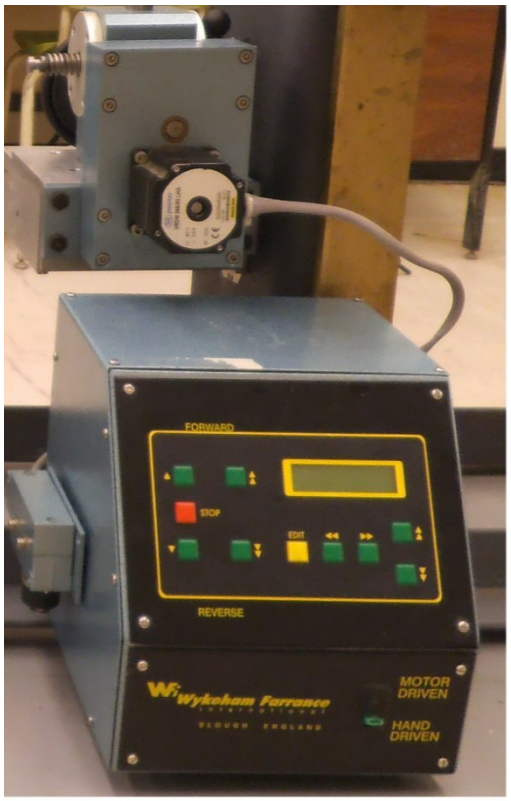

Fig.3.3. Gear box used

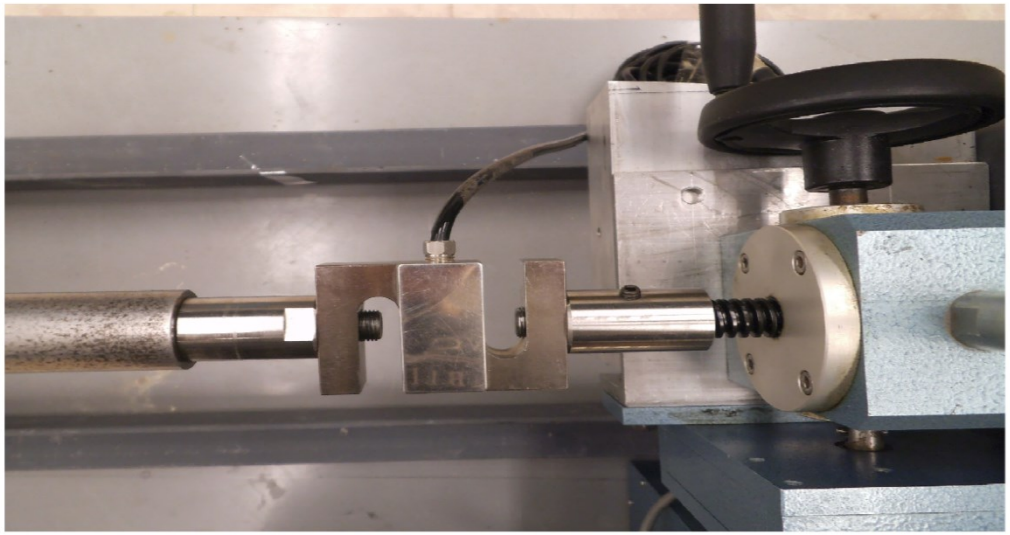

Fig.3.4. Load cell connections

- Water distribution system

In the present investigation collapsible soil was used as backfill material for the retaining wall. The collapse of the soil was achieved by inundation at the bottom of the testing tank. A water distribution system was built to simulate this condition. An elevated tank (Figure 3.5), made of Plexiglas, is connected to the testing tank by a plastic tube, which was branched into 12 tubes (Figure 3.6), through which the water was charged to the bottom of the test tank, simulating the rise of groundwater table. The water level in the water tank was kept constant during the inundation process, water was charged from a water source and an overflow pipe was fixed inside the water tank that kept the water at a constant level. To achieve the constant water level in the water tank before inundating the soil, a valve was placed on the "Out to test" tube. During the time that the water was allowed to flow in the water tank, this connection valve was kept closed. After the level of water started to have a constant flow, the valve was opened so that the water can pass through 12 thin tubes at the bottom of the testing tank inundating the soil.

During the inundation process the transparent thin tubes were monitored to prevent the entry of air bubbles in the system. When the test was finished and after the soil had been taken out of the tank, the tubes were cleaned with water to prevent any clogging in the system.

For the inundated samples, a layer of slightly compacted silica sand was placed at the bottom of the testing tank to ensure an even distribution of the water throughout the collapsible soil.

Fig.3.5. Water tank

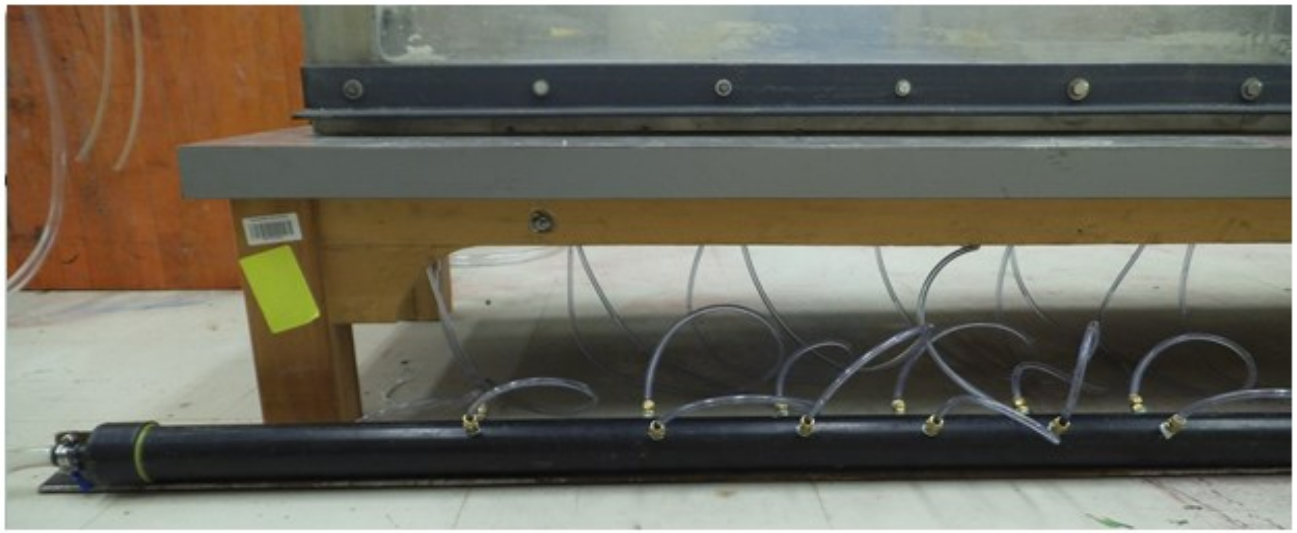

Fig.3.6 Water distribution system

Soil compaction was carried out prior to the loading of soil .The same compaction energy per unit volume *E* was maintained for each layer and throughout all the experiments to reach the desired soil properties, and accordingly the desired collapse potential.

The compaction unit consists of a 4.5kg hammer that drops from a height of 45.7 cm on an aluminum compaction plate of 19.4mm by 35.5mm as seen in figure 3.7.

The testing tank was divided into four equal layers. In order to achieve the desired height of the compacted sample, for the top layer a detachable wood frame was built to keep the soil from sliding during compaction figure 3.8. The wood frame was fixed to the steel frame of the system by screws and tightened with clamps. Prior to testing the frame was removed to allow the movement of the retaining wall.

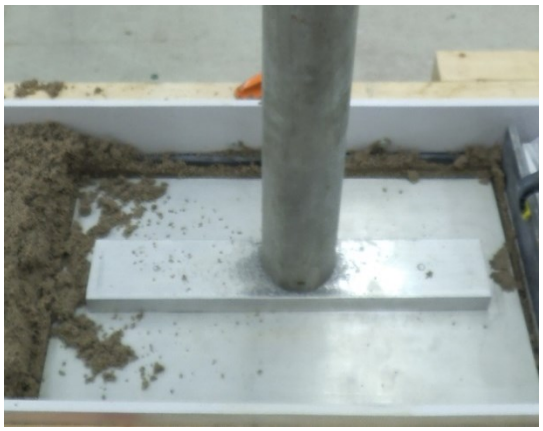

Figure 3.7 Compaction plate and hammer

Figure 3.8 Wood frame

3.3 Soil Mixture Preparation

Three different mixtures of collapsible soil were prepared and used in the experiments, in order to reach different levels of collapse potential. The mixtures consisted of sand and Kaolin clay with different content values (6%,8% and 10%) and water content of 5% as shown in table 3.1. The different soil characteristics were determined through a series of soil properties test presented in this chapter.

Sieve analysis was carried out for the soil mixtures .The diameter corresponding to percentage of soil passing sieves D_{10} , D_{30} and D_{60} was determined and the coefficient of curvature C_c and the uniformity coefficient C_u were calculated, where:

$$C_c = \frac{D_{30}^2}{D_{60} * D_{10}} \qquad \text{and} \qquad C_u = \frac{D_{60}}{D_{10}}$$

Classification of soils according to USCS and AASHTO are presented in table 3.1.

After compaction and just before carrying out the experiments, a series of soil tests were carried out in order to determine the unit weight, dry unit weight and the water content of the soil for each of the three soil mixtures and the results are summarized in table 3.1.

Standard Proctor test was carried out on the three soil mixtures to determine the maximum dry unit weight and the optimum moisture content.

In addition, direct shear test was performed for each of the mixtures to determine the shear strength parameters. For each soil mixture, four direct shear test were performed at different vertical stresses and Mohr-Coulomb criterion was used to determine the shear parameters of the soil. The results are presented in table 3.2.

Table 3.1 - Soil properties

Parameter	Soil type		
	Mix 1	Mix 2	Mix 3
Clay content (% Kaolin)	6	8	10
Initial moist content w_c (%)	5	5	5
Unit weight γ (kN/m^3)	16.28	16.25	16.2
Dry unit weight γ_d (kN/m^3)	15.6	15.5	15.4
Maximum dry unit weight $\gamma_{d\,max}$ (kN/m^3)	18.05	18.3	19.25
Optimum water content w_{opt} (%)	12.6	12.25	11.75
Specific gravity G_s	2.66	2.67	2.67
Void ratio e	0.67	0.69	0.70
Degree of saturation S (%)	19.77	19.35	19.05
Liquid limit (w_l)	-	9.2	15.9
Plastic limit (w_p)	N.P.	N.P.	13.35
Plasticity index (PI)	-	-	2.55
Coefficient of uniformity (C_u)	4	5.4	21.9
Coefficient of curvature (C_c)	1.27	1.65	6.47
Soil Classification (Unified Soil Classification System USCS)	SP-SC	SP-SC	SP-SC
AASHTO	A-3	A-3	A-2-4

Table 3.2 - Summary of shear strength parameters for the soil mixtures

Soil Type	Clay content (%)	Soil cohesion c' (kPa)	Angle of internal friction $\emptyset'$ (degrees)
Mix 1	6	9	40
Mix 2	8	12.5	38.5
Mix 3	10	15.5	35

The clay content used for the three soil mixtures was chosen so that the three different mixtures would have different collapse potentials. (Mashhour, 2009) (Soliman, 2010).

Odometer tests were carried out on the soil mixtures to determine the collapse potential C_p, following the procedure suggested by (Knight, 1963), where the soil specimen was being loaded up to a load of 200 kPa, then it was being flooded with water, while the load was maintained on the soil and the settlement upon wetting (collapse settlement) was measured.

The collapse potential is equal to the deformation of soil to the addition of water, divided by the initial height of the specimen, expressed in percentage as shown in the following equation:

$$C_p = \frac{\Delta H_0}{H_c}$$

Table 3.3 shows the collapse potential values obtained from the odometer test for each of the soil mixes and the severity of foundation problems as suggested by (Jennings, 1975).

Table 3.3 –Collapse potential and severity problem for the soil mixtures (Mashhour, 2009) (Soliman, 2010)

Soil mixture	Clay content (%)	Collapse potential C_p (%)	Severity of foundation problem (Jennings and Knight 1975)
Mix 1	6	4.2	Moderate trouble
Mix 2	8	9	Trouble
Mix 3	10	12.5	Severe trouble

Soil compaction has a great influence on the collapse potential of the soil. Prior to testing the compaction was carefully carried out. The same compaction energy per unit volume *E* was maintained for each layer and throughout all the experiments to reach the desired soil properties, and accordingly the desired collapse potential.

Energy of compaction was calculated using the equation:

$$E = \frac{N*W*H*L}{V}$$

Where:

E = energy per unit volume (g/cm/cm^3)

N = no. of blows

W = weight (g)

H = height (cm)

L = no. of layers

V = volume of soil being compacted (cm^3)

Table 3.4 –Calculation of the compaction energy

E (g.cm/cm^3)	N	W (g)	H (cm)	L	V (cm^3)	V (cm^3)
588.39	20	4500	45.7	4	19.4*35.5*40.6	27961.22

3.4 Test procedure

1. For the inundated samples, a 2.5 cm layer of coarse silica sand was placed and slightly compacted at the bottom of the testing tank to allow even and uniform distribution of water throughout the collapsible soil during inundation. Figure 3.9

Figure 3.9 Silica sand layer

2. The laboratory prepared collapsible soil was prepared by dry mixing the sand and clay in a mixer Figure 3.10. The dry mixing procedure ensured that the Kaoline and sand are thoroughly mixed. Five percent water by weight was added to the mix and all are mixed together for an additional period of time. A sensitive balance was used to measure the quantities of materials used.

Figure 3.10 Mixing of the samples

3. The mixed sample was placed in the tank in four layers and compacted, keeping the same compaction energy for each layer. The unit weight of the mixture in the tank was measured by means of density cans, which were placed in a staggered scheme in the vertical direction to avoid boundary effects. At the end of each test, these cans were carefully taken out and weighed. The unit weight of the mixture was taken as the average unit weight in these cans.

   The procedure was repeated for each test so that the unit weight will be the same as the one given in table 3.1. The mixing, spreading and compacting procedure was repeated until the third layer. For the last layer the wood frame was attached to the tank and the sample was placed and compacted for the last layer. Prior to testing the wood frame was detached. Fig.3.11

Figure 3.11 Wood frame for the compaction of the top layer

4. The LVDTs that measured the horizontal displacement of the wall and the collapse settlement were placed and carefully retracted to reach the zero value. Figure 3.12.
5. For the tests with only 5% initial water content, the test was carried out recording the force and displacement of the wall.

6. For the inundated samples, the water was introduced in the tank until the soil was 100% inundated. After saturation, the load on the retaining wall was applied at a constant loading rate. The constant loading rate was selected on the loading unit in terms of piston displacement of 0.5 millimeters per minute. The load applied on the retaining wall, measured by the load cell and the displacement of the wall measured by the LVDT was collected using the DAS program.
7. During inundation three LVDT's were placed along the tank to measure the collapse settlement of the sample (Figure 3.12). It was noticed that the LVDT's do not record any values and collapse settlement was not visible.

Figure 3.12 LVDT assembly

8. Prior to testing, all of the metal parts inside the tank were waterproofed by applying a thick water resisting grease.

The following parameters were being monitored:

- Collapse settlement (LVDT)
- The load applied on the soil (load cell)
- Displacement of the retaining wall (LVDT)

3.5 Friction force

To account for the development of the friction force in the bearings of the mechanism, and between the wall and the sides of the tank two tests were performed on the empty tank and the load applied on the retaining wall as well as its displacement were recorded. As can be observed in figure.3.13, the two load-displacement curves of the tests had close values.

An average friction force has been calculated and subtracted from the load readings of all the tests. In the present experimental investigation the presented values of the loads for all the tests will represent the net value of the load.

Table 3.5 - Test 1

Displacement (mm)	Load (N)
0.000	0.000
0.110	24.028
0.369	25.857
0.679	34.944
1.032	63.659
1.436	58.487
1.915	38.641
2.459	18.600
3.007	8.982
3.593	25.326
4.186	33.056
4.803	36.478
5.453	33.292
6.139	34.983
6.818	38.622
7.488	22.199
8.141	47.669
8.778	44.208
9.426	42.339
10.097	36.891
10.775	38.799
11.443	44.306
12.105	34.138

Displacement (mm)	Load (N)
12.744	45.368
13.211	54.710
13.858	38.700
14.515	34.787
15.193	27.096
15.848	24.009
16.491	32.918
17.129	29.929
17.767	32.721
18.418	38.248
19.097	38.189
19.790	30.833
20.462	43.401
21.112	39.055
21.751	37.638
22.402	32.879
23.066	31.797
23.738	63.738
24.405	50.718
25.071	29.260
25.713	36.262
26.363	28.434
27.033	30.814

Displacement (mm)	Load (N)
27.721	18.836
28.418	11.618
29.095	22.022
29.751	30.342
30.397	31.128

Test 2

Displacement (mm)	Load (N)
0.000	0.000
0.023	45.991
0.088	61.649
0.228	68.200
0.371	72.626
0.522	74.082
0.650	75.360
0.842	73.708
1.050	65.879
1.218	55.768
1.446	44.083
1.703	40.030
1.978	33.932
2.258	33.677
2.558	34.601
2.861	42.686
3.166	42.214
3.482	39.263
3.812	41.289
4.142	48.548
4.490	48.902
4.834	52.325
5.191	48.922
5.558	46.896
5.932	44.948
6.210	38.594
6.578	37.434
6.944	32.870
7.310	40.463
7.670	43.591
8.026	49.768
8.385	45.007
8.748	40.857
9.109	38.909
9.376	42.824
9.742	45.814
10.113	49.178
10.476	46.738

Displacement (mm)	Load (N)
10.849	41.073
11.212	42.155
11.569	54.568
11.921	64.266
12.278	63.459
12.636	59.033
12.988	64.325
13.340	75.065
13.698	64.639
14.064	52.423
14.428	41.053
14.827	39.027
15.163	45.420
15.519	51.991
15.871	49.768
16.226	51.125
16.583	51.027
16.934	46.994
17.286	45.991
17.644	44.909
18.008	45.814
18.373	49.040
18.746	45.479
19.115	47.289
19.485	44.122
19.856	45.460
20.221	54.390
20.585	50.456
20.943	49.060
21.298	49.178
21.568	50.004
21.928	45.755
22.204	47.506
22.567	47.938
22.931	44.476
23.301	40.168
23.668	48.863
24.027	54.155

Displacement (mm)	Load (N)
24.392	56.731
24.754	65.111
25.105	73.708
25.464	71.819
25.821	66.115
26.186	67.098
26.551	65.288
26.926	62.102
27.302	52.207
27.679	40.975
28.061	34.385
28.435	27.027
28.816	30.116
29.174	36.411
29.538	48.587
29.896	44.437
30.247	46.129

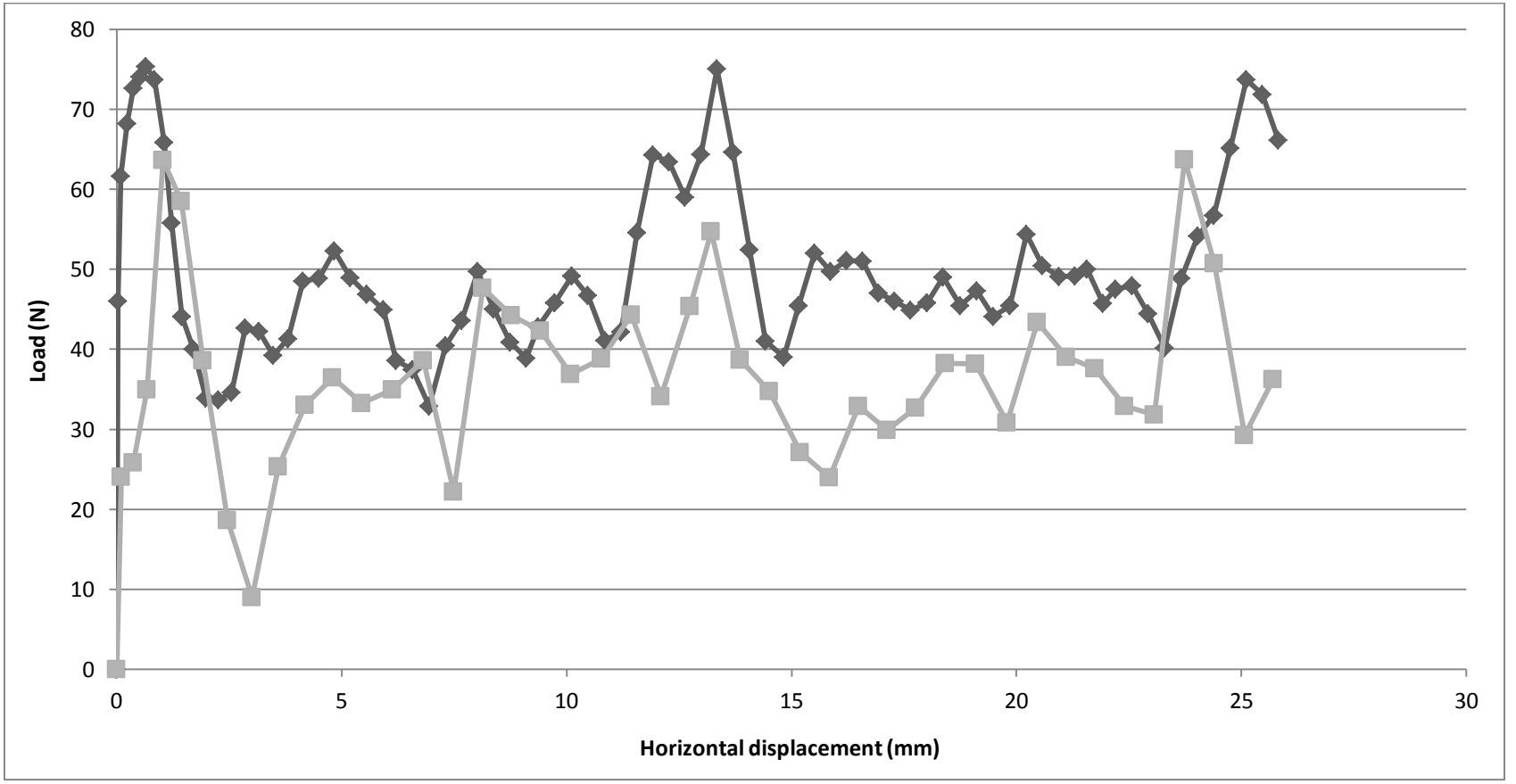

Graph 3.13- Friction force load-displacement curves

3.6 Calibration of the setup

To ensure that the results of the tests are accurate, a test was performed on pure sand and the coefficient of passive earth pressure (k_p) was calculated using Rankine's passive earth theory.

Prior to testing, the angle of friction and the unit weight of the sand were calculated by performing a series of shear tests. The unit weight of the sand in the tank was measured by means of density cans which were placed in a staggered scheme in the vertical direction. At the end of each test, these cans were carefully taken out and weighed. The unit weight of the sand was taken as the average unit weight of the sand in these cans. The placing of sand in the tank was developed so that the average unit weight of the sand would be the same as the unit weight in the shear test.

The wall was pushed toward the sand mass, and the loading system was turned on at a loading rate of 5 mm/ min. The DAS (Data Acquisition System) will record the load applied and the horizontal displacement of the wall.

The wall movement continued until failure was reached, at which the sand mass behind the wall will separate from the rest of the sand in the testing tank through a failure surface. The sand movement was observed from the glass sides of the testing tank until the failure mechanism was fully developed behind the wall.

The test was stopped when the sand started to overflow from the tank. The force applied on the wall recorded the maximum value when the failure mechanism was achieved and then the load will start decreasing. It was observed that after the soil has failed the load would start increasing again because under the movement of the wall, the soil would start to build up and overflow from the tank.

The results of the tests performed on the loose sand are presented in table 3.6. The maximum load and horizontal displacement corresponding to the failure are underlined. The load-displacement curve of the loose and is presented in graph 3.14.

Table 3.6 – Test results for loose sand

Displacement (mm)	Load (N)
0.000	0
0.023	6.91806
0.078	51.5317
0.172	73.1555
0.278	83.2611
0.324	90.3772
0.422	95.0743
0.630	112.546
0.801	134.707
0.952	155.371
1.110	173.75
1.278	183.445
1.452	200.625
1.644	207.248
1.836	217.885
2.036	227.283
2.245	247.843
2.463	265.398
2.686	273.071
2.926	282.011
3.166	293.102
3.406	302.871
3.659	315.629
3.913	330.528
4.176	343.874
4.443	347.983
4.709	359.862
4.978	375.918
5.247	384.864
5.524	393.656
5.801	399.963
6.082	407.12
6.356	423.355
6.643	432.205
6.911	444.906
7.194	452.121
7.477	459.04
7.762	474.274
8.037	489.866
8.331	492.673
8.612	500.913
8.892	507.755
9.175	508.834
9.455	513.869
9.741	523.284
10.018	534.035
10.294	541.348
10.577	559.693
10.846	580.725
11.128	592.282
11.402	596.492
11.673	603.24
11.947	613.838
12.226	619.595
12.506	627.124
12.785	628.752
13.060	631.096
13.337	641.414
13.608	656.81
13.881	666.242
14.155	673.323
14.426	679.22
14.700	684.173
14.974	692.331
15.248	699.844
15.522	***701.728***
15.797	692.334
16.075	694.723
16.350	700.577
16.628	710.299
16.906	713.857
17.179	716.178
17.460	720.782
17.735	728.13

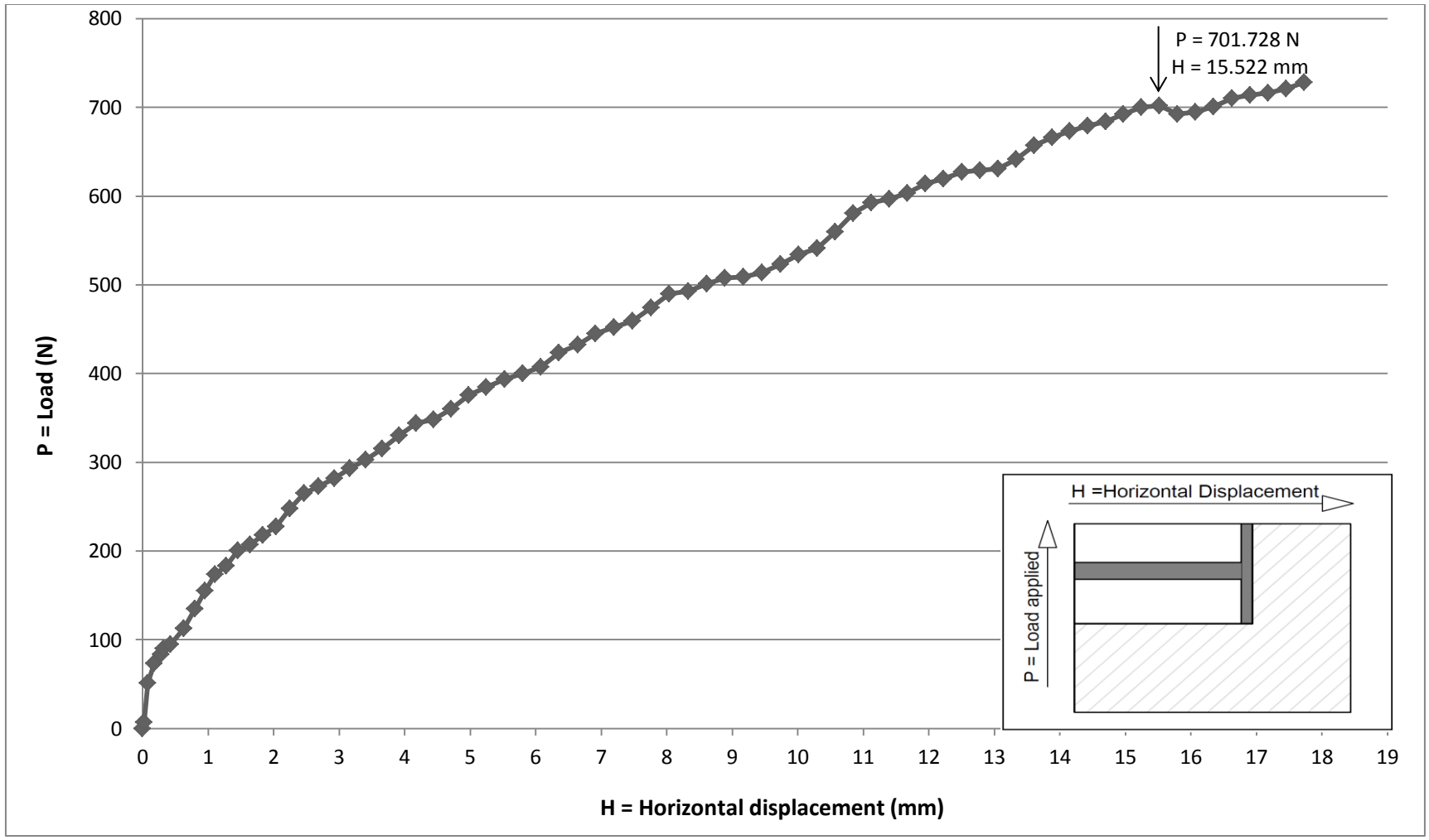

Graph 3.14 – Load - displacement curve for the test performed on loose sand

From the load-displacement curve it can be observed that after reaching the failure, the load decreased for three readings of the DAS. At 16.62 mm horizontal displacement, the load started to increase.

The horizontal component of the maximum passive earth pressure acting on the wall (P_h) was determined at the failure point on the load-displacement curve. The value of P_h measured by the load cell was used to calculate the coefficient of passive earth pressure K_p as follows:

$$P_p = \frac{P_h}{\cos\delta}$$

i.e.,

$$P_p = \frac{1}{2}\gamma h^2 d k_p$$

i.e.,

$$k_p = \frac{2 * P_p}{\gamma h^2 d}$$

where

P_h = horizontal component if the passive earth pressure acting in the wall

P_p = total passive earth pressure acting at an angle δ with the horizontal

γ = unit weight of the sand

d and h = width and height of the wall, respectively

The value of P_h measured by the load cell in this test was 701.728 N at a horizontal displacement of 15.522 mm. The dimensions of the retaining wall were 195mm x 215mm width and height respectively. The coefficient of passive earth pressure has been calculated as follows:

$$P_p = 701.728\ N$$

$$\gamma = 18.733\ \frac{kN}{m^3}$$

$$h = 216\ mm$$

$$d = 195\ mm$$

$$k_p = \frac{2 * P_p}{\gamma h^2 d} = 8.235$$

In order to validate the results given by the setup, the passive earth coefficient was calculated using Rankine's theory in case the soil is cohesionless as following:

$$k_p = \ tan^2\left(45^o + \frac{\emptyset}{2}\right)$$

The angle of friction for the sand is determined by plotting a graph of the maximum or peak shear stresses versus the corresponding normal stresses. The Mohr – Coulomb failure envelope was determined by drawing a straight line through the origin (cohesionless soil) and the points resulting from the experimental results. The slope of this line gives the peak friction angle of $\emptyset = 51$. The coefficient of passive earth pressure is calculated as follows:

$$k_p = \ tan^2\left(45^o + \frac{\emptyset}{2}\right) = 7.974$$

As can be observed, the passive earth coefficient calculated using the angle of friction $k_p = 7.974$ has a close value to the one calculated using the maximum force recorded from the test performed on loose sand $k_p = 8.235$.

The horizontal component of the passive earth pressure was first calculated using the passive earth coefficient $k_p = 7.974$ as follows:

$$P_p = \frac{1}{2}\gamma h^2 d k_p = 679.551\ N$$

The net value of P_h measured by the load cell in this test was 701.728 N.

Following the result given above the setup constructed to measure the horizontal component of the passive earth pressure is considered to be accurate.

CHAPTER 4

TEST RESULTS AND ANALYSIS

4.1 General

In this chapter the test results are presented in the form of tables and graphs showing the soil behavior under the movement of the retaining wall. Also a series of graphs have been developed to show the difference of the soil behavior under the same loading conditions.

Table 4.1 shows a summary of the tests performed, in terms of the different soil mixtures at the initial condition and fully saturated condition. The first three tests have been performed at the initial condition of 5% water content. To show the loss of strength after inundation, tests 4, 5 and 6 are conducted on the fully saturated samples.

Test No.	Soil mix	Collapse potential C_p	Clay content (%)	Water content %	Load at failure (N)	Wall displacement at failure (mm)	Table number
Test 1	Mix 1	4.2	6	5	1644.64	11.32	4.4
Test 2	Mix 2	9.0	8	5	1920.03	12.7	4.5
Test 3	Mix 3	12.5	10	5	2331.8	14.074	4.6
Test 4	Mix 1	4.2	6	100	558.55	1.249	4.7
Test 5	Mix 2	9.0	8	100	289.114	0.081	4.8
Test 6	Mix 3	12.5	10	100	130.153	0.076	4.9

Table 4.1- Summary of test results

4.2 Results of the tests performed on the collapsible soil mixtures

Test no.1- Soil mix 1

The test no.1 was performed on a soil mixture of sand and 6% Kaolin clay at an initial water content of 5% by weight. The results of the test are presented in table 4.2. The force recorded by the load cell at the failure point and the horizontal displacement of the wall are highlighted. The load-displacement diagram was constructed and presented in graph 4.1.

Table 4.2 – Test results for Soil Mix 1 (6% Clay content at 5% initial water content)

Displacement (mm)	Load (N)
0.000	0.0000
0.051	107.0725
0.255	545.8774
0.531	742.5964
0.871	879.8691
1.256	992.1132
1.721	1087.0870
2.106	1160.8786
2.524	1197.9819
2.966	1233.8066
3.426	1274.4292
3.914	1316.3282
4.403	1365.1782
4.910	1400.8730
5.433	1417.3802
5.967	1452.1482
6.505	1481.7913
7.047	1505.5131
7.587	1515.9117
8.127	1534.9370
8.652	1560.4843
9.182	1587.6602
9.707	1592.4065
10.245	1605.5620
11.050	1630.2700
11.321	***1644.6390***
11.689	1627.0694
12.401	1630.6126
12.936	1633.7573
13.473	1633.6393
14.003	1635.6092
14.544	1601.1162
15.089	1574.4014
15.634	1569.3904
16.424	1581.4268
16.970	1559.4731
17.500	1562.4632
18.038	1558.0397
18.572	1562.8933
19.111	1552.2784
19.658	1563.9189

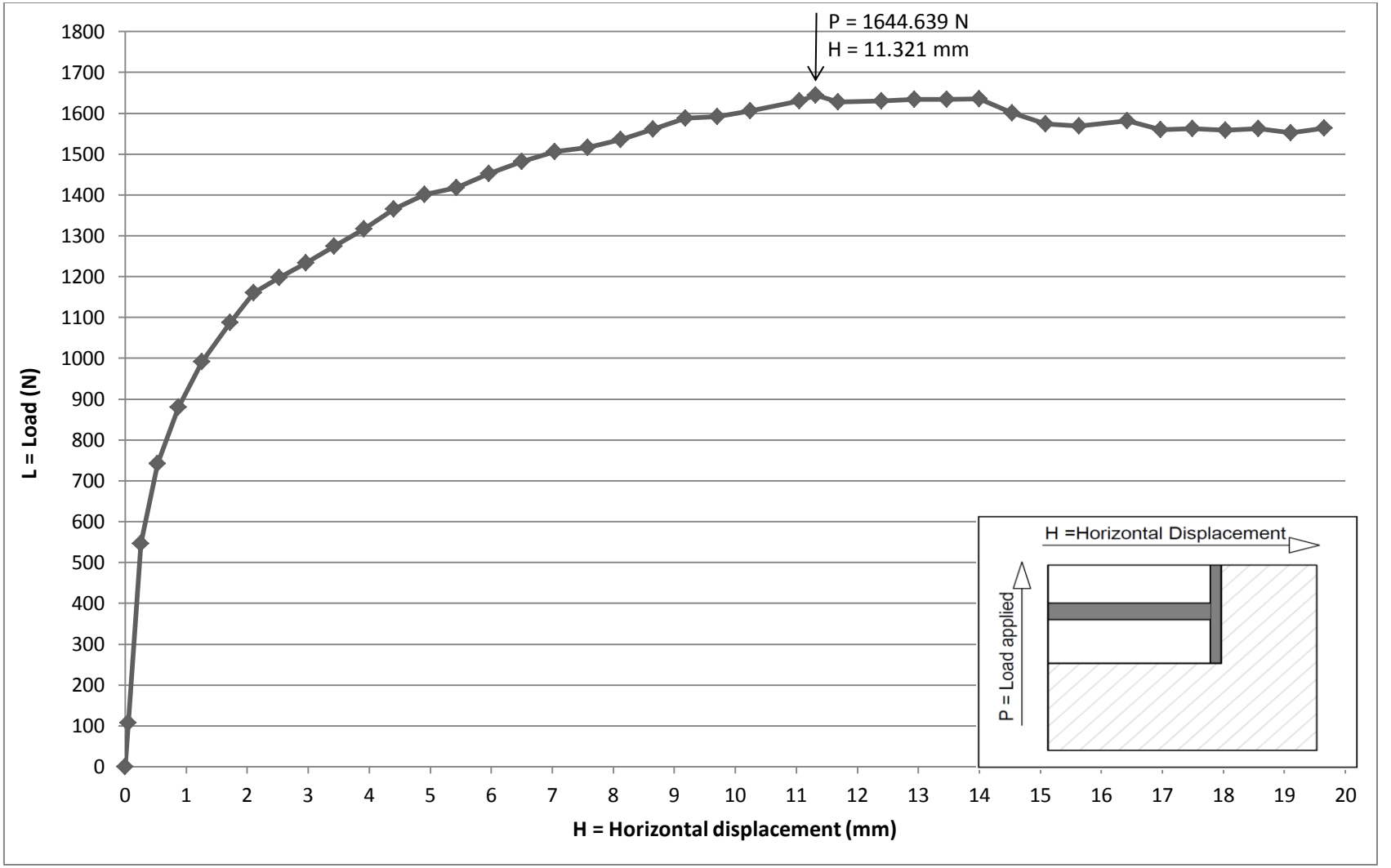

Graph 4.1 – Load - displacement curve for the test performed on Mix 1 (6% clay content at 5% initial water content)

Test no.2- Soil mix 2

Test no.2 was performed on a soil mixture of sand and 8% Kaolin clay at an initial water content of 5% by weight. The results of the test are presented in table 4.3. The horizontal displacement of the wall and the force recorded by the load cell at the soil failure are highlighted. The load-displacement diagram was constructed and presented in graph 4.2.

Table 4.3 – Test results for Soil Mix 2 (8% Clay content at 5% initial water content)

Displacement (mm)	Load (N)
0.000	0.000
0.002	416.970
0.080	735.207
0.191	874.338
0.319	973.052
0.462	1049.290
0.622	1117.241
0.787	1179.928
0.978	1228.224
1.178	1273.290
1.397	1313.394
1.626	1371.812
2.060	1426.034
2.479	1457.819
2.913	1495.134
3.376	1535.249
3.859	1571.264
4.357	1604.302
4.873	1617.147
5.401	1655.269
5.936	1688.819
6.483	1712.226
7.025	1728.305
7.574	1749.913
8.112	1776.458
8.650	1805.167
9.198	1821.809
9.735	1839.596
10.275	1856.924
10.821	1864.268
11.357	1889.028
11.896	1894.962
12.434	1904.785
12.700	***1920.03***
13.241	1904.807
13.780	1938.710
14.305	1968.171
14.834	1990.525
15.356	1981.130
15.878	1986.876
16.402	1976.288
16.923	1993.554
17.191	1982.762
17.727	1988.311
18.264	1987.061
18.803	2010.073
19.351	2006.437
19.891	2022.475

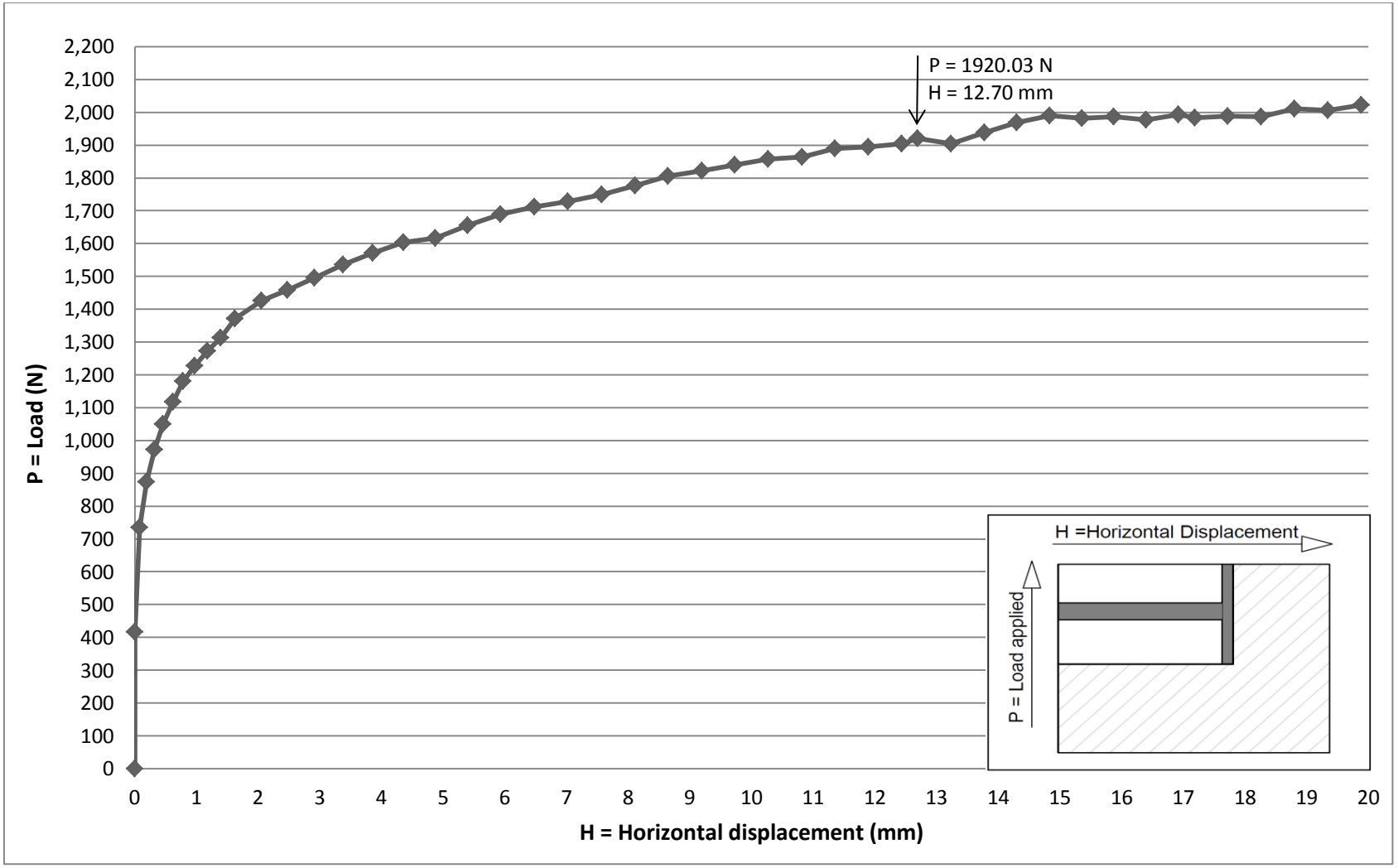

Graph 4.2 – Load - displacement curve for the test performed on Mix 2 (8% clay content at 5% initial water content)

Test no.3- Soil mix 3

The results of the test no.3 are presented in table 4.4. The test was performed on a soil mixture of sand and 10% Kaolin clay at an initial water content of 5% by weight. The force recorded at the failure point of the soil and the horizontal displacement of the wall is highlighted. The load-displacement diagram was constructed and presented in graph 4.3.

Table 4.4 – Test results for Soil Mix 3 (10% Clay content at 5% initial water content)

Displacement (mm)	Load (N)
0.000	0.000
0.074	476.872
0.138	789.549
0.229	939.069
0.431	1121.95
0.682	1248.03
0.957	1341.54
1.267	1425.59
1.597	1503.46
1.963	1570.47
2.359	1636.83
2.786	1692.36
3.232	1752.88
3.706	1795.63
4.197	1830.8
4.709	1864.24
5.228	1911.61
5.766	1951.99
6.300	1994.4
6.837	2017.82
7.371	2053.46
7.912	2074.4
8.446	2102.49
8.984	2119
9.525	2154.77
10.064	2169.36
10.611	2192.49
11.143	2209.43
11.671	2243.11
12.202	2255.91
12.733	2285.88
13.267	2304.68
14.074	***2331.8***
14.608	2328.9
15.144	2332.41
15.675	2340.18
16.208	2371.03
16.734	2384.38
17.269	2403.13
17.802	2412.02
18.336	2434.19
18.869	2436.23
19.409	2439.59
19.951	2456.83

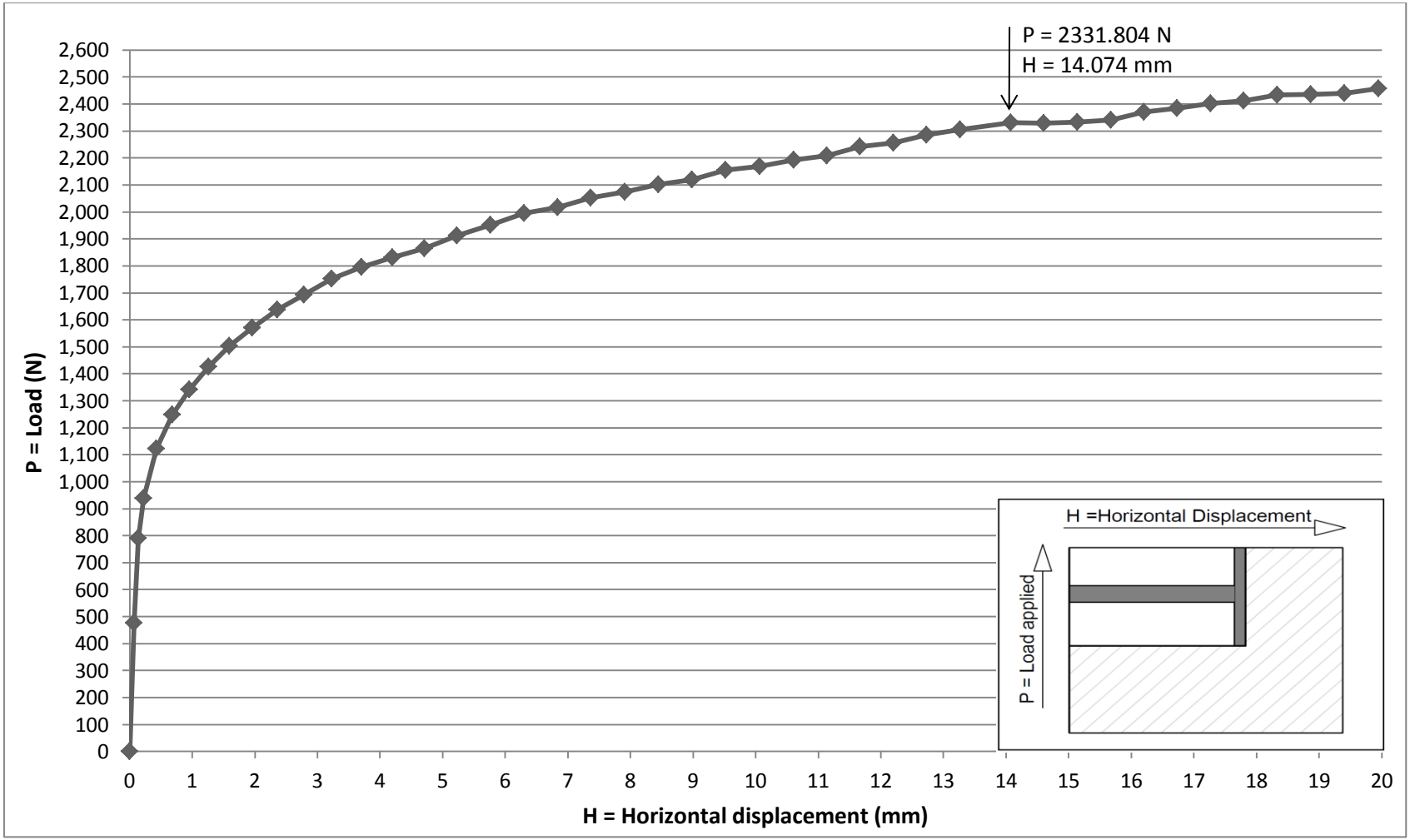

Graph 4.3 – Load - displacement curve for the test performed on Mix 3 (10% clay content at 5% initial water content)

Test no.4- Soil mix 1

The test number 4 was performed on a soil mixture of sand and 6% Kaolin clay at an initial water content of 5% by weight. The sample was inundated from the bottom until full saturation was achieved. The test was performed after inundation. The collapse potential C_p of the soil mix is 4.2% and the severity of foundation problems as suggested by (Jennings and Knight 1975) is “moderate trouble”. The results of the test are presented in table 4.5. The force recorded at the failure point of the soil and the horizontal displacement of the wall is highlighted. The load-displacement diagram was constructed and presented in graph 4.4.

Table 4.5 – Test results for Soil Mix 1, C_p = 4.2% (6% Clay content at full saturation)

Displacement (mm)	Load (N)
0.000	0.000
0.057	385.102
0.172	483.183
0.310	503.732
0.471	511.876
0.639	521.023
0.828	526.821
1.035	545.037
1.249	***558.55***
1.483	557.348
1.735	567.927
1.999	567.576
2.281	562.422
2.568	564.863
2.869	557.586
3.183	566.435
3.499	581.833
3.824	604.567
4.156	612.36
4.496	614.58
4.852	602.998

Displacement (mm)	Load (N)
5.210	602.051
5.572	599.872
5.932	607.561
6.290	604.234
6.656	611.594

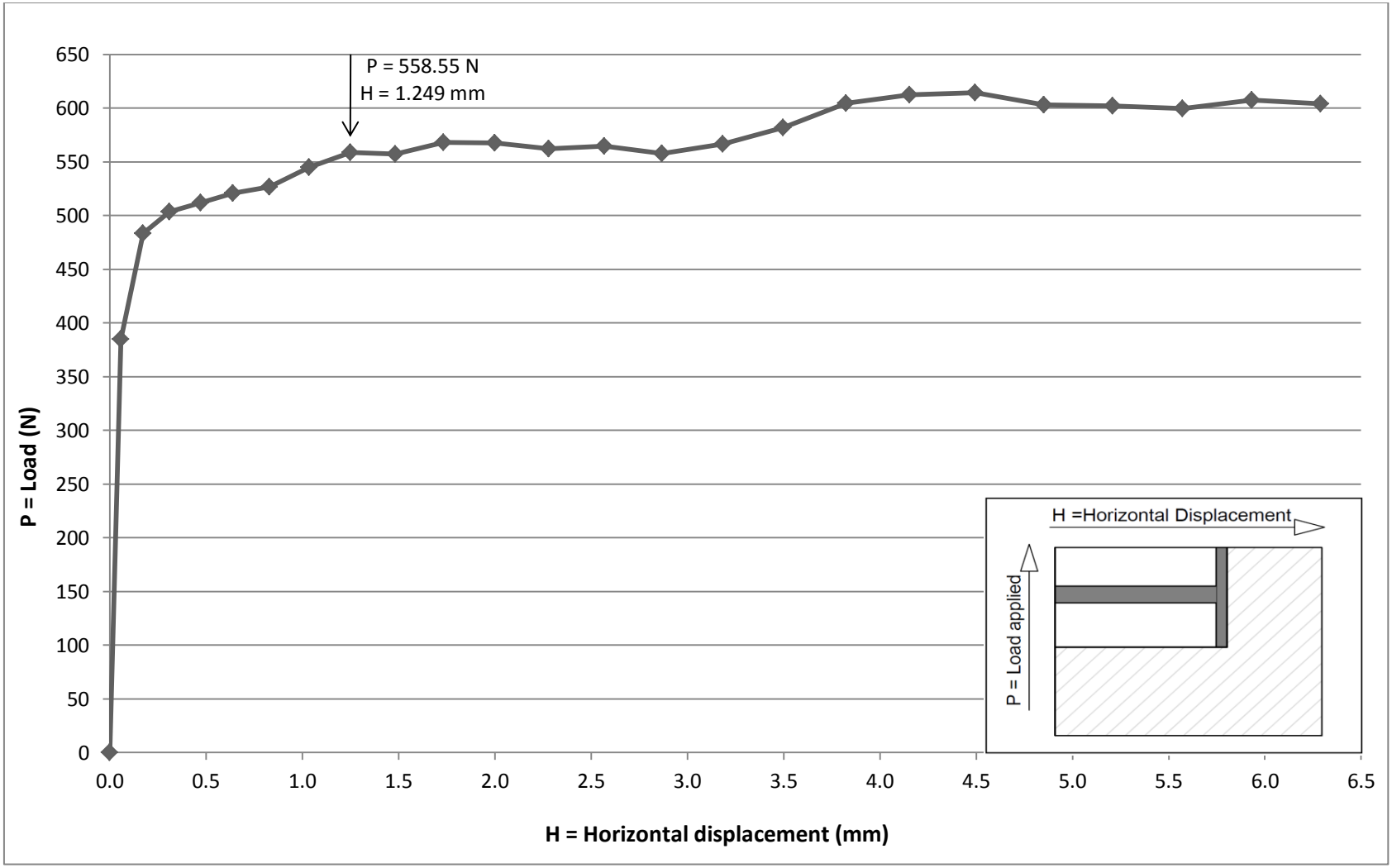

Graph 4.4 – Load - displacement curve for the test performed on Mix 1 (6% clay content full saturation) – collapse potential 4.2%

Test no.5- Soil mix 2

The test number 5 was performed on a soil of 8% Kaolin clay at full saturation. The collapse potential C_p of the soil mix is 9% and the severity of foundation problems as suggested by (Jennings and Knight 1975) is “trouble”. The results of the test are presented in table 4.6. The force recorded at the failure point of the soil and the horizontal displacement of the wall is highlighted. The load-displacement diagram is constructed and presented in graph 4.5.

Table 4.6 – Test results for Soil Mix 2, C_p = 9% (8% Clay content at full saturation)

Displacement (mm)	Load (N)
0.000	0.000
0.015	131.905
0.030	239.364
0.081	***289.114***
0.144	285.162
0.209	284.139
0.280	267.551
0.355	242.925
0.427	237.814
0.507	235.809
0.584	239.859
0.667	248.980
0.759	252.617
0.849	253.637
0.941	258.745
1.036	254.990
1.141	253.205
1.264	259.296
1.363	264.446
1.476	276.377
1.580	291.961
1.707	291.827
1.817	289.602
1.945	292.416
2.068	287.286
2.197	284.258
2.337	291.688
2.472	292.806
2.608	292.297
2.741	296.642

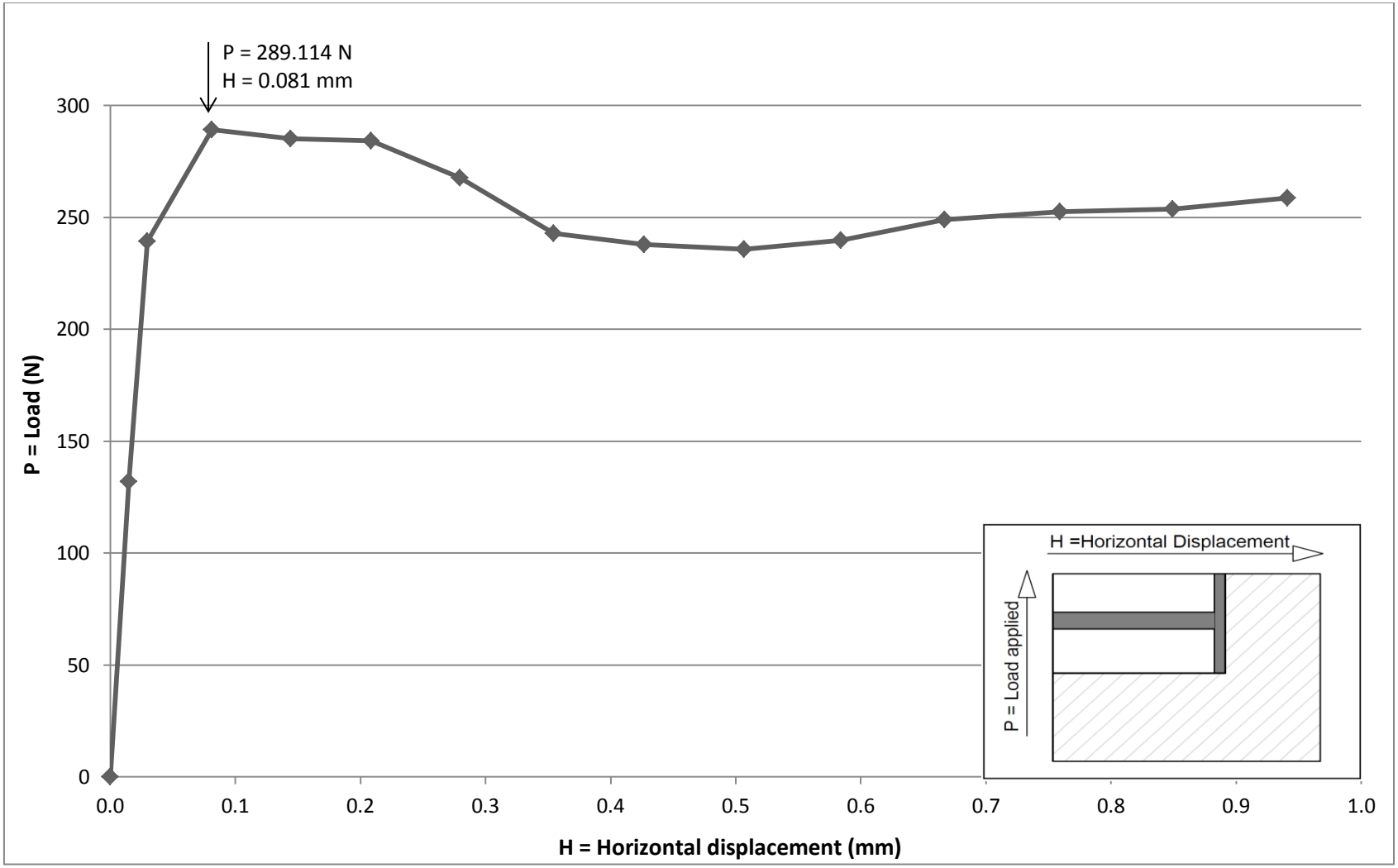

Graph 4.5 – Load - displacement curve for the test performed on Mix 2 (8% clay content full saturation) – collapse potential 9%

Test no.6 - Soil mix 3

The test number 6 was performed on a soil containing 10% Kaolin clay. The sample was inundated from the bottom until full saturation was achieved. The test was performed after inundation. The collapse potential C_p of the soil mix is 12.5% and the severity of foundation problems as suggested by (Jennings and Knight 1975) is “severe trouble”. The results of the test are presented in table 4.7 and the constructed load-displacement diagram is presented in graph 4.6.

Table 4.7 – Test results for Soil Mix 3, C_p = 12.5% (10% Clay content at full saturation)

Displacement (mm)	Load (N)
0.000	0.000
0.001	114.813
0.016	128.575
0.076	***130.153***
0.157	119.462
0.247	113.854
0.339	110.336
0.439	109.615
0.542	109.297
0.655	110.213
0.770	111.940
0.893	113.429
1.021	114.941
1.152	114.226
1.290	112.868
1.442	111.874
1.590	109.788
1.744	109.417
1.907	110.071
2.071	111.383
2.243	111.224
2.417	112.104
2.597	112.431
2.788	114.583
2.976	119.657
3.167	122.378
3.369	121.672
3.570	121.274
3.776	118.879
3.982	118.353

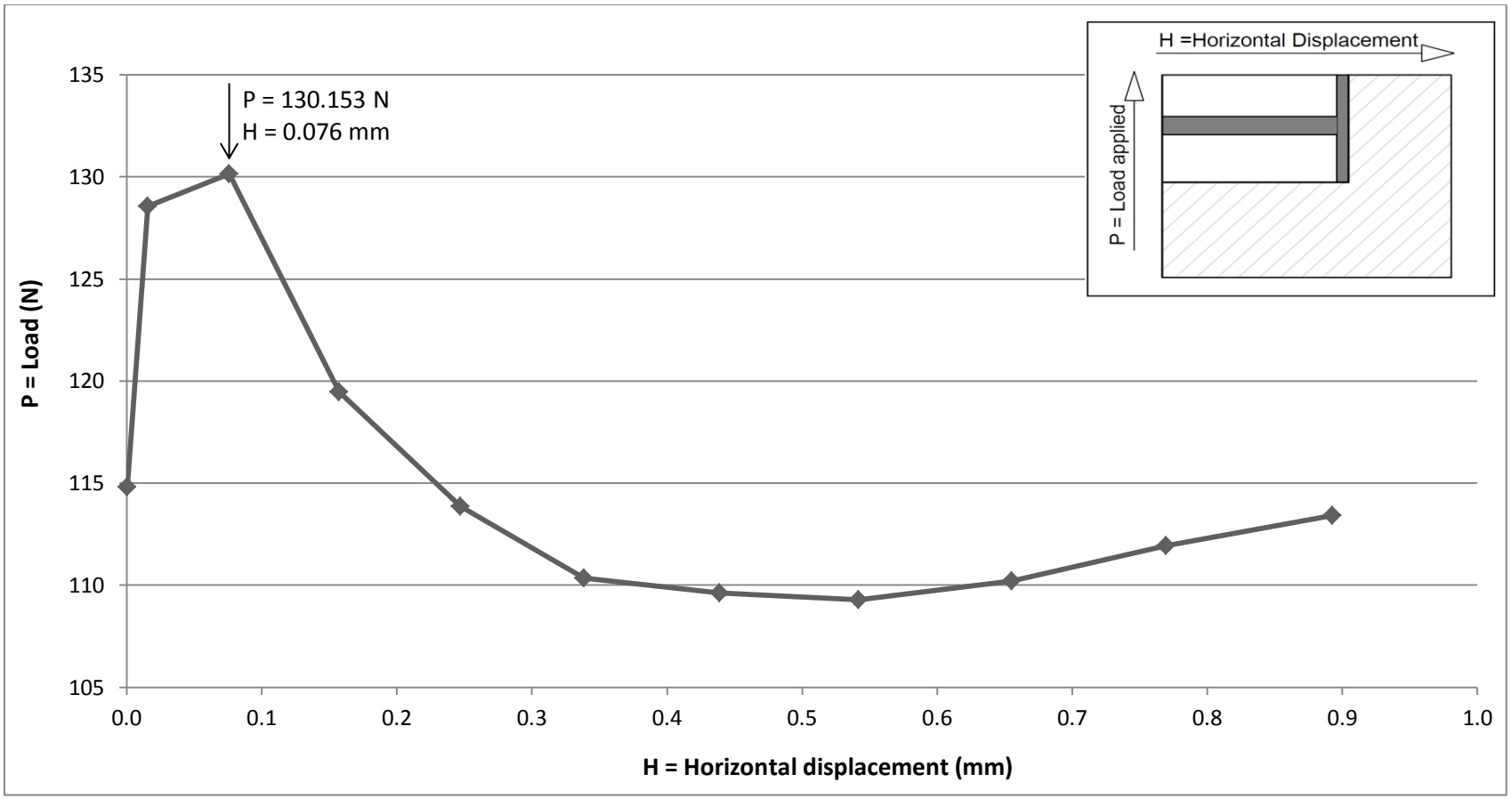

Graph 4.6 – Load - displacement curve for the test performed on Mix 3 (10% clay content full saturation) – collapse potential 12.5%

4.3 Reproducibility of the test data

To ensure the reproducibility of the data one test from each series of tests was repeated. A set of test is represented by the water content of the samples tested. Based on this in the present investigation are presented two series of sets. The first set of repeated tests was conducted on samples at the initial 5% water content. The second sets of tests were performed on the inundated samples. To check the results of the tests performed on fully samples the test number on the Mix 1 was repeated.

In table 4.8 are presented the results of two tests performed on the soil mixture of sand and 6% Kaolin clay at an initial water content of 5% by weight. The force recorded by the load cell at the failure point of the soil and the horizontal displacement of the retaining wall are highlighted in the table. Graph 4.7 shows the load-displacement relationship for these two tests. The two curves presented are almost identical, which means that the results obtained from the experimental setup were repeatable.

Table 4.9 shows the results of two tests performed on the soil mixture of sand and 6% Kaolin clay at an initial water content of 5% by weight. This set of tests was performed on fully saturated samples that present loss of strength due to collapse of the soil. The collapse potential C_p of the soil mix is 4.2% and the severity of foundation problems as suggested by (Jennings and Knight 1975) is “moderate trouble”. The force recorded by the load cell at the failure point of the soil and the horizontal displacement of the retaining wall are highlighted in the table. The load-displacement curves for these tests are presented in Graph 4.8 The two curves are almost identical, which means that the results obtained from the experimental setup are repeatable.

For the analysis of the results the tests that had a higher value of the failure force were kept.

Table 4.8 – Test results for Soil Mix 1 (6% Clay content at 5% initial water content)

Test number 1:

Displacement (mm)	Load (N)
0	0
0.051	107.072
0.255	545.877
0.531	742.596
0.871	879.869
1.256	992.113
1.721	1087.087
2.106	1160.878
2.524	1197.981
2.966	1233.807
3.426	1274.429
3.914	1316.328
4.403	1365.178
4.91	1400.873
5.433	1417.38
5.967	1452.148
6.505	1481.791
7.047	1505.513
7.587	1515.912
8.127	1534.937
8.652	1560.484
9.182	1587.66
9.707	1592.407
10.245	1605.562
11.05	1630.27
11.321	**1644.639**
11.689	1627.069
12.401	1630.613
12.936	1633.757
13.473	1633.639
14.003	1635.609
14.544	1601.116
15.089	1574.401
15.634	1569.39
16.424	1581.427
16.97	1559.473
17.5	1562.463
18.038	1558.04
18.572	1562.893
19.111	1552.278
19.658	1563.919

Table 4.8 – Test results for Soil Mix 1 (6% Clay content at 5% initial water content)

Test number 2:

Displacement (mm)	Load (N)
0.000	0
0.088	216.478
0.257	573.008
0.465	725.754
0.715	809.949
0.846	877.056
1.284	1010.06
1.619	1055.59
1.993	1125.21
2.392	1181.34
2.829	1215.04
3.051	1269.84
3.518	1308.82
4.000	1347.55
4.498	1389.84
5.014	1414.22
5.544	1452.37
6.081	1469.04
6.613	1502.35
7.157	1519.59
7.698	1543.74
8.235	1553.49
8.769	1582.94
9.303	1592.65
9.845	1616.39
10.386	1617.74
10.929	1622.36
11.470	***1641.1***
12.014	1628.54
12.554	1632.61
13.087	1634.49
13.621	1635.13
14.156	1644.89
14.687	1608.6
15.224	1584.88
15.750	1575.1
16.282	1576.97
16.812	1556.08
17.350	1568.96
17.623	1572.22

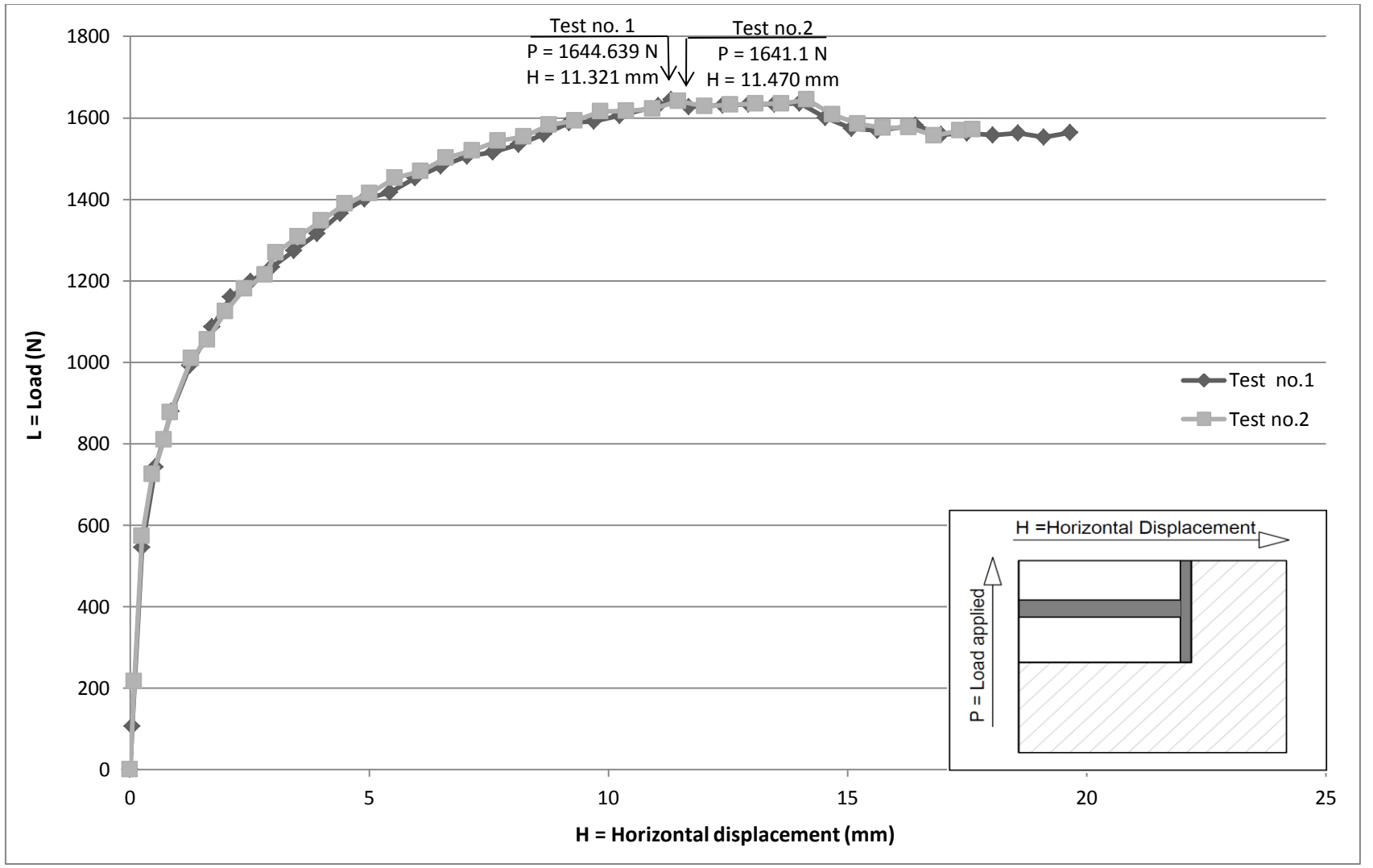

Graph 4.7 – Load - displacement curve for the repeated tests performed on Mix 1

Table 4.9 – Test results for Soil Mix 1, C_p = 4.2% (6% Clay content at full saturation)

Test number 1	
Displacement (mm)	Load (N)
0	0
0.057	385.102
0.172	483.183
0.31	503.732
0.471	511.876
0.639	521.023
0.828	526.821
1.035	545.037
1.249	***558.55***
1.483	557.348
1.735	567.927
1.999	567.576
2.281	562.422
2.568	564.863
2.869	557.586
3.183	566.435
3.499	581.833
3.824	604.567
4.156	612.36
4.496	614.58
4.852	602.998
5.21	602.051
5.572	599.872
5.932	607.561
6.29	604.234
6.656	611.594

Test number 2	
Displacement (mm)	Load (N)
0.000	0
0.030	339.364
0.144	435.162
0.280	487.551
0.427	507.814
0.584	519.859
0.759	522.617
0.941	538.745
1.141	549.205
1.363	***557.446***
1.580	556.961
1.817	567.602
2.068	567.286
2.337	563.688
2.608	565.297
2.889	561.926
3.176	567.785
3.482	582.833
3.793	591.506
4.112	611.841
4.434	615.402
4.759	602.531
5.087	602.786
5.425	588.881
5.751	599.505
6.089	606.75
6.291	604.785

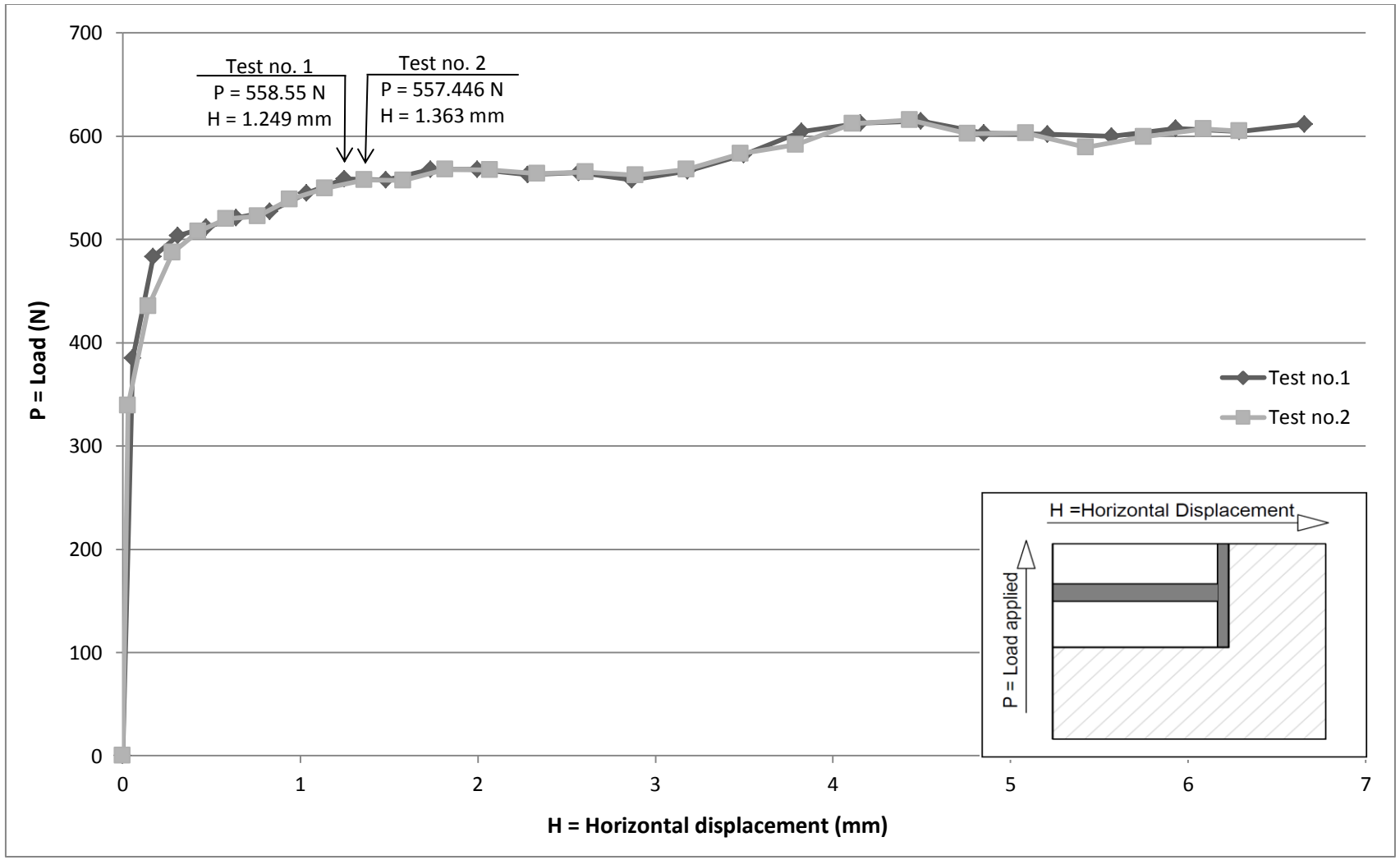

Graph 4.8 – Load - displacement curve for the repeated tests performed on Mix 1(C_p = 4.2%) at full saturation

4.4 Comparison of results

The experimental study was conducted on laboratory prepared collapsible soils by mixing Kaoline clay with sand at different percentages. In general the higher the clay content the higher the collapse potential. (Adnan, 1992) and (Miller, 1998) concluded that the maximum collapse occurs at approximately 18% clay content.

(Lawton EC, 1992) indicated that the maximum collapse potential, for the natural soils studied, is obtained when the clay fraction is situated in the range 10% and 40%. (Abbeche Khelifa, 2007) concluded that the soil is not susceptible to collapse it its clay fraction is greater than 30%.

The soil mix in the present investigation was chosen in different percentages of kaolin clay content of 6,8 and 10% to achieve the collapse potentials of 4.2%, 9% and 12.5% respectively. (Soliman, 2010) concluded that at a constant percentage of clay content and constant compaction energy the collapse potential decreased sharply due to increasing the water content, especially in the range of 5% to 7%. (Abbeche Khelifa, 2007) stated that the collapse potential decreases or even can be equal to zero above a certain value of the initial water content.

In the present investigation the first series of tests was performed on soil mixes on 6, 8, and 9% clay content at an initial water content of 5%. The tests measured the horizontal force applied on the retaining wall and the horizontal displacement of the wall. Graph 4.9 shows the load- displacement curves for the three mixtures used in the present investigation.

Clay is the bonding agent that gives the soil mix its cohesive nature. As can be observed in graph 4.9 the failure force and wall displacement increased with the increase of the clay content. (Sheeler, 1968) stated that cohesive strength increases with increasing clay content.

(Bayoglu, 1995) made an experimental study on the effects of the fine particles on the shear strength and compressibility properties of the soil. Soil mixtures having wide range of grain size from sand to silt-clay mixtures were studied. He concluded that for a fine content less than 50% the angle of internal friction varied between 30-38 degrees with small variations and only after 50% fine content the friction angle decreased significantly.

The soil properties of the mixes used in this investigation are presented in Table 3.3.2. It can be observed that the friction angles of the mixes decrease with the increase of clay content ranging between 40 to 35 degrees.

Graph 4.9 presents the load- displacement curves for the samples tested at 5% initial moisture content. In order to show the different soil behavior of the three soil mixtures used in the experimental investigation, the load-displacement curves for the tests are presented in the same chart. It can be observed that increasing the clay content of the mix leads to the increasing of the load that the soil can sustain.

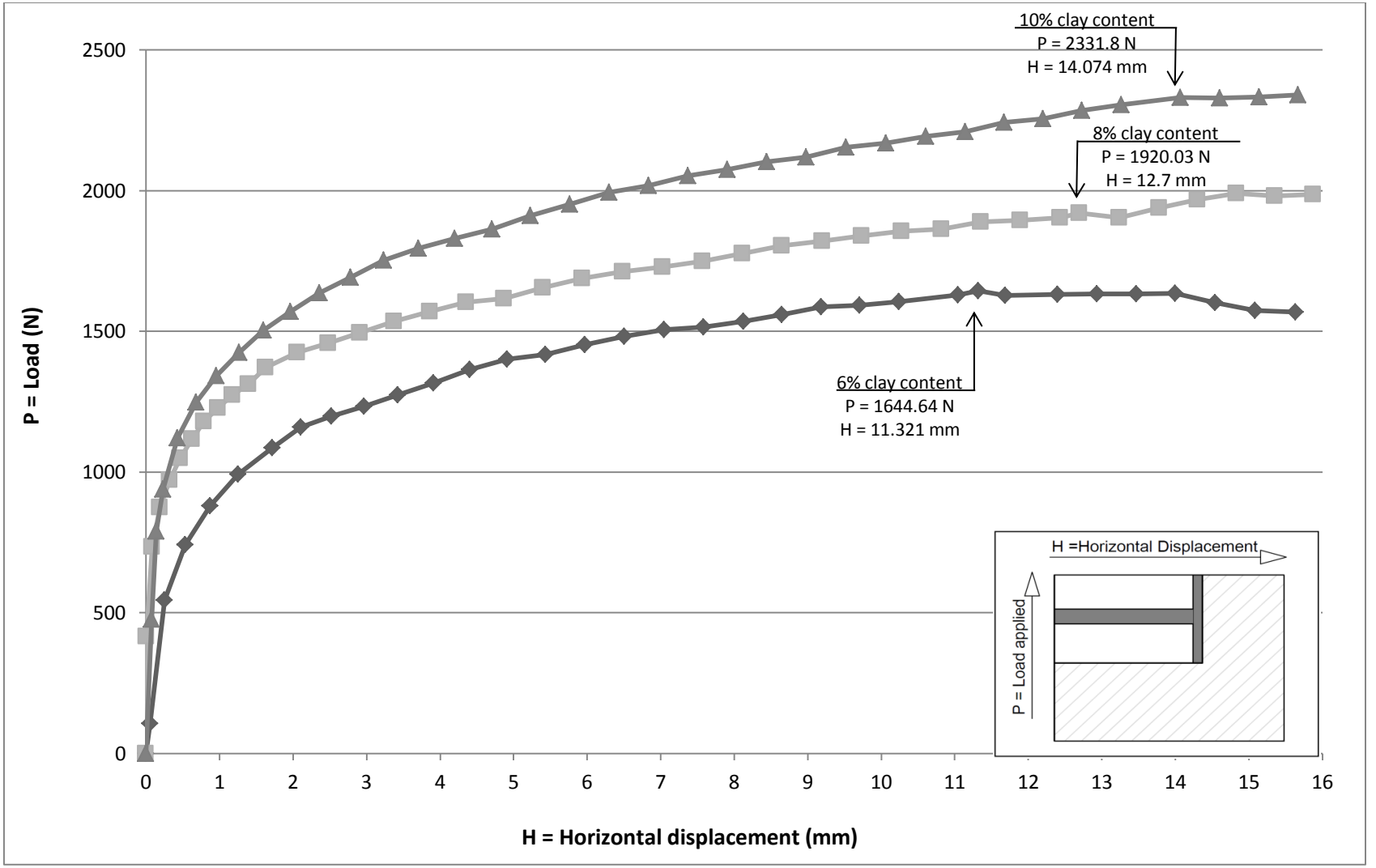

Graph 4.9 – Load - displacement curve for the tests performed on Mix 1, Mix 2 and Mix 3 at 5% initial water content

The horizontal force applied on the retaining wall at the soil failure for the 6% clay content soil mixture was 1644.64 N at a horizontal displacement of 11.321 mm. At 8% clay content, the failure force increased with 14%. By increasing the clay content from 8% to 10%, the force increased with almost 18%.

In the case of passive earth pressure on retaining wall with horizontal cohesive backfill Rankine presents the passive force per unit length of the wall as:

$$P_p = \frac{1}{2} k_p \gamma d h^2 + 2c'h\sqrt{k_p}$$

P_p = total passive earth pressure

γ = unit weight of the soil

c' = cohesion

d and h = width and height of the wall, respectively

In the present investigation the horizontal force of the earth pressure is measured by the load cell. Knowing the soil properties, the only unknown in Rankine's equation remains the coefficient of passive earth pressure which can be taken out of the equation and be calculated.

The coefficient of passive earth pressure for the three mixtures is presented in Table. 4.10

Mix	Clay content (%)	Collapse potential C_p (%)	Force (N)	Coefficient of passive earth pressure (k_p)
Mix 1	6	4.2	1644.64	4.151
Mix 2	8	9	1920.03	3.762
Mix 3	10	12.5	2331.8	3.157

It can be observed that by increasing the clay content, the coefficient of passive earth pressure decreased.

The graph 4.10 shows the relation between the collapse potential and the coefficient of passive earth pressure. As can be observed the coefficient of passive earth pressure decreased with almost 10% from the 4.2% to 9% collapse potential. The decrease from 9% to 12.5% collapse potential is in the range of 16%.

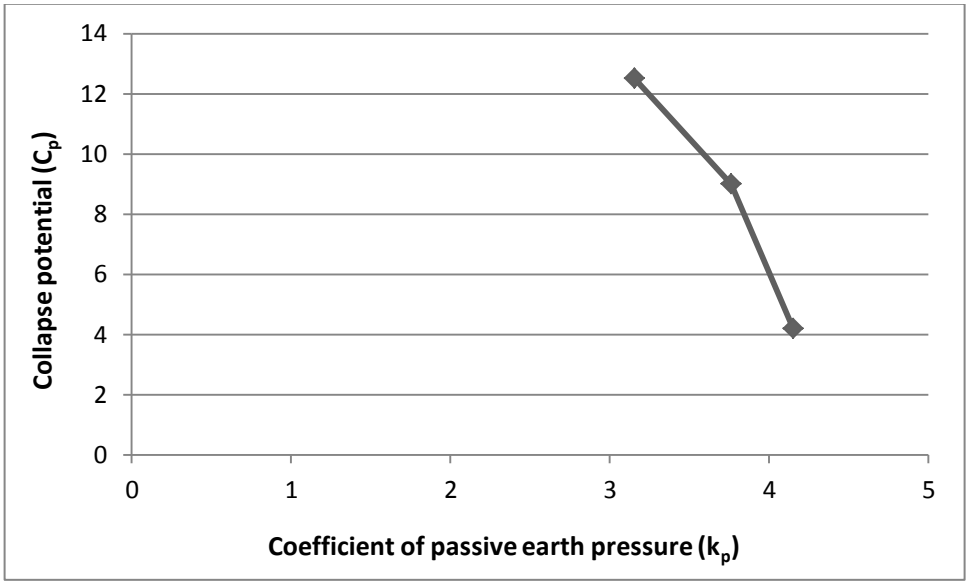

Graph 4.10 Relation between collapse potential and coefficient of passive earth pressure at 5% initial water content

In the present investigation, the soil mixes tested had the collapse potential increased from 4.2% to 12.5% which resulted in the decrease of the coefficient of passive earth pressure k_p with almost 76%. This underlines that the passive pressure developed on the retaining wall decrease with the increase of the collapse potential of the soil mix.

- Tests performed on the soil mixes at full saturation

The collapsible soil is known to have a loss of strength when inundated. The second set of tests performed in this investigation was performed on the soil mixtures with 6, 8 and 9% clay content but under the condition that the ground water level kept being risen until the soil became fully saturated. The increase of the moisture caused the clay bonds to weaken reducing the original soil strength. During the testing, the force applied on the retaining wall was measured as well as its horizontal displacement. Graph 4.11 shows the load- displacement curves for the three mixtures used in the investigation. The force and displacement at the soil failure are highlighted on the chart.

From the load-displacement curves presented in graph 4.11, it can be observed that by increasing the collapse potential of the soil mixture, the force required to push the retaining wall until reaching soil failure decreased. The soil mix 1 that with a collapse potential of 4.2% exhibited a value of the failure force of 48% higher than the soil mix with a 9% collapse potential and 78% higher than soil mix with 12.5% collapse potential. Soil mix 2 and 3 recorded a small value of the horizontal displacement of the wall showing that failure of the soil will occurred practically immediately because of the loss of strength after collapse.

Comparing the values from the tests performed on the soil mixes of 5% initial water content and the fully saturated mixes, it can be observed that once the collapse of the soil is achieved the force required to push the retaining wall decreased considerably. This implies that due to the collapse, the soil lost its ability to sustain driving forces. In the following section a comparison between the samples with 5% initial water content and fully saturated samples is extended.

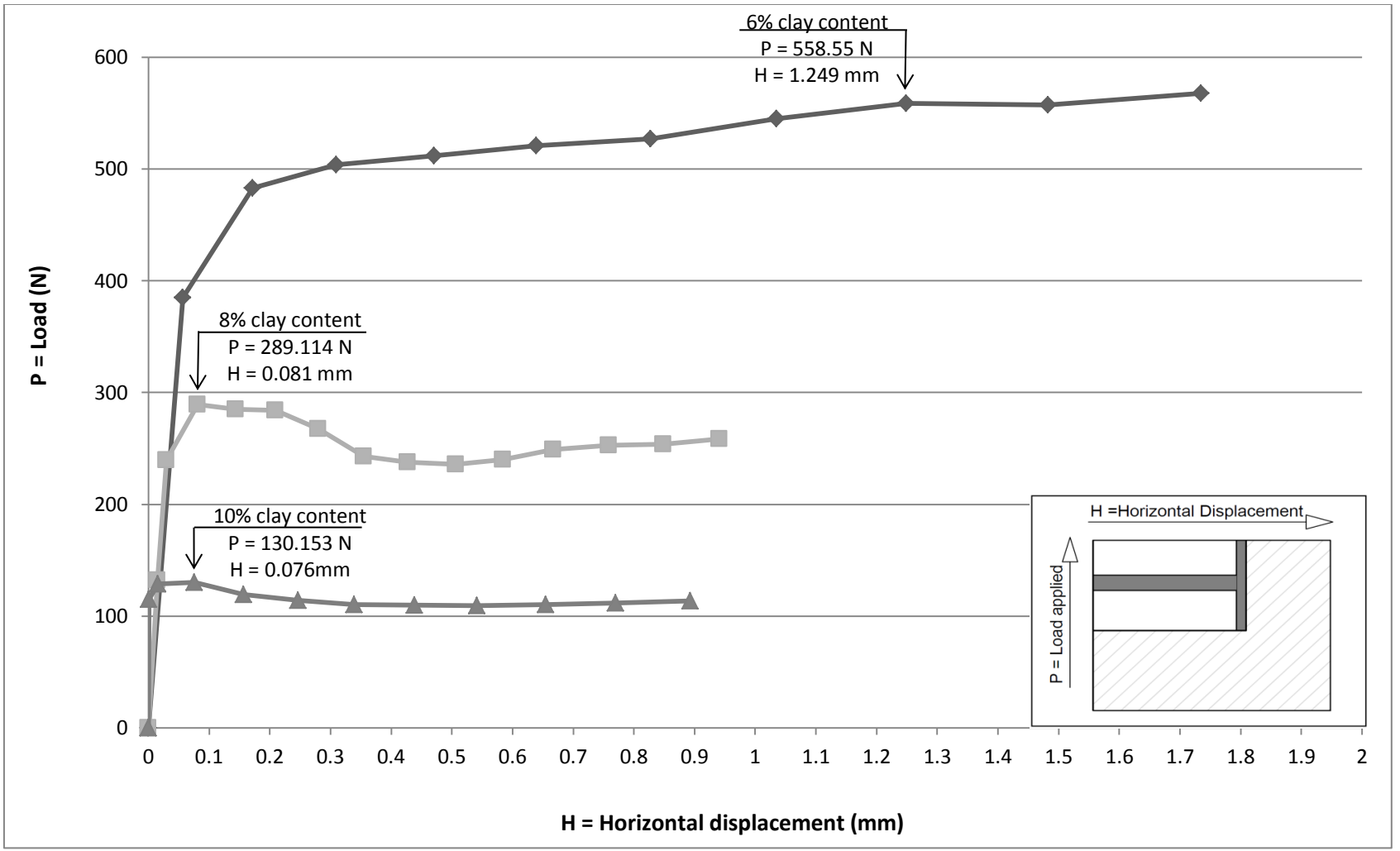

Graph 4.11 – Load - displacement curve for the tests performed on Mix 1, Mix 2 and Mix 3 at full saturation

The collapse potential of the mixes, the failure force and the calculated coefficient of passive earth pressure for the three mixtures are presented in Table. 4.11

Mix	Clay content (%)	Collapse potential C_p (%)	Force (N)	Coefficient of passive earth pressure (k_p)
Mix 1	6	4.2	558.55	0.54
Mix 2	8	9	289.114	0.075
Mix 3	10	12.5	130.153	0.009

Table. 4.11 – Collapse potential for soil mixes at 5% initial moisture content

The coefficient of passive earth pressure decreased as the collapse potential increased. (Graph 4.12) shows the relation between the collapse potential and the coefficient of passive earth pressure.

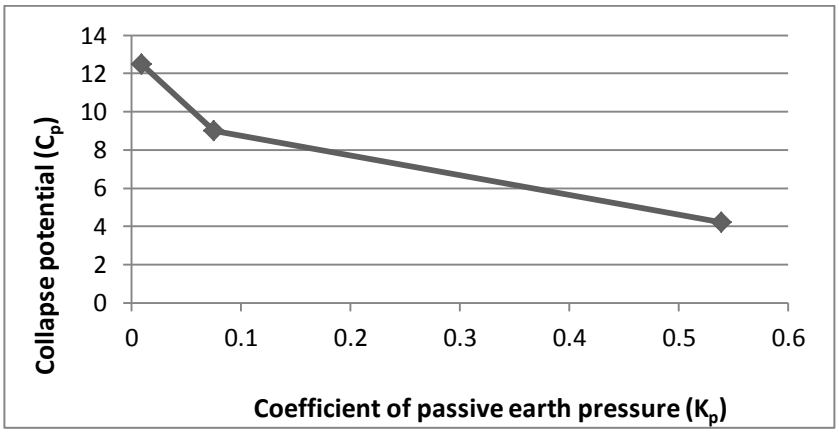

Graph 4.12 Relation between collapse potential and coefficient of passive earth pressure at full saturation

As can be observed in the above table, the coefficient of passive earth pressure decreased significantly from C_p = 4.2% to C_p = 9%. The decrease in value is almost of 86% between the two mixes. For C_p = 9% and C_p = 12.5%, the decrease in K_p value is almost in the same range of 88%.

- Comparison of the results of Test 1 and Test 4 performed on Soil Mix 1

Soil mix 1 contained 6% clay content and had a collapse potential of 4.2% being classified by (Jennings and Knight 1975) as “moderate trouble”. Test no.1 was performed on the soil mix at 5% initial water content and Test no.4 was performed after the soil was inundated from the bottom until full saturation was achieved.

In the dry state, the clay particles act as a cementing agent between the grains and are responsible for an inter-granular connection that can support high loads. However, the saturation, even without additional loading, causes the disintegration of the connections, giving a denser structure followed by a sudden collapse of the soil particles.

(Gibbs, 1960) reported that an increase in moisture content is often a more important contributor to collapse than loading.

For the test performed on the soil mix at 5% water content, it is observed that the force required to push the retaining wall until soil failure was almost 66% bigger than after the collapse of the soil. The collapse of the soil was not visible during the test, but could be observed clearly when comparing the difference in the horizontal loading and displacement of the retaining wall.

The coefficient of passive earth pressure K_p is calculated for both of the cases and the results given in table 4.12.

Soil Mix	Water content %	Clay content (%)	Collapse potential C_p (%)	Horizontal Displacement (mm)	Force (N)	Coefficient of passive earth pressure (K_p)
Mix 1	5	6	4.2	11.321	1644.64	4.151
	100			1.249	558.55	0.54

Table.4.12 Coefficient of passive earth pressure for Soil Mix 1

As can be observed, the coefficient of passive earth pressure decreased with almost 87% after the collapse of the soil. This was due to the loss of strength of the soil after collapse.

Graph 4.13 shows the relation between the load applied on the retaining wall and the horizontal displacement of the wall for two cases of 5% initial water content and fully submerged.

The horizontal displacement corresponding to the failure force of 558.55N had a small value. This underlines the collapse of the soil influenced greatly the strength of the soil. The collapse was almost immediate.

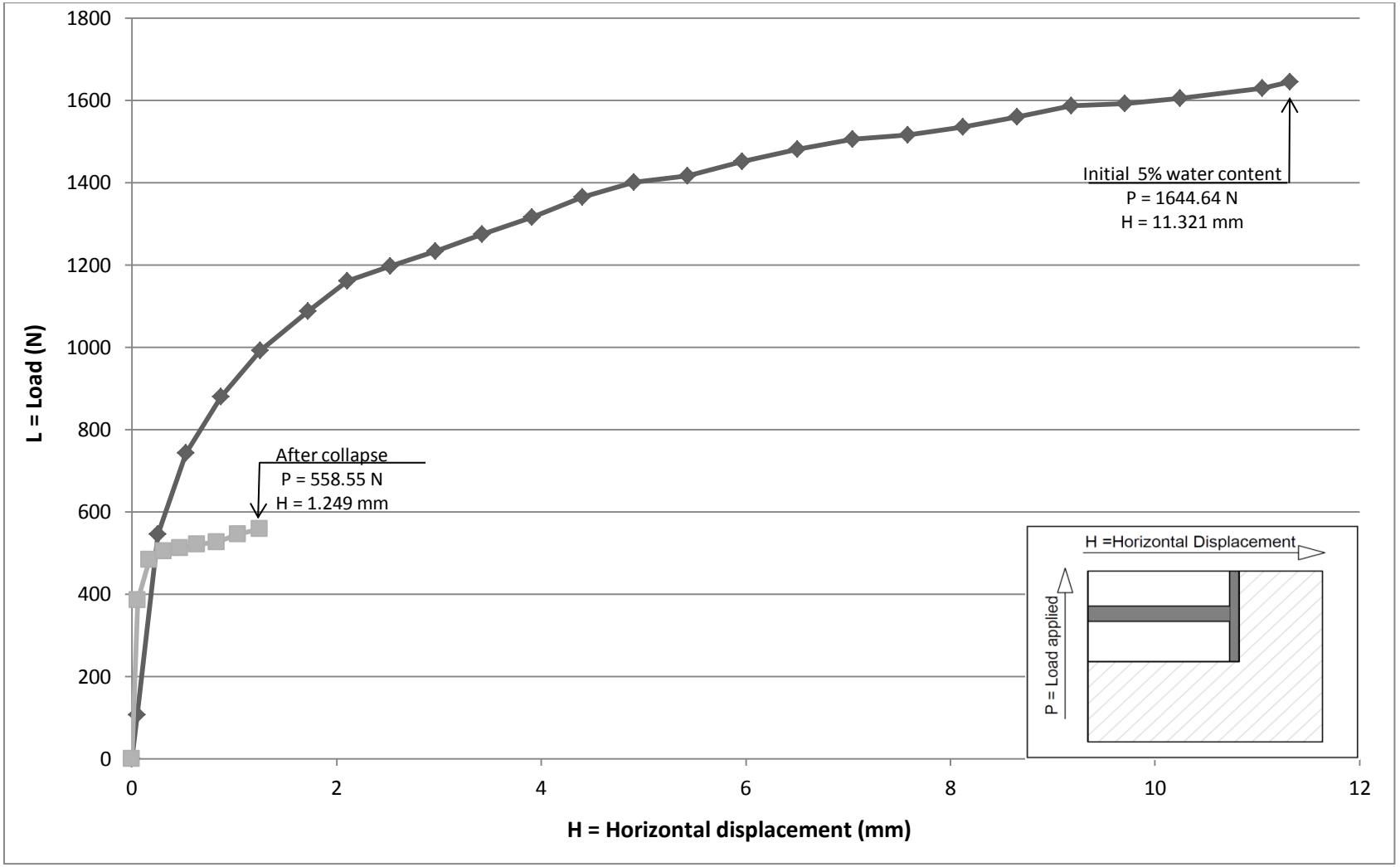

Graph 4.13 – Load - displacement curve for the tests performed on Mix 1 at 5% initial water content and full saturation

- Comparison of the results of Test 2 and Test 5 performed on Soil Mix 2

Soil mix 2 contained 8% clay content and had a collapse potential of 9% being classified by (Jennings and Knight 1975) as “trouble”. Test no.2 was performed on the soil mix at 5% initial water content and Test no.5 was performed after the soil was inundated from the bottom until full saturation was achieved.

The force required to push the retaining wall towards the soil and the horizontal displacement of the wall were measured and the load- displacement curves are presented in graph 4.14. The failure force at soil failure is underlined on the graph.

For the test performed on the soil mix at 5% water content, it was observed that the force required to push the retaining wall until soil failure is almost 85% bigger than after the collapse of the soil. The small value of the horizontal displacement of the retaining wall underlined that the soil failed almost immediately after the load was applied on the wall.

The coefficient of passive earth pressure K_p is calculated for both of the cases and the results given in table 4.13:

Soil Mix	Water content %	Clay content (%)	Collapse potential C_p (%)	Horizontal Displacement (mm)	Force (N)	Coefficient of passive earth pressure (K_p)
Mix 2	5	8	9	12.7	1920.03	3.762
	100			0.081	289.114	0.075

Table 4.13 Coefficient of passive earth pressure for Soil Mix 2

The coefficient of passive earth pressure decreases with 98% from the calculated value at 5% initial moisture content. The loss of strength of the collapsed soil influenced greatly the passive earth pressure which decreased significantly.

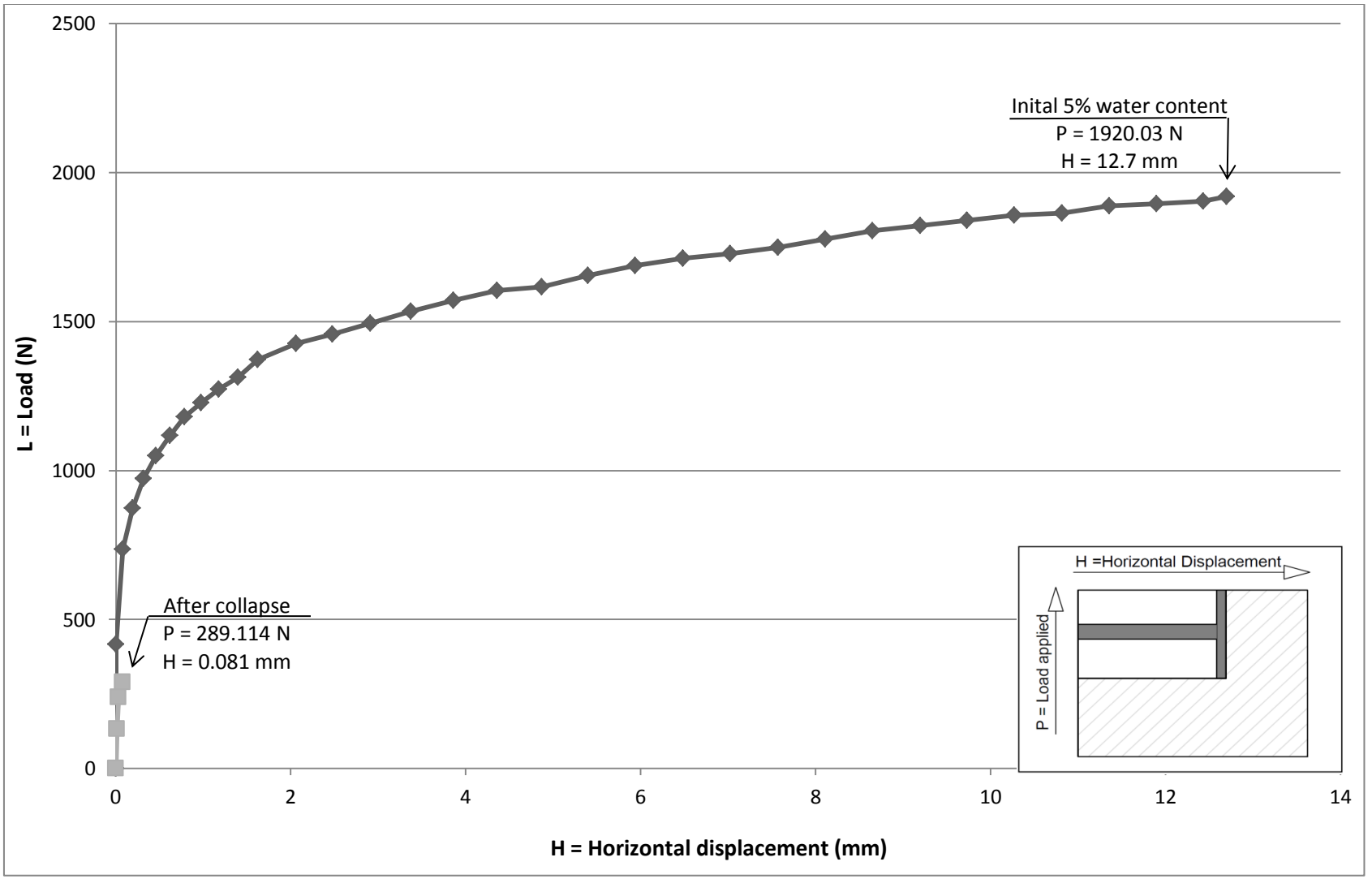

Graph 4.14 – Load - displacement curve for the tests performed on Mix 2 at 5% initial water content and full saturation

- Comparison of the results of Test 3 and Test 6 performed on Soil Mix 3

Soil mix 3 contained 10% clay content and had a collapse potential of 12.5% being classified by (Jennings and Knight 1975) as “severe trouble”. Test no.3 was performed on the soil mix at 5% initial water content and Test no.6 was performed after the soil was inundated from the bottom until full saturation was achieved.

The force required to push the retaining wall towards the soil and the horizontal displacement of the wall were measured and the load- displacement curves are presented in graph 4.15. The failure force at soil failure is underlined in the graph.

The classification of the soil according to (Jennings and Knight 1975) is as severe trouble for foundation problems. This is underlined when comparing the force required to push the retaining wall until soil failure from test 3 which is 95% higher than after the collapse of the soil. From all the tests performed on the soil mixes at 5% initial moisture content, soil mix 3 that contained 10% clay presents the greatest failure force, but also the highest collapse potential of 12.5%. After collapse, the soil lost almost all its strength and it failed at small values of force applied on the retaining wall. The failure occurred immediately after loading at a very small value of the horizontal displacement.

The coefficient of passive earth pressure K_p is calculated for both of the cases and the results given in table 4.14:

Soil Mix	Water content %	Clay content (%)	Collapse potential C_p (%)	Horizontal Displacement (mm)	Force (N)	Coefficient of passive earth pressure (K_p)
Mix 3	5	10	12.5	14.074	2331.8	3.157
	100			0.076	130.153	0.00936

Table 4.14 Coefficient of passive earth pressure for Soil Mix 3

The coefficient of passive earth pressure decreases with 99.7% from the calculated value at 5% initial moisture content. It can be clearly observed that after the collapse, the soil lost almost all its strength.

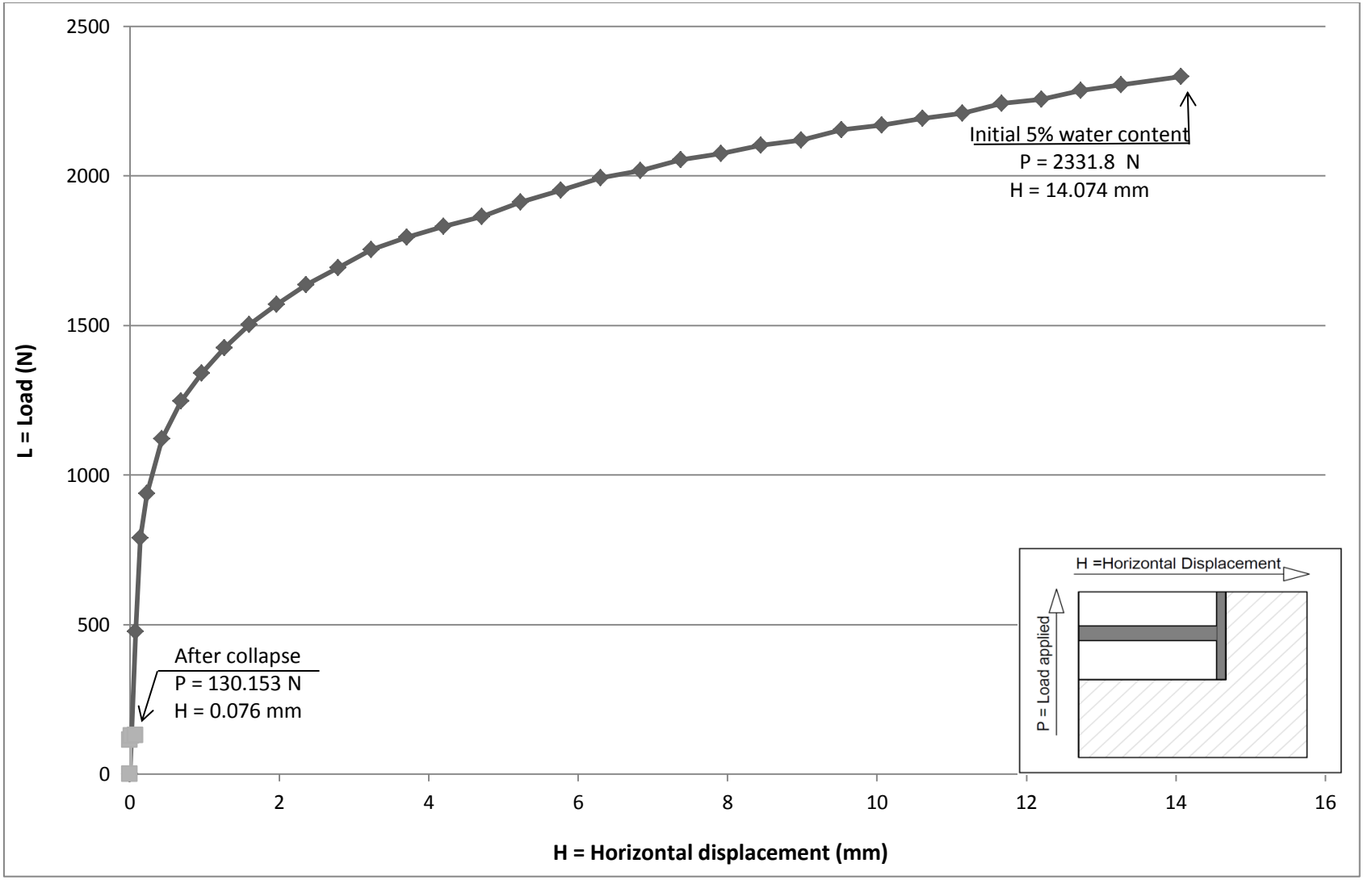

Graph 4.15 – Load - displacement curve for the tests performed on Mix 3 at 5% initial water content and full saturation

- Comparison of the results with the theoretical values

Rankine's equations for passive earth pressure are presently used for design of earth structures due to its easy maneuverability. Table 4.15 shows the soil properties for all the mixes and the coefficient of passive earth pressure calculated using Rankine's equation as follows:

$$k_p = tan^2\left(45^o + \frac{\emptyset}{2}\right)$$

k_p = passive earth coefficient

$\emptyset$ = angle of internal friction

Soil Mix	Clay content (%)	Initial water content (%)	Angle of internal friction $\emptyset'$ (degrees)	Rankine's Coefficient of passive earth pressure (K_p)
Mix 1	6	5	40	4.599
Mix 2	8	5	38.5	4.298
Mix 3	10	5	35	3.69

Table 4.15 Rankine's coefficient of passive earth pressure

In the present investigation, the coefficient of passive earth coefficient was calculated using Rankine's equation for the passive force per unit length of the wall as:

$$P_p = \frac{1}{2}k_p\gamma dh^2 + 2c'h\sqrt{k_p}$$

P_p = total passive earth pressure

γ = unit weight of the soil

c' = soil cohesion

d and h = width and height of the wall, respectively

All of the coefficients in the above equation are known and the coefficient of passive earth pressure can be taken out and calculated for each of the mixtures at 5% initial water content and presented in table 4.16.

Test number	Soil Mix	Initial water content %	Clay content (%)	Soil cohesion c' (kPa)	Unit weight γ (kN/m^3)	Collapse potential C_p (%)	Coefficient of passive earth pressure (K_p)
Test 1	Mix 1	5	6	9	16.28	4.2	4.151
Test 2	Mix 2	5	8	12.5	16.25	9	3.762
Test 3	Mix 3	5	10	15.5	16.2	12.5	3.157

Table 4.16 Coefficient of passive earth pressure for Soil Mixes at 5% initial water content

The comparison between the experimental and theoretical values of the passive earth coefficient is presented in table 4.17.

Soil Mix	Clay content (%)	Water content (%)	Experimental Coefficient of passive earth pressure (K_p)	Rankine's Coefficient of passive earth pressure (K_p)
Mix 1	6	5	4.151	4.599
Mix 2	8	5	3.762	4.298
Mix 3	10	5	3.157	3.69

Table 4.17 Comparison between Experimental and Rankine's coefficient of passive earth pressure

Based on the frictional resistance only (friction angle $\emptyset'$) the Rankine's passive earth coefficient is slightly higher than the experimental values obtained.

The coefficient of passive earth pressure for the soil mixes that were inundated from the bottom until full saturation is presented in table 4.18.

Test number	Soil Mix	Water content %	Clay content (%)	Collapse potential C_p (%)	Coefficient of passive earth pressure (K_p)
Test 1	Mix 1	100	6	4.2	0.54
Test 2	Mix 2	100	8	9	0.075
Test 3	Mix 3	100	10	12.5	0.00936

Table 4.18 – Coefficient of passive earth pressure for the collapsed samples

CHAPTER 5

FINITE ELEMENT MODEL

5.1 General

The finite element software known as Plaxis (Version 8.2) was used to perform the finite element studies presented in this report. The manner in which no deformable retaining wall was modeled, and the procedures were followed to calculate the displacements and stresses are presented in this chapter.

5.2 Modeling the physical space

The generation of a two-dimensional finite element model in Plaxis is based on a geometry model. This model was created in the x-y plane of the global coordinate system, where the z direction was in the out-of-plane direction.

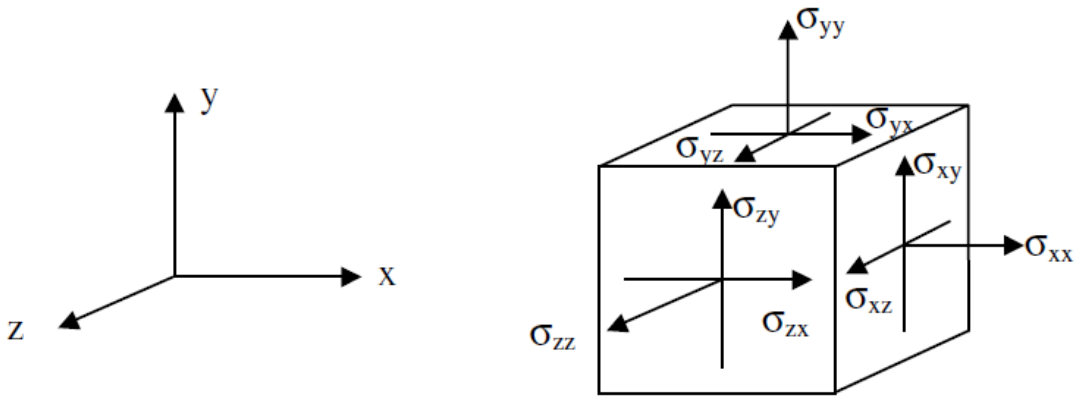

Figure 5.1 Coordinate system and indication of positive stress components (Plaxis, 2005)

The graphical interface allows the Plaxis user to draw a cross-section of the physical space. In the present study the physical space has three main components: the

backfill, the containing tank and the retaining wall. An example of the cross-section is shown in figure 5.1. The geometry model will be composed of points, lines and plates. The material properties and the boundary conditions have been specified for all components.

Before creating the geometry menu, the input menu of Plaxis requires the selection of the model type. Because the geometry of the model has a uniform cross-section and the loading scheme over a certain length was perpendicular to the cross-section in the present investigation the Plane strain model was selected. Plaxis program assumes displacements and strains in the z direction to be zero but the normal stresses on this direction are taken into account.

The next input in the menu was the element type. For the present numerical model a 15 node triangular element was chosen. It provides a fourth order interpolation for displacements and the numerical integration involves 15 stress points. The mesh consisted of 15 node triangular elements performs better than the other option of 6 node triangular elements because it has a larger number of nodes. During the finite element calculation displacements (u_x and u_y) are calculated at the nodes. Stresses and strains are calculated at the stress points and not in the nodes. The distribution of the nodes and stress points of a 15 node element are shown in figure 5.2.

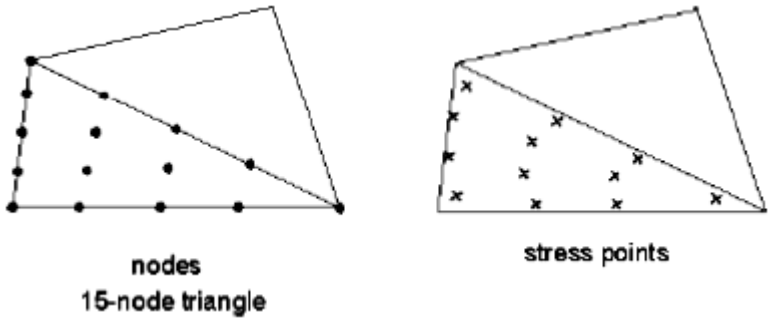

Figure 5.2 Example of nodes and stress points for 15-node triangular elements (Plaxis, 2005)

The experimental setup was modeled by constructing the geometry model from points, lines and plates. The points and lines define the geometry contour. The plates are structural objects used to model slender structures in the ground. In the present case the plate was used to model the testing tank and the retaining wall. The material properties used for defining the plate elements are presented in table 5.2. The most important parameters are the flexural rigidity (EI) and the axial stiffness (EA). Knowing the dimensions of the testing tank and the retaining wall and the modulus of elasticity of aluminum the material properties of the plates were calculated. The retaining wall was selected to behave elastically.

To model the interaction between the soil and the retaining wall an interface was placed on the face of the plate. During the experimental investigation the face of the retaining wall that interacts with the soil was covered with a thick layer of heavy grease. This was done to eliminate the friction between the soil and the retaining wall. In Plaxis the roughness of the interaction between the soil and the retaining wall was done by entering a value for the coefficient R_{inter}. This factor relates the interface strength (wall friction and adhesion) to the soil strength (friction angle and cohesion). In order to keep the same conditions as the experimental testing the value of R_{inter} was kept as 0.1 for all the numerical models.

Interfaces are composed of interface elements. Each element is connected to other elements or to a boundary. Triangular elements will share the nodes along each side of the triangle. When a triangle is connected to an interface element, they also share nodes. When using 15 node soil elements, the corresponding interface elements are defined by five pair of nodes as shown in Figure 5.5.

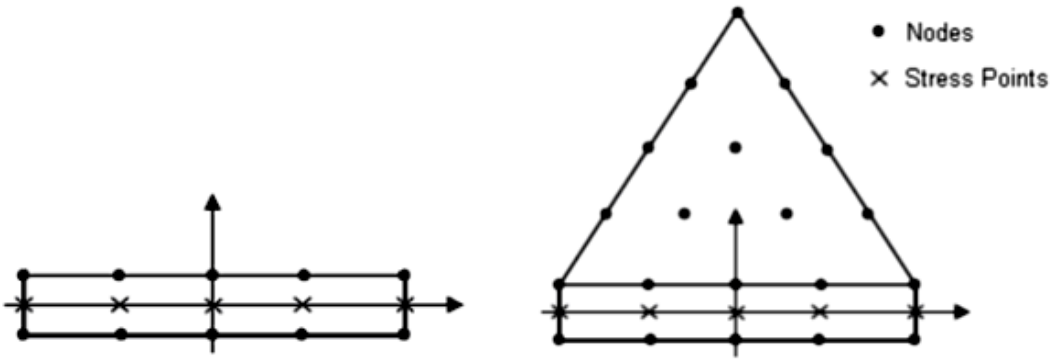

Figure 5.3 Locations of nodes and stress points when a 15-node triangular element is connected to a 5-node interface element (Plaxis, 2005)

The Plaxis Reference manual presents several cases when, in the corners of structures high peaks of stresses and strains develop as shown in Figure 5.6

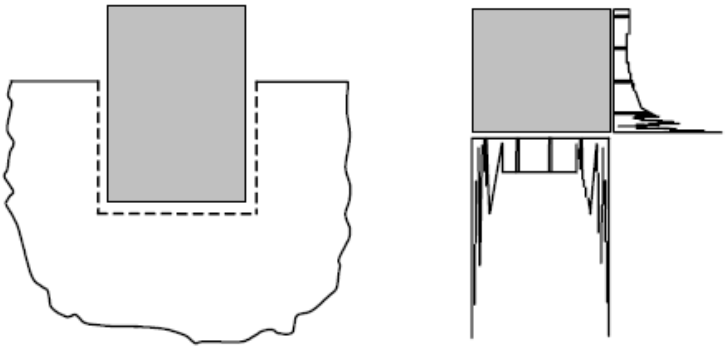

Figure 5.4 Stress peaks (Plaxis 2005)

These inflexible points will cause poor quality stress results. To account for this in the present numerical modeling the interface has been extended beyond the bottom corner of the retaining wall.

To model the confinement of the soil in the testing tank from the experimental investigation, to the plates in the geometry model from Plaxis total fixities are applied. Total fixities will prevent any movement in any direction (displacements u_x=u_y=0).

In the experimental setup the retaining wall was connected to the loading machine by a steel rod that passes through a series of bearing supports. The vertical movement of the wall was restricted by this connection. The retaining wall had the same width as the testing tank so the horizontal displacements will be null. The wall was connected to the loading steel rod by a series of plates and screws. This connection will restrict the rotation of the retaining wall.

To ensure the same wall movement of the retaining wall from the experimental setup, the plate in the numerical model was fixed in the vertical direction but it was allowed to move horizontally. This was achieved by placing a vertical fixity from the Plaxis program. To account for the zero rotation the top and bottom points of the wall were fixed using the rotation fixities for plates from the program.

To model the loading of the retaining wall from the experimental setup, in the Plaxis model a concentrated force was applied on the plate. The point of application of the force was placed so that it coincided with the connection point of the retaining wall to the steel rod from the experimental setup. The values of the applied forces used in the numerical modeling were the forces recorded at soil failure from the experimental investigation. To maintain the sign convention from the program the values of the forces have been introduced with a negative sign.

The plate used to model the structural elements of the model and their fixities, as well as the loading force applied on the retaining wall are presented in Figure 5.5.

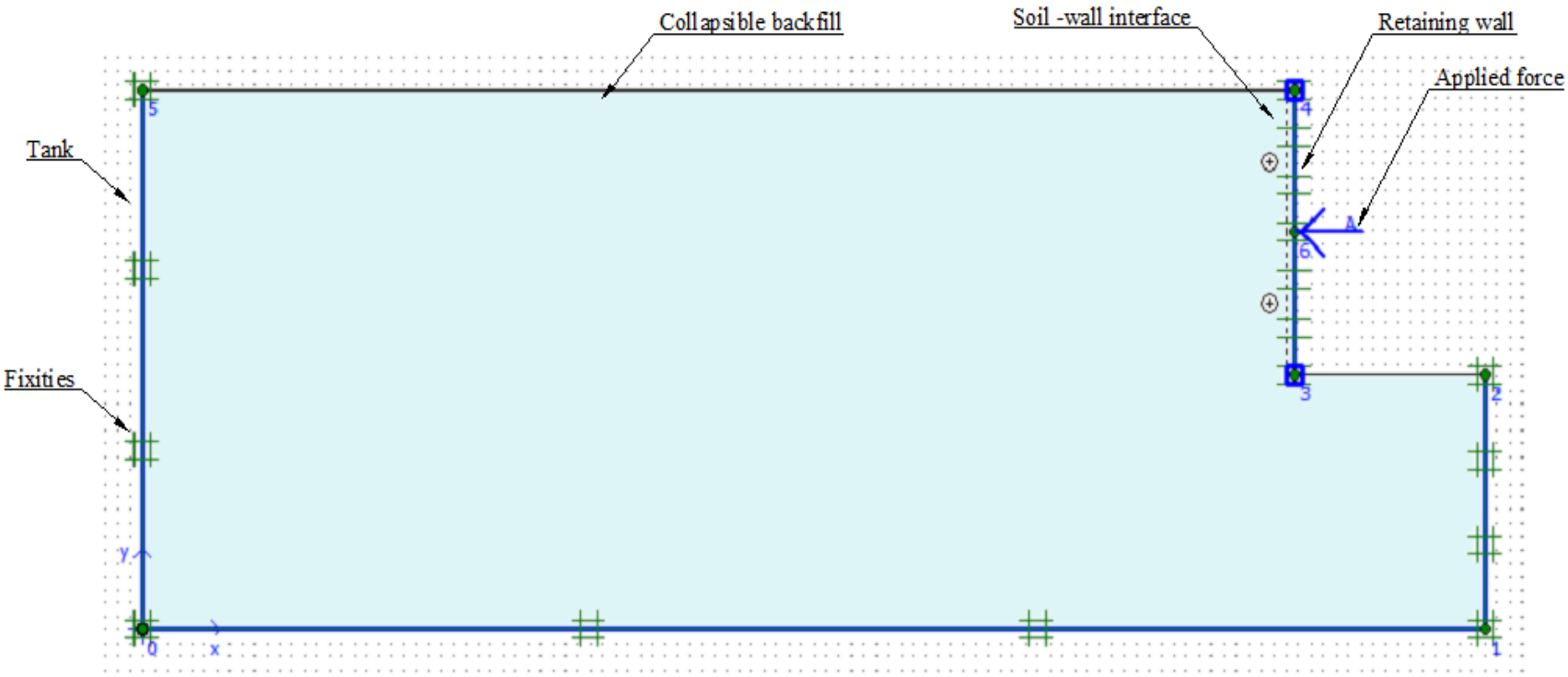

Figure 5.5 Geometry and boundary conditions of the physical space in Plaxis

In order to model the soil backfill a soil model had to be constructed in Plaxis. The soil behaviour was defined by Mohr-Coulomb (MC) constitutive law, which simulates the soil behaviour based on soil parameters known in most practical situations. In this model a yield surface is defined such that when the soil reaches or surpasses a predefined stress state, deformation is no longer completely recoverable. Five soil constitutive parameters are required for the Mohr-Coulomb model: Young's Modulus (E), Poisson's ratio (v), angle of internal friction (φ'), cohesion (c'), and dilatancy angle (ψ). The soil properties used in the present numerical modelling are presented in table 5.1.

In the experimental investigation in order to inundate the soil from the bottom, 12 tubes were connected to the bottom of the testing tank. These tubes remained fixed and unblocked throughout all the tests. The loading rate of the gear box used was set at a slow rate. To model this conditions in Plaxis, in the soil properties input the drained soil behavior was chosen.

When the geometry model was fully defined and the material properties were assigned to all clusters and structural objects, the geometry was divided into finite elements by generating the mesh.

In Plaxis, the default element size used for generating the mesh is referred to as "coarse." In the present numerical models the coarseness of the mesh was kept at default and the generated mesh contained around 100 elements. A typical mesh generated using the "coarse" mesh option in Plaxis is illustrated in Figure 5.6.

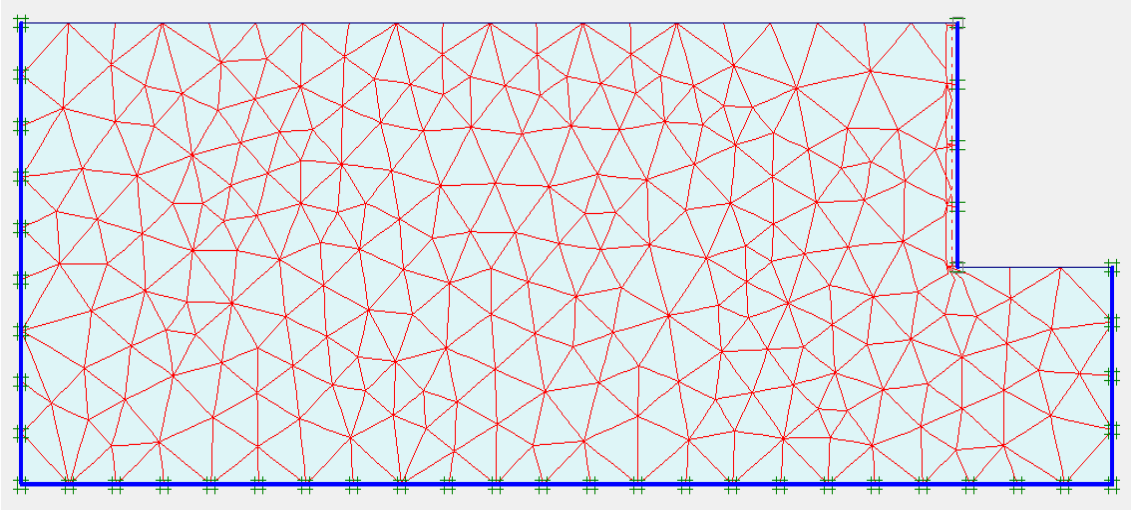

Figure 5.6 Typical mesh generated using the “coarse” mesh option in Plaxis

Once the mesh was generated the finite element model was complete. Initial condition must be generated that comprise the initial groundwater conditions, the initial geometry configuration and the initial effective stress state. The initial soil effective stresses were automatically generated from the given general phreatic level and the input of the coefficient of earth pressure at rest (k_0). The k_0 procedure was used to generate the initial soil stresses using k_0 to relate the initial horizontal effective stresses ($\sigma'_{h,0}$) and the initial vertical effective stresses ($\sigma'_{v,0}$) as follows:

$$\sigma'_{h,0} = k_0 * \sigma'_{v,0}$$

In generating the initial effective stresses, no external load or the weights of the walls and the interfaces are taken into account. After the generation of the initial conditions the calculation program is active and can be performed.

For the calculation part of the model an elasto-plastic deformation analysis was considered. This is termed Plastic calculation in Plaxis program. The stiffness matrix in a normal plastic calculation is based on the original undeformed geometry. This type of calculation does not take into consideration the decay of the excess pore water pressure

during the time period considered. During all the calculation models used in all the numerical models the Updated mesh option was activated, which makes the calculations to be performed according to large deformation theory.

Each calculation was defined in separate phases of staged construction. Only one type of loading input can be activated in each calculation phase. The first phase was represented by the initial condition phase. In the next phase a point load was applied on the retaining wall. The phases defined above can simulate wall loading in soil at constant moisture content. The model was further extended to incorporate the effect of inundation later on.

5.3 Numerical model for retaining wall pushing in the soil with 5% initial moisture content

The numerical model was used to simulate the case of the first experimental tests performed on the three soil mixtures with 6%, 8% and 10% kaolin content at initial water content of 5%. During the experimental setup, the model retaining wall was connected to the testing tank before the soil was placed in the tank. The installation of the retaining wall was ignored in the numerical model. Collapsible soils, used in the model tests, were found strong when dry, that is a characteristic property of unsaturated collapsible soil at initial moisture condition (5% water content).

Collapsible soil behavior (at constant moisture content, representing either partially or fully saturated state) was defined as drained material and modeled by the Mohr-Coulomb (MC) constitutive law. Material parameters (including cohesion (c), angle of shearing resistance (υ), Poisson‘s ratio (υ), Young‘s modulus (E) and angle of dilatancy (ψ)) in the MC model, were given as input parameters, according to the soil constant soil moisture content state (corresponding to either the unsaturated or

saturated condition). The properties of the soil backfill modeled in all numerical models are presented in the following table:

Soil Mix	Cohesion c (kPa)	Angle of internal friction ϕ (degrees)	Modulus of elasticity E (kPa)	Dilatancy Ψ (degrees)	Unsaturated unit weight γ_{usat} (kN/m^3)	Saturated unit weight γ_{sat} (kN/m^3)
Mix 1	9	40	30000	10	16.28	19.54
Mix 2	12.5	38.5	30000	8.5	16.25	19.49
Mix 3	15.5	35	30000	5	16.2	19.43

Table 5.1 Soil properties used in the numerical analysis

The testing tank and retaining wall were modeled as plate elements and the properties imputed in the program are the ones in the following table:

Plate element	Poisson's ratio ν	Modulus of elasticity E(kPa)	Unit weight γ_{plate} (kN/m^3)
Retaining wall Tank walls	0.3	6.89E07	27

Table 5.2 Material Properties for the plates in the numerical analysis

The boundary conditions and material properties were applied for all the clusters in the model as described in the previous sub-chapter.

The initial conditions must be generated. For the first set of tests the general phreatic line was placed at the bottom of the geometry model. Hence the pore water pressure remains zero for the full depth of the homogeneous strata (figure 5.7). In generating the initial effective stresses, no external load or the weights of the walls and the interfaces are taken into account. Figure 5.8 shows the initial effective stresses developed in the numerical model. After generating the initial conditions of the soil the program will move to the calculation part.

When defining the Staged construction of the second phase, the program allows us to return to the geometry model and activate the walls, interfaces and external load.

After the application of the force the calculation program and the plastic calculation was chosen. The points for the stress and displacement curves were selected. Several stress points were chosen along the height of the wall. The horizontal stress for each point was compared and the point with the maximum horizontal stress was used for calculations.

Figure 5.9 shows that the maximum horizontal displacement of 11.29mm is close to the recorded experimental displacement of 11.321mm.

For the point at the bottom of the wall, that presented the maximum horizontal stress, the curve of horizontal and vertical effective stress is plotted from Plaxis and it is presented in Figure 5.10. The horizontal effective stress from the curve presented is $\sigma_h' = 0.111\ \frac{N}{mm^2}$ and the corresponding vertical stress $\sigma_v' = 0.023\ \frac{N}{mm^2}$.

The stresses are used to find the coefficient of passive earth pressure using Rankine's formula:

$$\sigma_h' = \sigma_v' * k_p + 2c\sqrt{k_p}$$

Where:

σ_h' = horizontal effective stress

σ_v' = vertical effective stress

k_p = coefficient of passive earth pressure

c = cohesion of the soil

The comparison between the coefficient of passive earth pressure from the experimental results and Plaxis model are presented in table 5.3:

	Coefficient of passive earth pressure k_p
Experimental investigation results	4.151
Rankine's calculation	4.599
Plaxis results	4.456

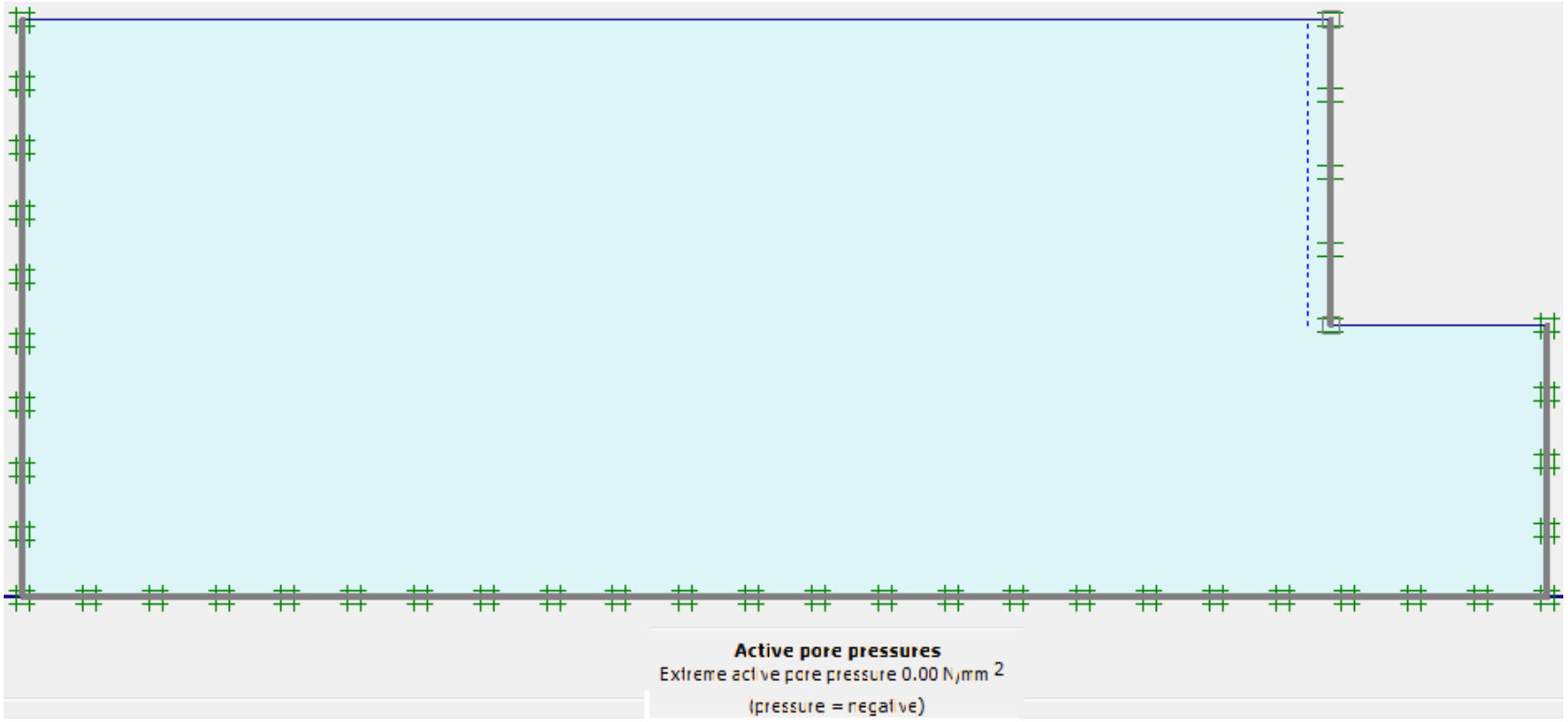

Figure 5.7 Initial pore water pressure

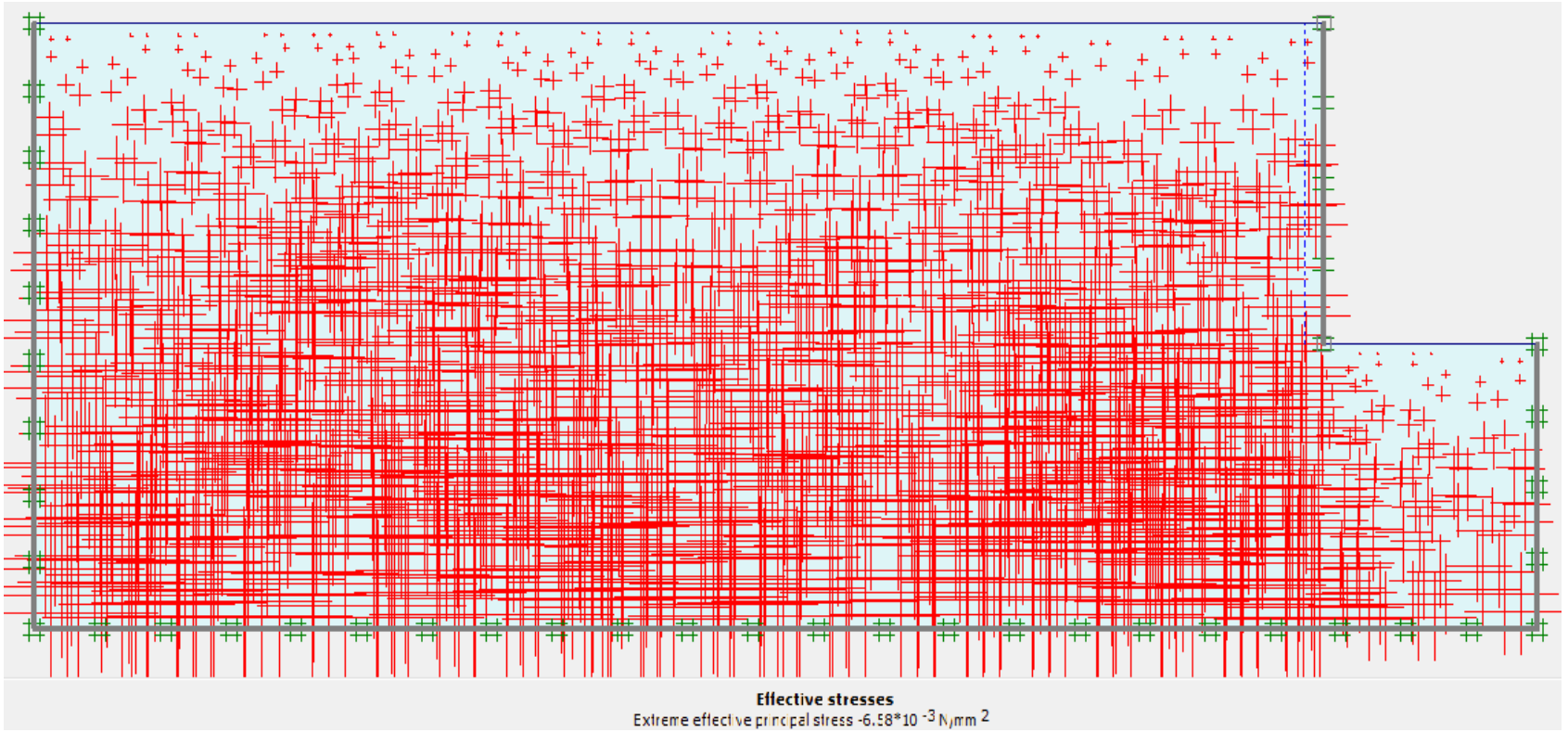

Figure 5.8 Initial effective stresses in the soil mass

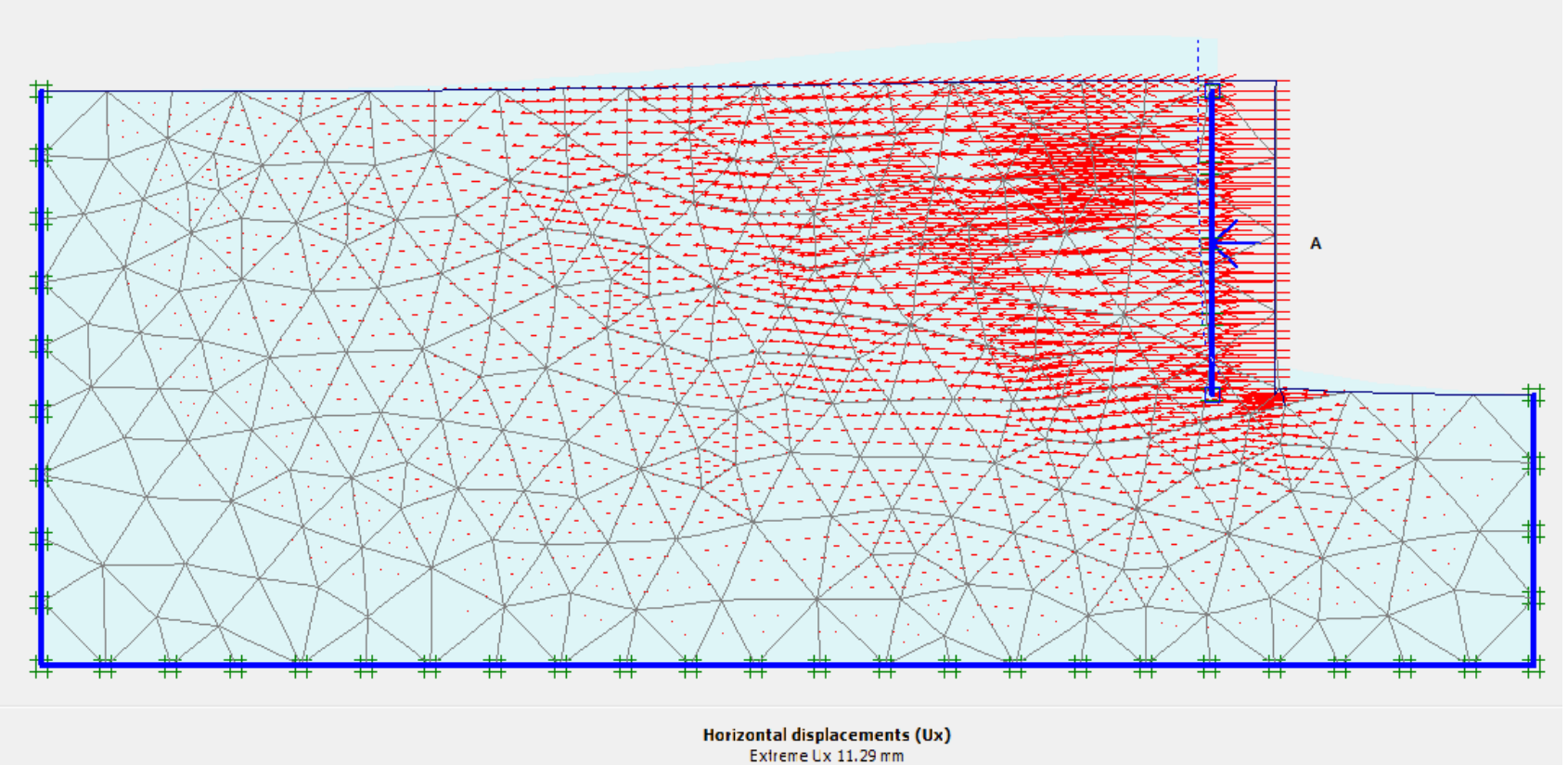

Figure 5.9 Horizontal displacements for Mix 1 (6% clay content) at 5% moisture content

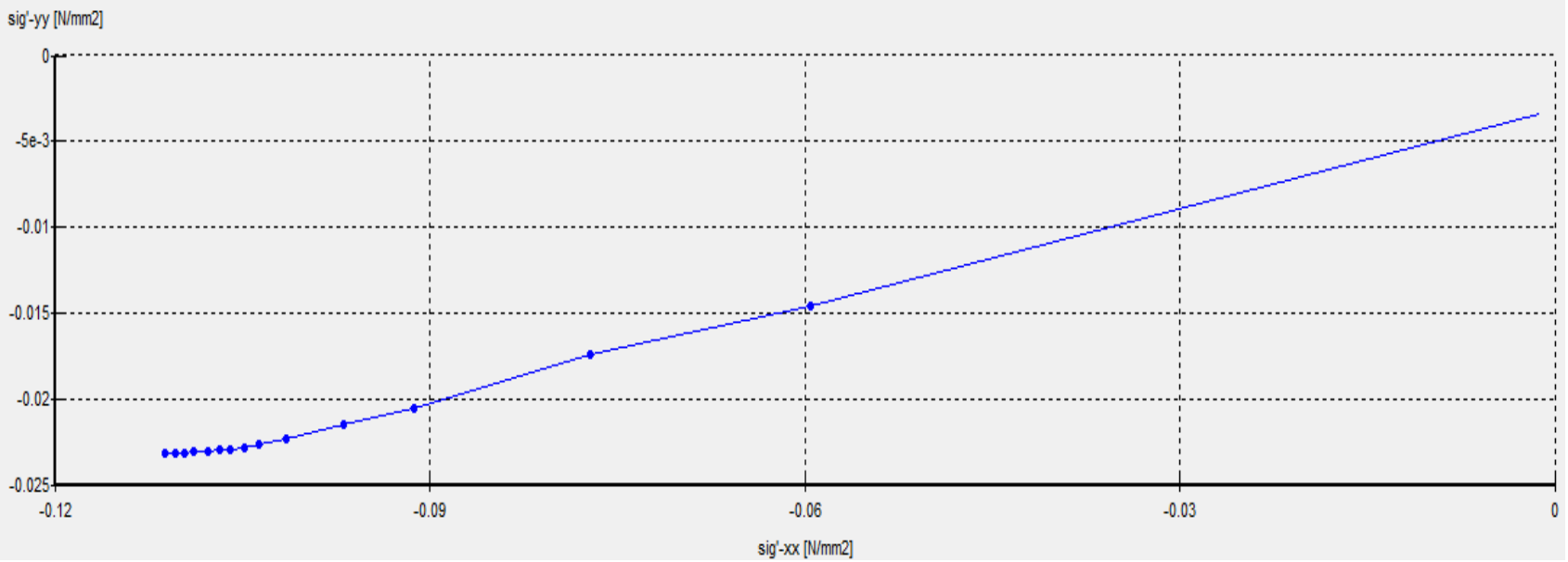

Figure 5.10. Horizontal and vertical effective stress plotted from Plaxis (point F) for Mix 1 (6% clay content) at 5% moisture content

For the Plaxis geometric model of the soil mix 2 that contains 8% clay content the same procedure has been applied.

The soil properties have been changed and the force applied on the wall was the maximum force recorded from the experimental results of 1920.03N. The program has been run under the Plastic calculation model.

The displacement output of the program shows a maximum displacement of 12.42 mm (Figure 5.11) which is close to the experimental displacement of 12.70 mm.

Stress points have been selected along the height of the wall and the point of maximum horizontal stress has been found as being point C located at the bottom of the wall. For this point the horizontal and vertical stresses have been plotted as shown in Figure 5.12.

Using these values the coefficient of passive earth pressure has been calculated using formula 5.1 where the horizontal effective stress of point C is $\sigma_h' = 0.101\ \frac{N}{mm^2}$ and the corresponding vertical stress $\sigma_v' = 0.022\ \frac{N}{mm^2}$.

The calculated coefficient of passive earth pressure was calculated and compared with the experimental results in table 5.4.

	Coefficient of passive earth pressure k_p
Experimental investigation results	3.762
Rankine's calculation	4.298
Plaxis results	3.99

Table 5.4 Coefficient of passive earth pressure for Soil Mix 2 at 5% moisture

As can be observed in the above table the coefficient of passive earth pressure has close values for all the different cases.

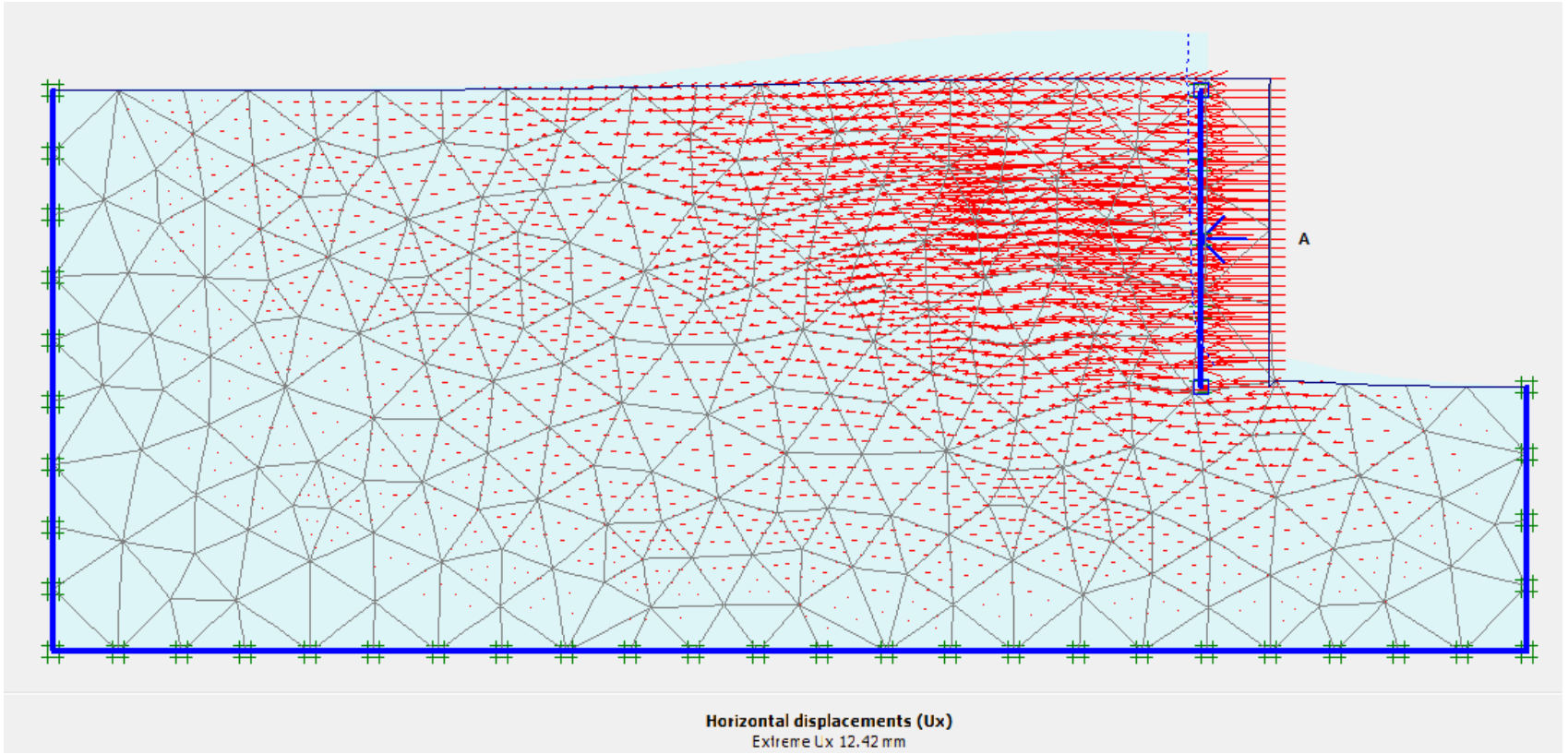

Figure 5.11 Horizontal displacements for Mix 2 (8% clay content) at 5% moisture content

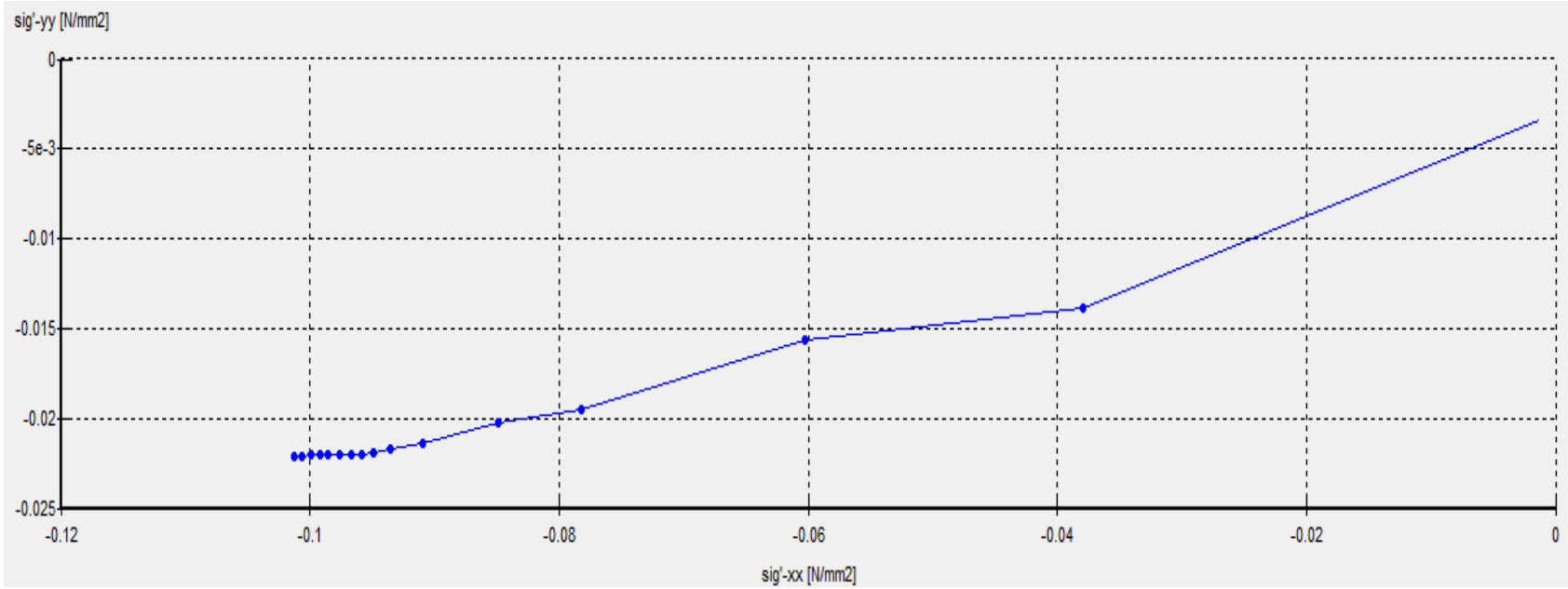

Figure 5.12. Horizontal and vertical effective stress plotted from Plaxis (point C) for Mix 2 (8% clay content) at 5% moisture content

To model the soil mix 3 that contains 10% clay content the soil properties have been changed and the Plaxis model procedure has been repeated.

In the calculation part of the model the horizontal force applied on the retaining wall has been replaced by the maximum force recorded from the experiments of 2331.8N. After the model has been run the maximum displacement given by the program presented in figure 5.13 is of 14.96 mm which is close to the horizontal displacement recorded during the experiment of 14.074mm.

Before the program his run several stress points are taken along the height of the wall and the point of maximum horizontal stress has been selected for calculations. For this point C located at the bottom of the wall, the effective stresses presented in figure 5.14 are considered for calculation of the coefficient of passive earth pressure using formula 5.1. The effective stresses of the point are as follows: the horizontal effective stress as $\sigma_h' = 0.108\ \frac{N}{mm^2}$ and the corresponding vertical stress $\sigma_v' = 0.022\ \frac{N}{mm^2}$.

The calculated coefficient of passive earth pressure is presented in table 5.5 along with the one obtained from the experimental results and the one calculated using Rankine's equation.

	Coefficient of passive earth pressure k_p
Experimental investigation results	3.157
Rankine's calculation	3.69
Plaxis results	3.395

Table5.5 Coefficient of passive earth pressure for Soil Mix 3

Table 5.5 shows that the values of passive earth pressure are close for all the three different cases.

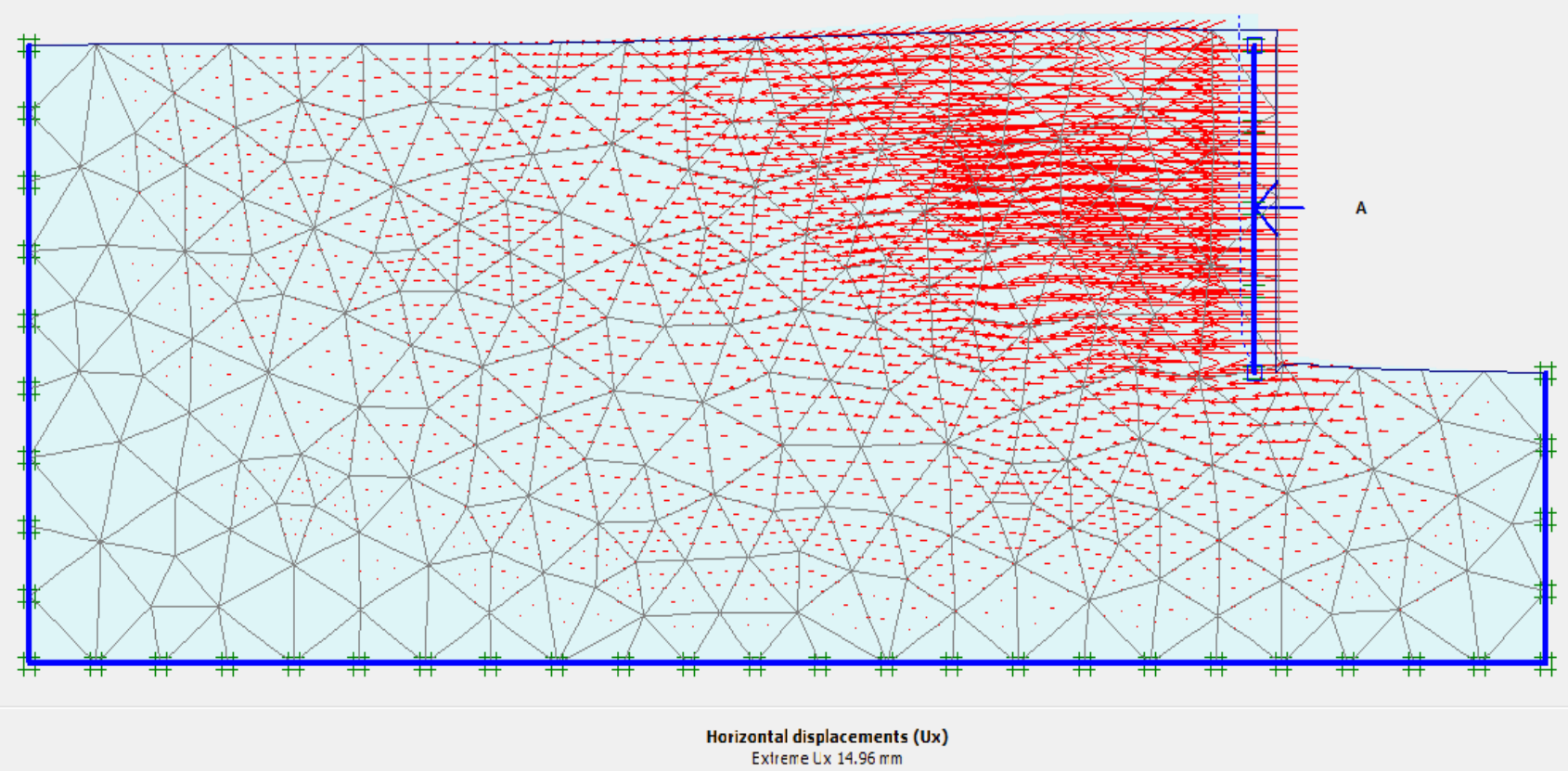

Figure 5.13 Horizontal displacements for Mix 3 (10% clay content) at 5% moisture content

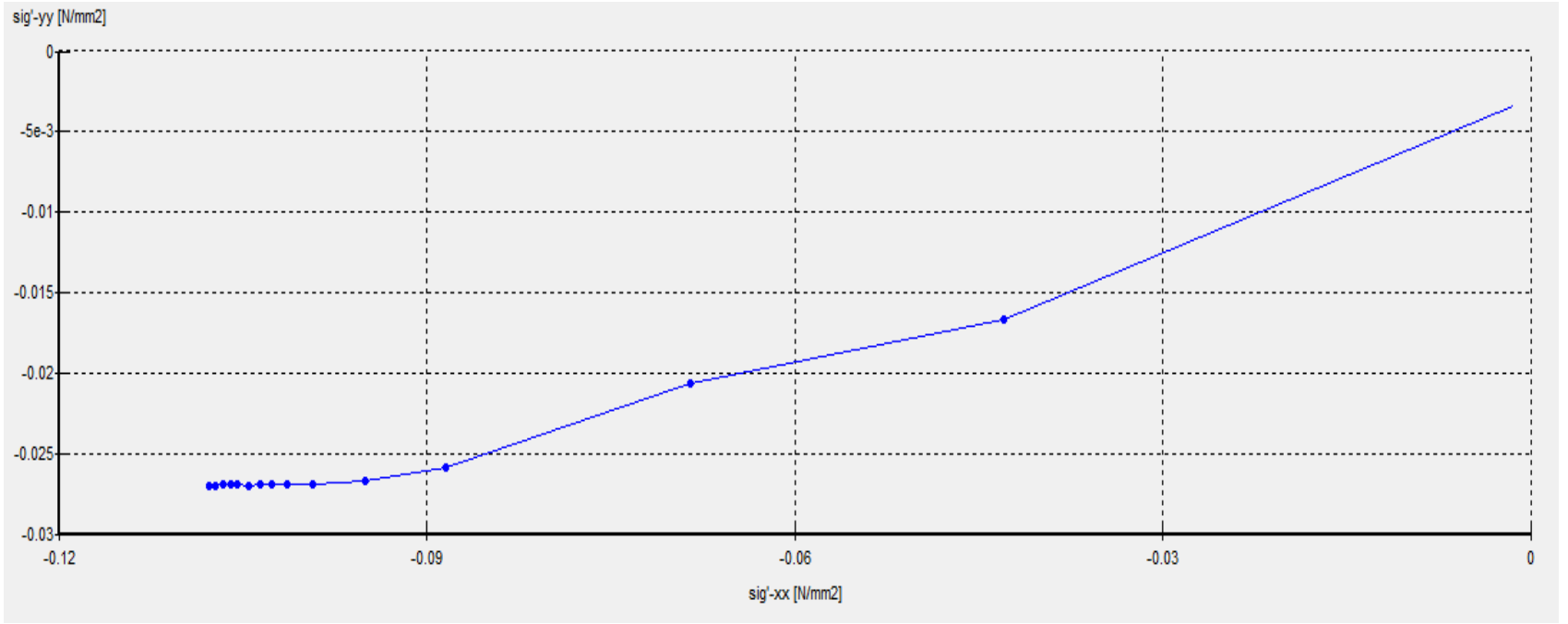

Figure 5.14 Horizontal and vertical effective stress plotted from Plaxis (point C) for Mix 3 (10% clay content) at 5% moisture content

5.4 Numerical model for retaining wall pushing in the soil at full saturation

In the present experimental investigation the simulation of the rise of the ground water table was made by inundating the soil from the bottom up, until full saturation was achieved. To model this condition in Plaxis before loading the retaining wall the ground water table was moved from the bottom of the tank to the upper part of the retaining tank as shown in Figure 5.15.

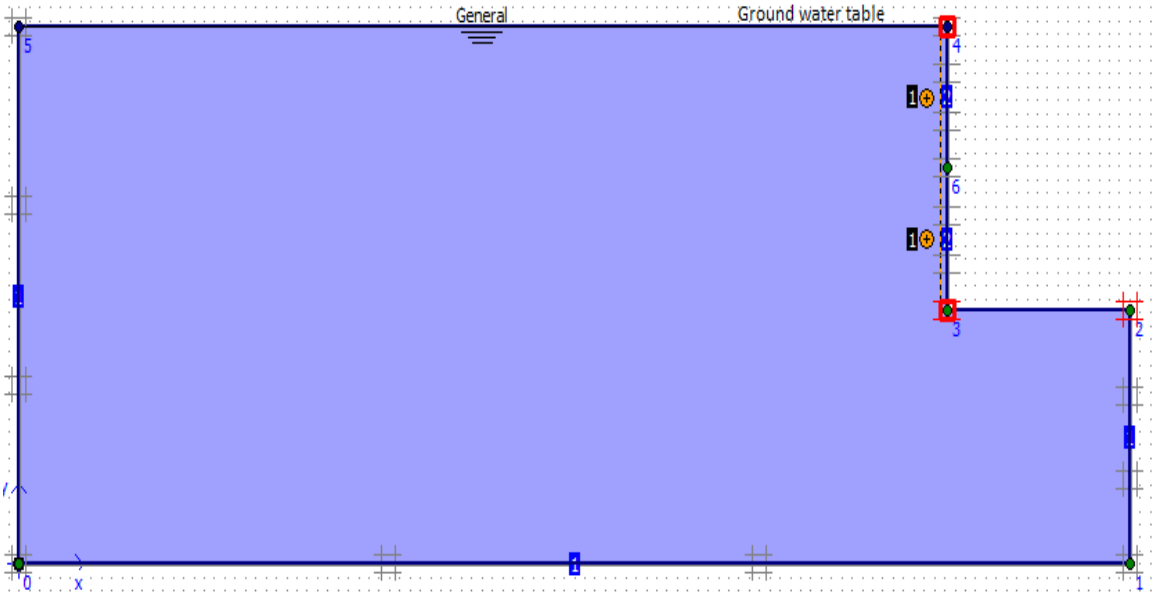

Figure 5.15 – Ground water table for inundated samples

In order to account for the loss of soil strength after the collapse of the soil, in the calculation part the “Phi-c reduction” calculation was used as second stage of calculation after the initial condition phase. In the Phi-c reduction approach the strength parameters tanϕ and c are successively reduced until the all the additional steps are completed. In order to prevent the failure of the soil and achieve only reduction of the soil parameters the number of the additional steps is kept at 1. This will ensure the desired strength reduction but not failure. For the Phi-c reduction calculation in the multipliers menu of the program the ΣM_{sf} is defined as the quotient of the original strength parameters and the

reduced strength parameters and controls the reduction of tanϕ and c at a given stage in the analysis. This increment was kept at the value of 0.1 which according to the Plaxis Reference manual was found to be a good starting value.

The third phase of the calculation was a plastic calculation where the horizontal force recorded at soil failure from the experimental part was applied on the retaining wall. The plastic calculation followed the same elasto-plastic deformation analysis. The Plastic phase started at the end of the Phi-s reduction phase so the soil will present reduced strength parameters. When using Phi-c reduction in combination with the Plastic calculation the model will behave as a standard Mohr-Coulomb model, since the stress-dependent stiffness behavior and hardening effects are excluded from the analysis.

After application of the horizontal force on the retaining wall in the Plastic calculation Phase, from the output part of Plaxis the horizontal displacement of the wall (Figure 5.16) was found as 1.88mm which is only slightly higher than the experimental displacement of 1.249mm.

Before the start of the calculation along the height of the retaining wall several stress points have been selected in order to find the point that presents the maximum horizontal stress. This point has been found at the bottom of the wall, the same as for the other numerical models. The horizontal versus vertical stress diagram for this point is presented in Figure 5.17.

For this point C located at the bottom of the wall, the effective stresses presented in figure 5.17 were considered for calculation of the coefficient of passive earth pressure using formula 5.1. The effective stresses of the point are as follows: the horizontal effective stress as $\sigma_h' = 0.015\ \frac{N}{mm^2}$ and the corresponding vertical stress $\sigma_v' = 0.011\ \frac{N}{mm^2}$.

The calculated coefficient of passive earth pressure is presented in table 5.6 along with the one obtained from the experimental results.

	Coefficient of passive earth pressure k_p
Experimental investigation results	0.54
Plaxis results	0.572

Table 5.6 Coefficient of passive earth pressure for collapsed Soil Mix 1

Comparing the results in the above table it can be observed that the values of the coefficient of passive earth pressure calculated using the stresses from Plaxis is close to the coefficient of passive earth pressure calculated from the experimental investigation. This verifies the results from the numerical model analysis.

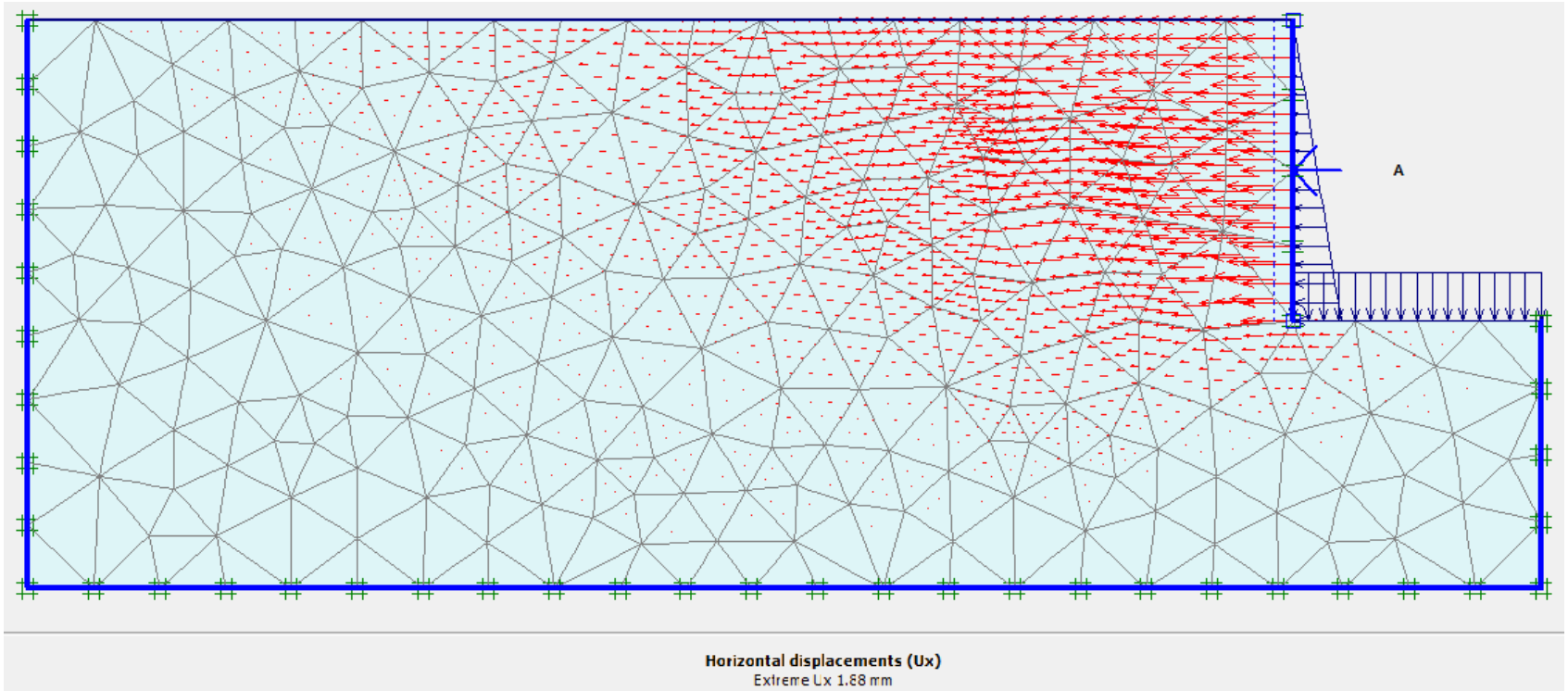

Figure 5.16 Horizontal displacements for Mix 1 (6% clay content) at full saturation

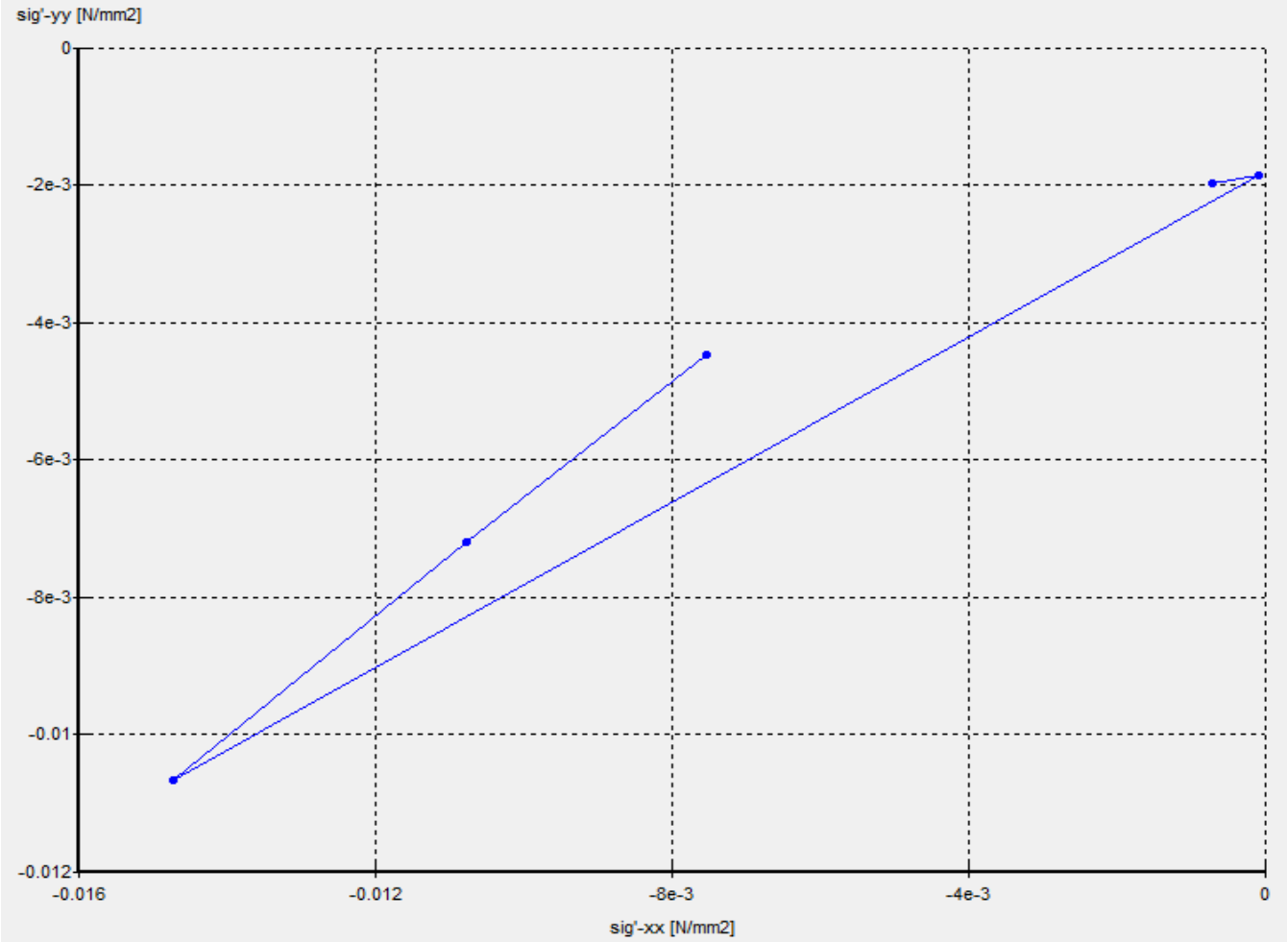

Figure 5.17 Horizontal and vertical effective stress plotted from Plaxis (point C) for Mix 1 (6% clay content) at full saturation

To model the soil mix 2 at full saturation in Plaxis the same procedure has been adopted. The soil properties have been changed in the Geometry of the model and the load applied on the retaining wall was changed to the horizontal force recorded at soil failure from the experimental investigation for this soil which has the value of 289.114N.

After the calculation was performed the horizontal displacement of the wall as can be observed in Figure 5.18 has a value of 0.181 mm which is slightly higher than the one presented after the experimental investigation.

For the several stress points selected along the height of the wall the one that presented the highest horizontal stress was used for calculation. The horizontal versus vertical stresses diagram for this point is presented in Figure 5.19. The horizontal effective stress of the point is $\sigma_h' = 0.00764 \frac{N}{mm^2}$ having the corresponding vertical stress $\sigma_v' = 0.004842 \ \frac{N}{mm^2}$.

The calculated coefficient of passive earth pressure is presented in table 5.7 along with the one obtained from the experimental results and the one calculated using Rankine's equation.

	Coefficient of passive earth pressure k_p
Experimental investigation results	0.075
Plaxis results	0.093

Table 5.7 Coefficient of passive earth pressure for collapsed Soil Mix 2

In the above table we can observe that the values of the coefficient of passive earth pressure are close, which means that the experimental results verify the numerical model.

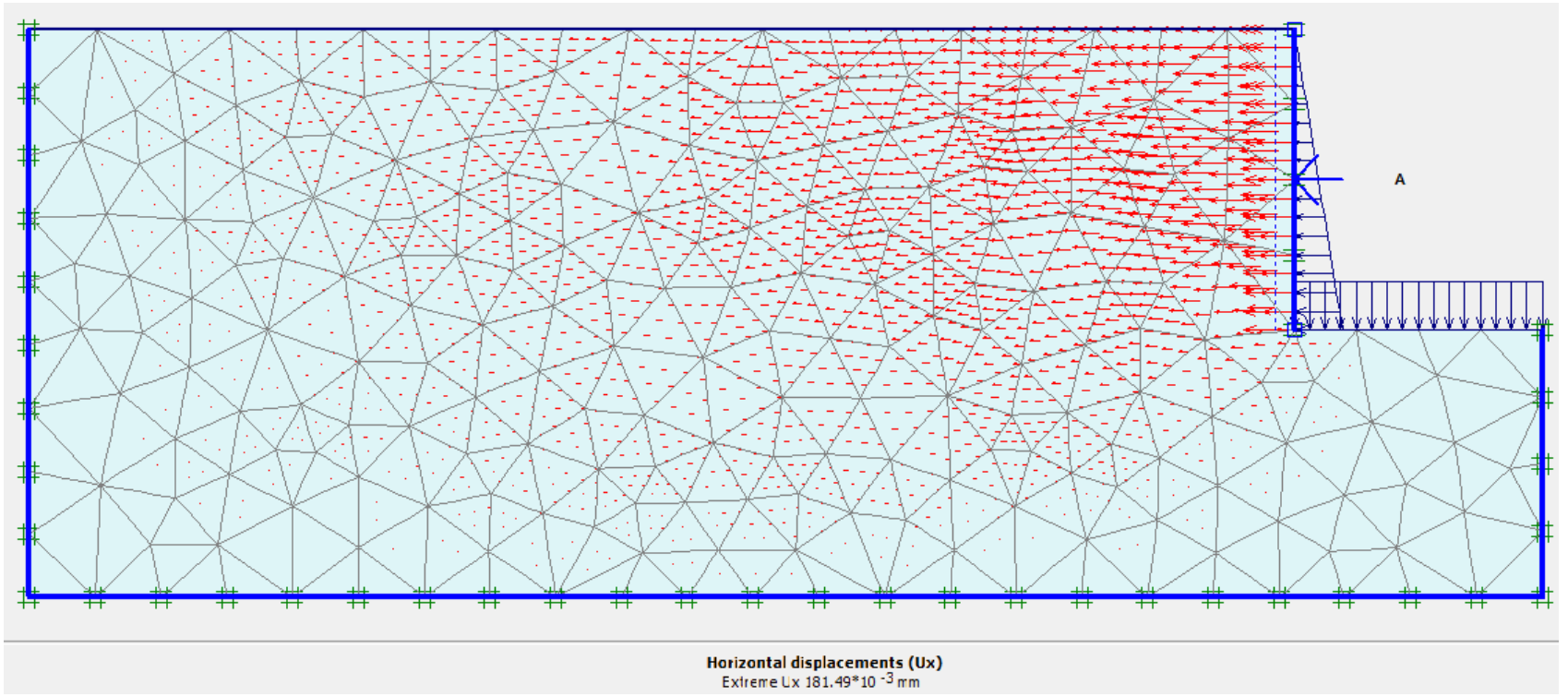

Figure 5.18 Horizontal displacements for Mix 2 (8% clay content) at full saturation

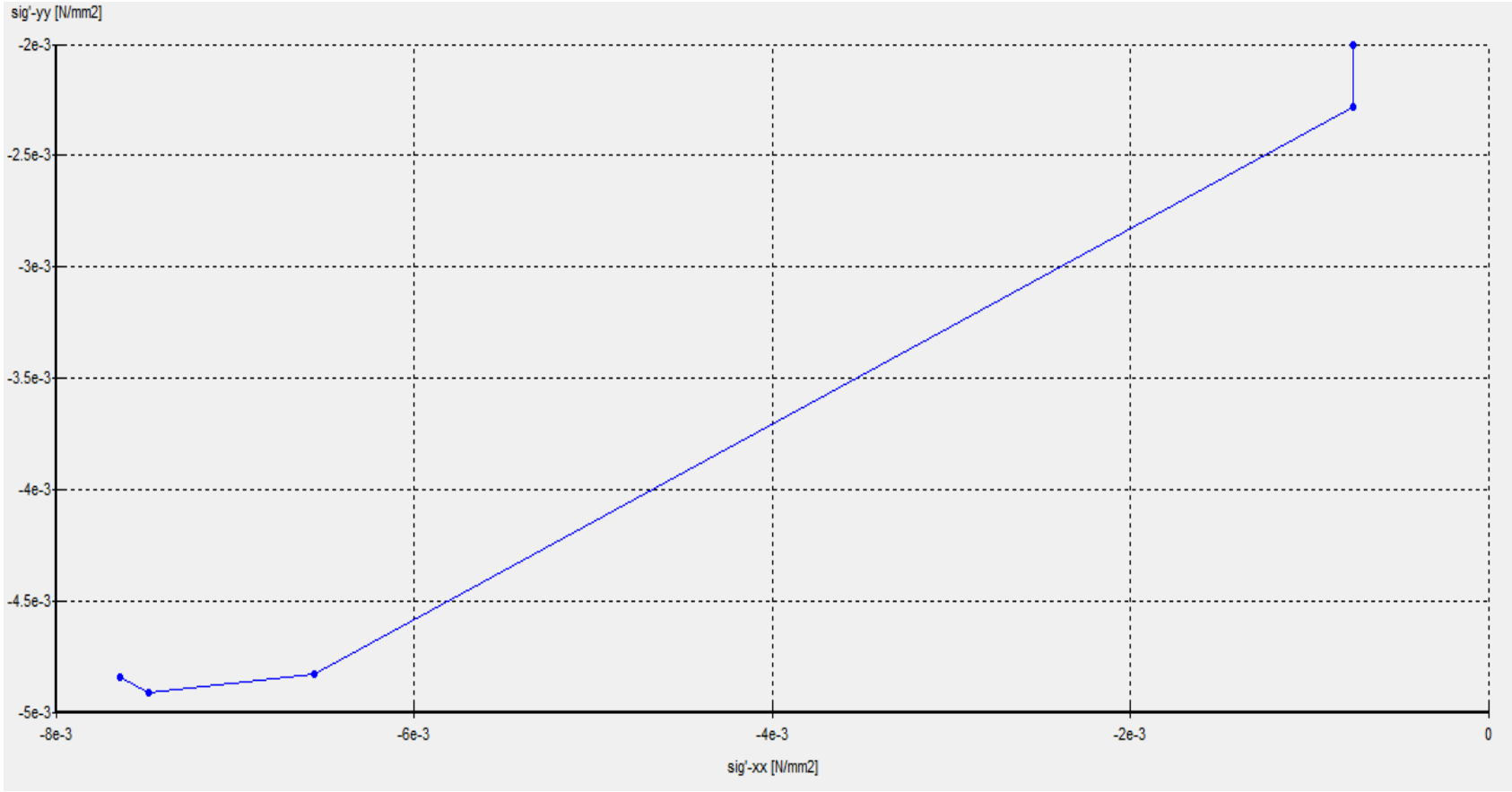

Figure 5.19 Horizontal and vertical effective stress plotted from Plaxis (point C) for Mix 2 (8% clay content) at full saturation

To model the soil mix 3 that contains 10% clay content the soil properties have been changed and the Plaxis model procedure has been repeated.

In the calculation part of the model the horizontal force applied on the retaining wall has been replaced by the maximum force recorded from the experiments of 130.153N. After the model has been run the maximum displacement given by the program presented in Figure 5.20 is of 1.52 mm is only slightly higher than the horizontal displacement recorded during the experiment of 0.076mm.

Before the program his run several stress points are taken along the height of the wall and the point of maximum horizontal stress has been selected for calculations. For this point C located at the bottom of the wall, the effective stresses presented in figure 5.21 are considered for calculation of the coefficient of passive earth pressure using formula 5.1. The horizontal effective stress of the point is $\sigma_h' = 0.003762 \frac{N}{mm^2}$ and the corresponding vertical stress is $\sigma_v' = 0.002799 \frac{N}{mm^2}$.

The calculated coefficient of passive earth pressure is presented in table 5.8 along with the one obtained from the experimental results.

	Coefficient of passive earth pressure k_p
Experimental investigation results	0.00936
Plaxis results	0.015

Table 5.8 Coefficient of passive earth pressure for collapsed Soil Mix 3

The coefficient of passive earth pressure calculated using the stresses obtained from Plaxis for the point at the bottom of the wall has a slightly higher value than the experimental calculated coefficient. The small difference between the values makes valid the verification of the numerical modeling with the experimental results.

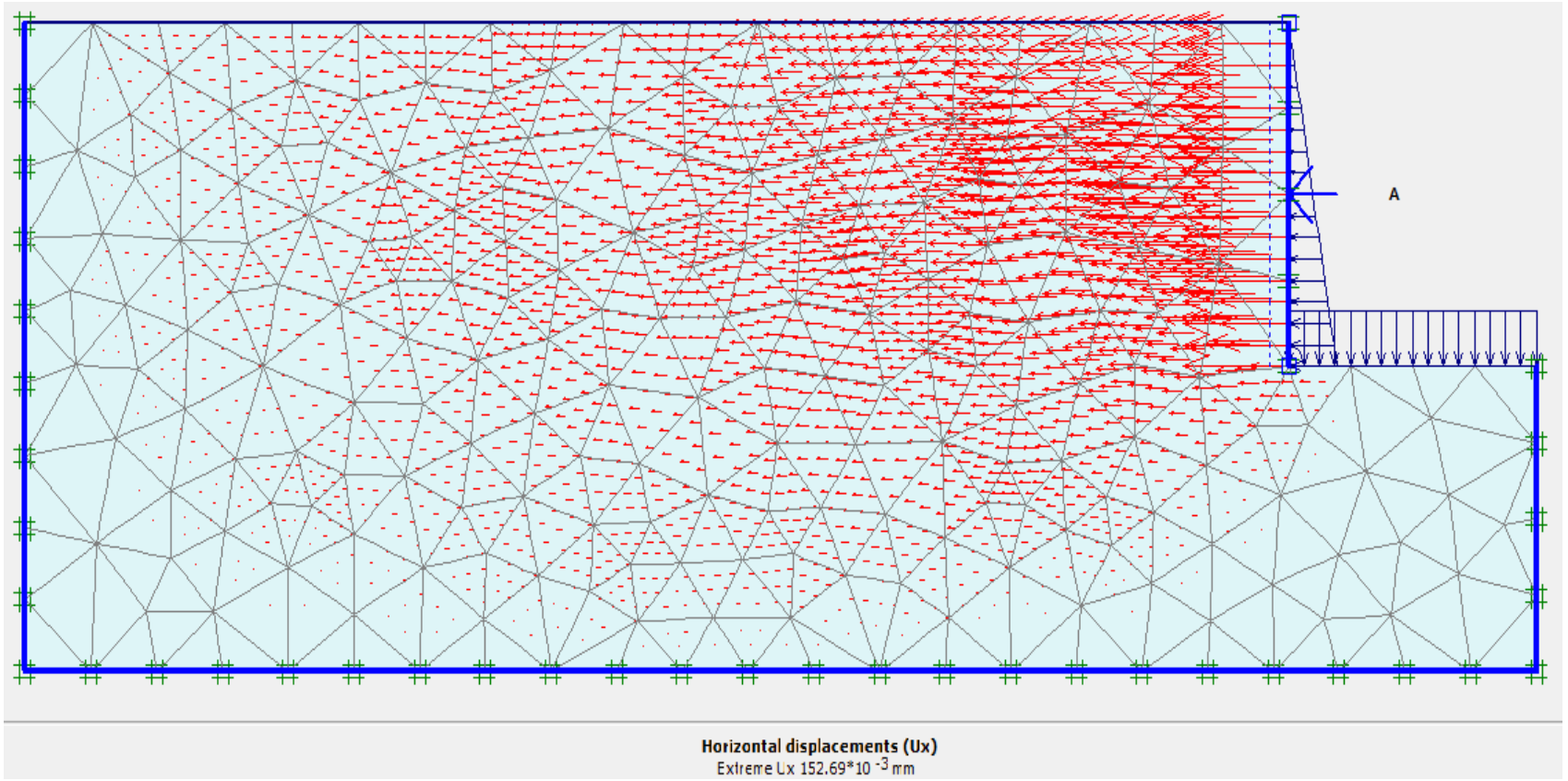

Figure 5.20 Horizontal displacements for Mix 3 (8% clay content) at full saturation

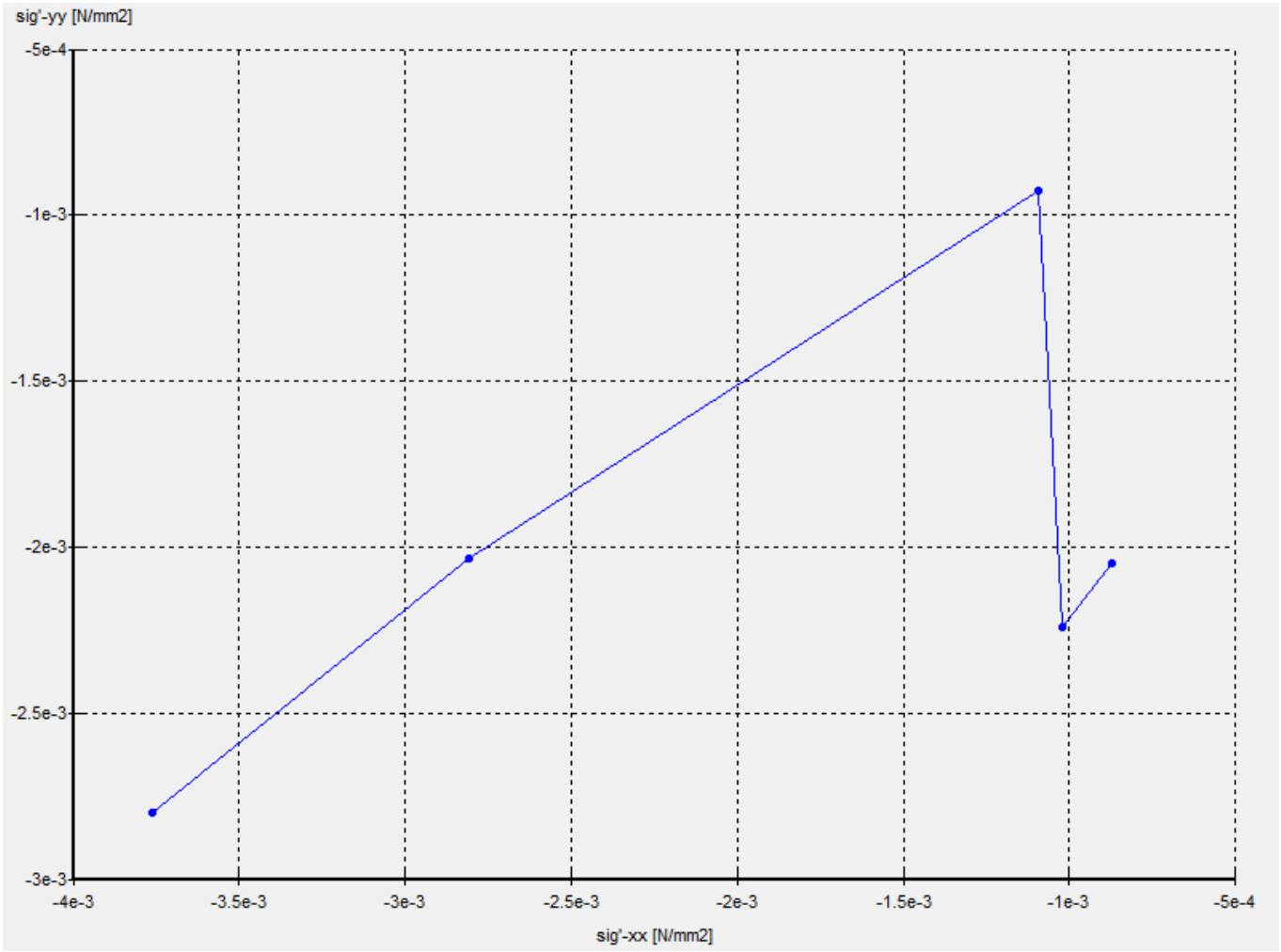

Figure 5.21 Horizontal and vertical effective stress plotted from Plaxis (point C) for Mix 3 (10% clay content) at full saturation

5.5 Numerical model for retaining wall pushing into the soil at full saturation for different soil mixtures

The results of the experimental investigation were used to validate the results of the numerical model developed in this investigation. After the validation the numerical model was used to generate results for a new range of soil mixtures of 7.5, 9 and 11% clay content. In order to compare the parametric changes of the soil mixtures, the force applied on the retaining wall was kept the same as in the experimental investigation for the soil mix from the same severity classification according to (Jennings and Knight 1975) presented in Table5.9.

Soil mixture	Clay content (%)	Collapse potential C_p (%)	Severity of foundation problem (Jennings and Knight 1975)
Mix 1	6	4.2	Moderate trouble
	7.5	6.5	Trouble
Mix 2	8	9	
	9	10.5	
Mix 3	10	12.5	Severe trouble
	11	14	

Table.5.9 Classification of soil mixtures of 7.5, 9 and 11 % clay content

The geometry model and the calculation procedure was the same as for the numerical model constructed for the inundated samples presented in the above chapter. From the output program for the new mixtures the maximum effective horizontal stress and the corresponding vertical stress were collected and used to calculate the coefficient of passive earth pressure for all the mixtures.

To model the soil mix that contains 7.5% clay content the soil properties have been changed and the Plaxis model procedure performed on the inundated Soil Mix 2 was repeated.

For point C located at the bottom of the wall, the effective stresses presented in figure 5.22 were considered for calculation of the coefficient of passive earth pressure using formula 5.1. The horizontal effective stress of the point is $\sigma_h' = 0.011 \frac{N}{mm^2}$ and the corresponding vertical stress is $\sigma_v' = 0.007754 \frac{N}{mm^2}$.

The coefficient of passive earth pressure is presented in Table 5.10 along with the numerical model results for the 6% and 8% clay content mixtures.

Clay content (%)	6%	7.5%	8%
Coefficient of passive earth pressure k_p	0.572	0.243	0.093

Table 5.10 Comparison between Kp for soil mixes of 6, 7.5 and 8% clay content

The coefficient of passive earth pressure of the soil mix containing 7.5% clay decreases from the value calculated for the Soil Mix 1 but still remains higher than the one calculated for the Soil Mix 2. The value for the new soil mix calculated is in the expected range.

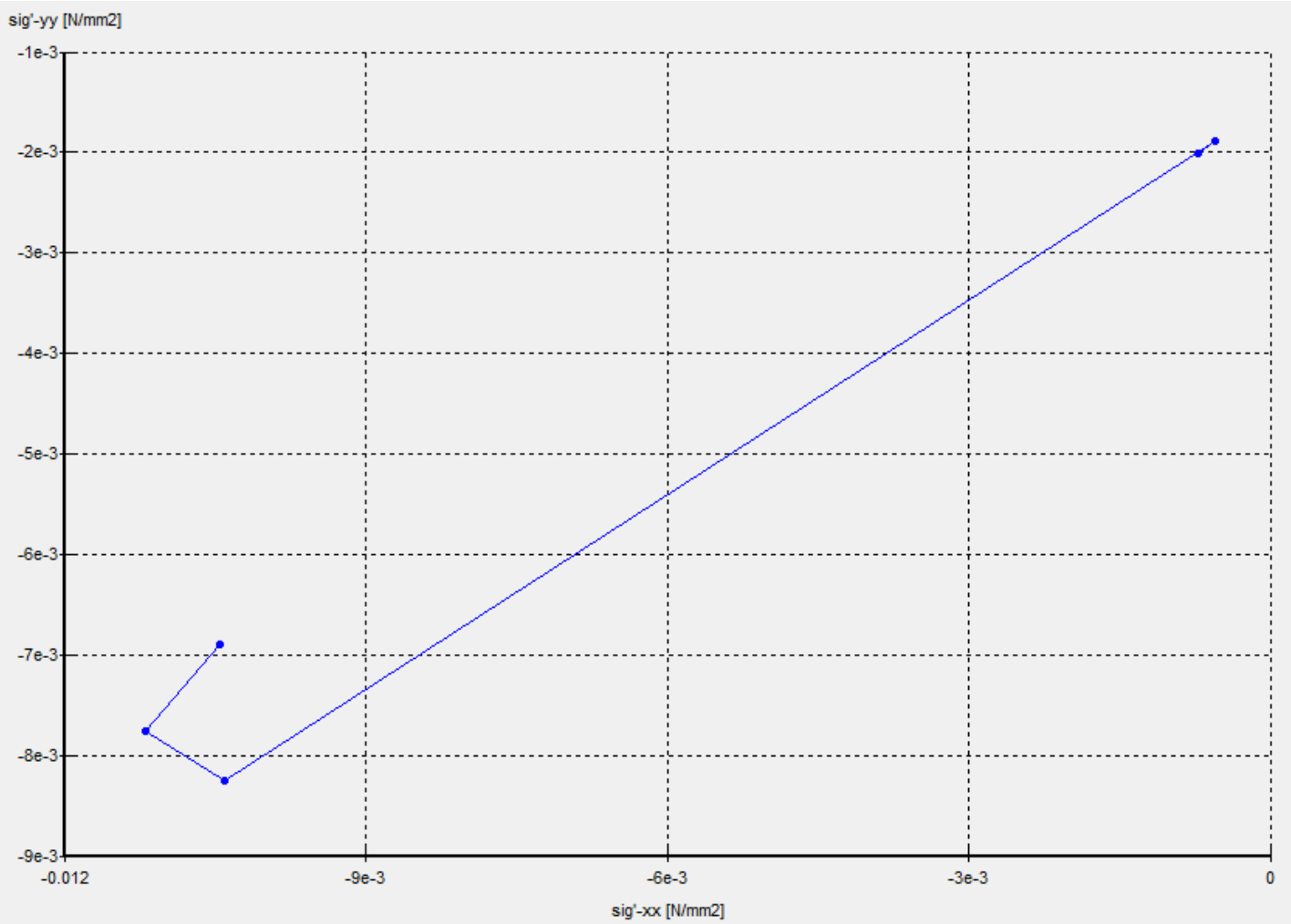

Figure 5.22 Horizontal and vertical effective stress plotted from Plaxis (point C) for Mix with 7.5% clay content at full saturation

The numerical model procedure performed on the Soil Mix 2 was repeated for the new mixture containing 8% clay content.

From the curve resulted at the end of the finite element calculation performed for the soil mix of 8% clay content (Figure 5.23) the horizontal effective stress was found as $\sigma_h' = 0.00642\ \frac{N}{mm^2}$ and the corresponding vertical stress was $\sigma_v' = 0.003872\ \frac{N}{mm^2}$.

The values of the effective stresses collected are used to calculate the coefficient of passive earth pressure and the result is presented in table 5.11.

Clay content (%)	8%	9%	10%
Coefficient of passive earth pressure k_p	0.093	0.053	0.015

Table 5.11 Comparison between Kp for soil mixes of 8, 9 and 10% clay content

To ensure that the numerical model was properly constructed for the soil mixture of 9% clay content the coefficient of passive earth pressure is compared with the results of the Soil Mix 2 and 3. As expected the coefficient of passive earth pressure is between the values of the two mixtures.

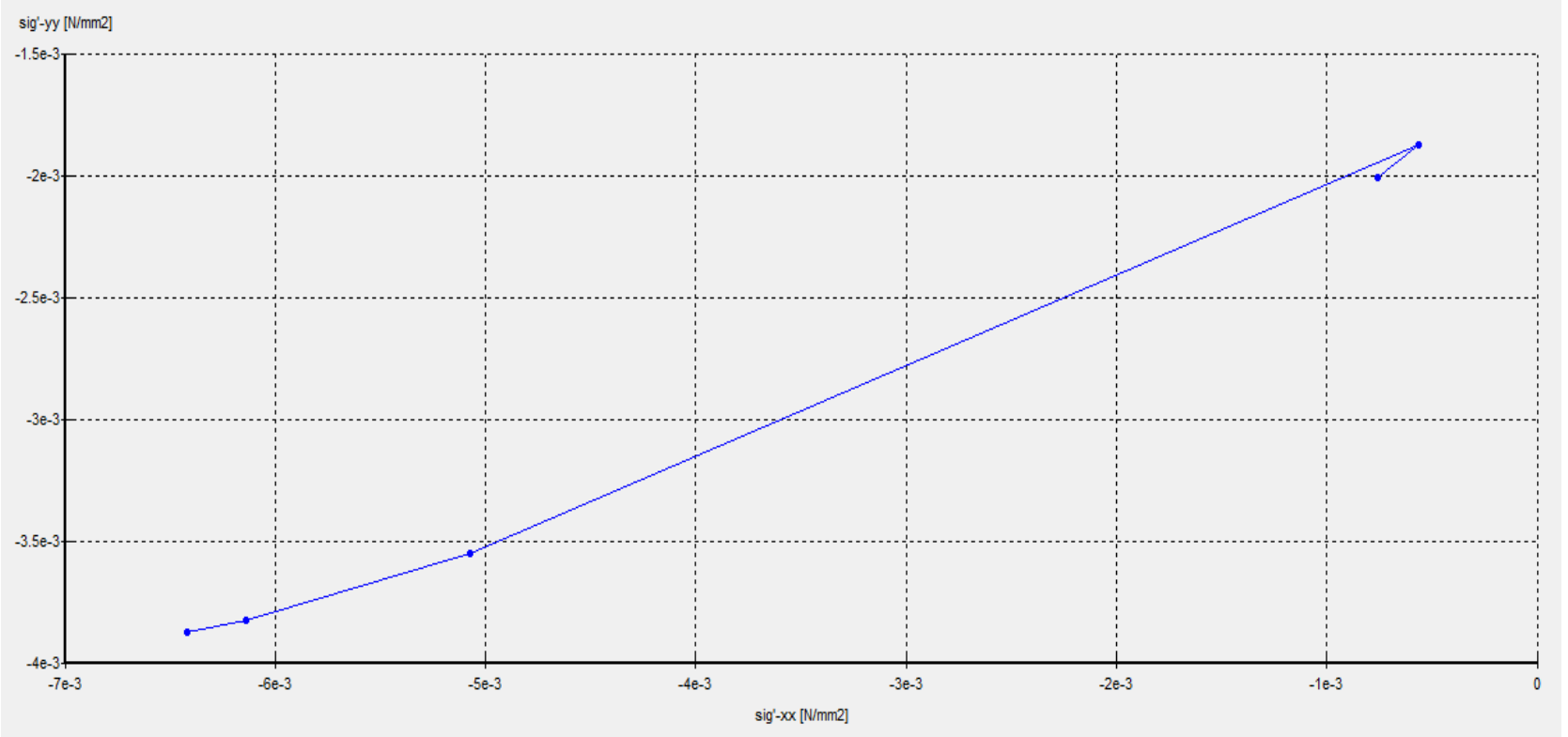

Figure 5.23 Horizontal and vertical effective stress plotted from Plaxis (point C) for Mix with 9% clay content at full saturation

To model the soil mix containing 11% clay the soil properties have been modified in Plaxis and the calculation procedure performed on the inundated Soil Mix 3 was repeated.

Based on the curve presented in Figure 5.24 the horizontal effective stress was found as $\sigma_h' = 0.003636\ \frac{N}{mm^2}$ and the corresponding vertical stress was $\sigma_v' = 0.001948\ \frac{N}{mm^2}$. The effective stresses are selected for the point that presented the highest effective horizontal stress on the height of the retaining wall.

The values of the effective stresses collected are used to calculate the coefficient of passive earth pressure and the result is presented in table 5.12.

Clay content (%)	10%	11%
Coefficient of passive earth pressure k_p	0.015	0.0091

Table 5.12 Comparison between soil mixes of 10 and 11% clay content

The calculated coefficient of passive earth pressure has a value that is smaller than the one calculated for the Soil Mix 3. This decrease is expected because of the increased clay content in the new soil mixture. This clay content will give the soil a higher collapse potential.

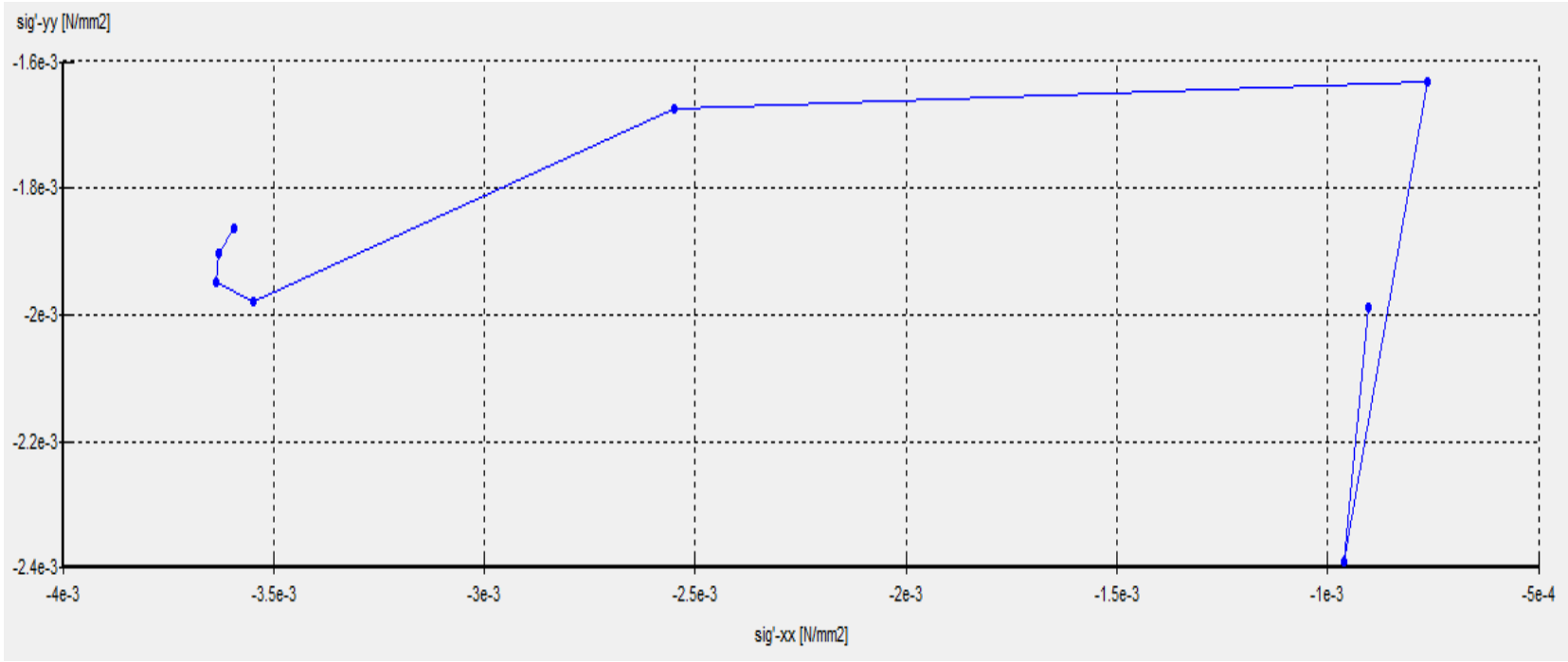

Figure 5.24 Horizontal and vertical effective stress plotted from Plaxis (point C) for Mix with 11% clay content at full saturation

Using the results from the numerical analysis the coefficient of passive earth pressure for all the inundated soil samples analyzed are presented in table 5.13.

Clay content (%)	6%	7.5%	8%	9%	10%	11%
Coefficient of passive earth pressure k_p	0.572	0.243	0.093	0.053	0.015	0.0091

Table 5.13 – Coefficient of passive earth pressure for all collapsed samples

The decrease of the passive resistance of the soil depends greatly upon the collapse potential of the soil mixture. A graphical representation between the collapse potential and the coefficient of passive earth pressure is presented in graph 5.25.

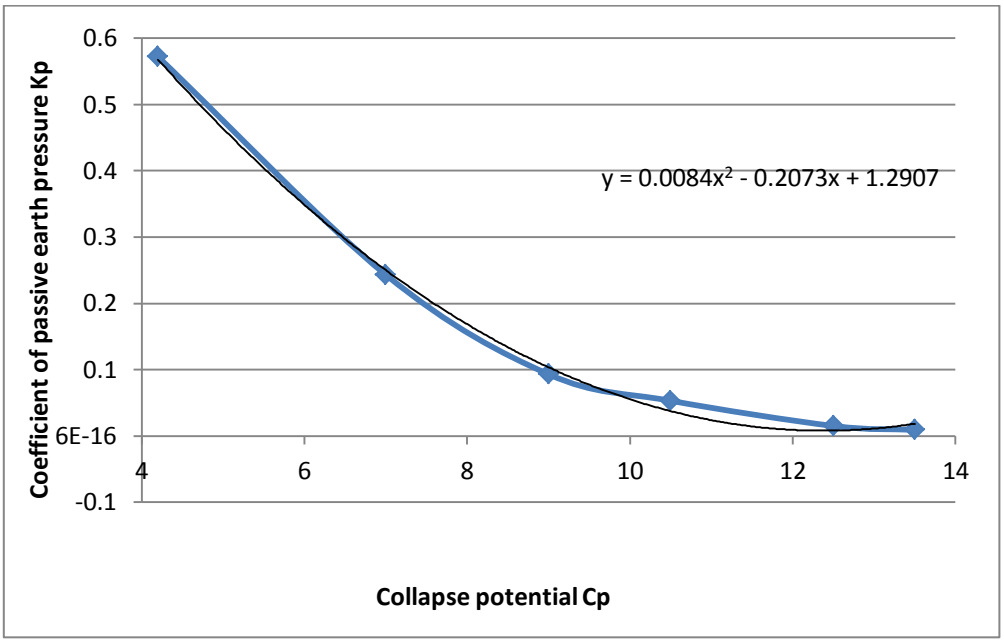

Graph 5.25 Collapse potential versus Coefficient of passive earth pressure for all collapsed samples

From the above chart it can be observed that the coefficient of passive earth pressure decreases with the increase of the collapse potential. The curve allows the construction of a two degree polynomial trendline. The equation of the trendline can be used to estimate the coefficient of passive earth pressure function of the collapse potential as:

$$k_p = 0.0084\, c_p^2 - 0.2073 c_p + 1.2907$$

CHAPTER 6

CONCLUSION

Based on the experimental and numerical investigations on passive earth pressure on walls retaining dry and wet collapsible soils, the following can be concluded:

1. The collapse potential decreased due to the increase of the initial moisture content.
2. Increasing the clay content of the dry soil mixtures increased the strength of the soil.
3. The collapse potential increased with the increase in clay content of the soil mixture.
4. After collapse, the failure forces supported by the soil decreased with the increase of collapse potential.
5. In case of dry soils, the coefficient of passive earth pressure decreased with the increase in clay content.
6. After collapse, the coefficient of passive earth pressure decreased with the increase of collapse potential of the soil.
7. After the soil was inundated, the coefficient of passive earth pressure decreased with almost 90% from the values calculated at low initial water content.
8. An empirical formula was developed to predict the coefficient of passive earth pressure after collapse as a function of the collapse potential.

RECOMMENDATIONS FOR FUTURE WORK

- Measure the distribution of the earth pressure on the retaining wall by means of pressure sensors must be applied on the face of the retaining wall. The pressure sensors have to be water resistant.
- Model the collapsible soil behavior for the cases of active and at rest earth pressure.

BIBLIOGRAPHY

Abbeche K, Hammoud F. and Ayadat T. 2007. *"Influence of relative density and clay fraction on soil collapse".* : Experimental unsaturated soil mechanics vol.112, p:3-9, 2007.

Adnan B.A. and Erdil T.R. 1992. *"Evaluation and control of collapsible soils".* s.l. : Journal of geotechnical engineering, ACCE,VOl.118,No.10,p:1491-1504, 1992.

Aitchinson G.D. and Donald I.B. 1956. *"Effective stresses in unsaturated soils".* s.l. : Proceedings of the second Australia-New Zealand Soils Mechanics Conference,p:192-199, 1956.

Arman A. and Thorton S.I. 1972. *"Collapsible soils in Louisiana".* s.l. : Engineering Research Buletin 111,Louisiana State University,U.S.A., 1972.

Bara and Gibbs. 1967. *"Stability problems of collapsing soils".* s.l. : Journal of soil mechanics and foundation engineering,ASCE,Vol.93 p:577-594, 1967.

Bara J.P. 1976. *"Collapsible soils".* Philadephia, USA : Presented at the ASCE Annual Convention and Exposition, 1976.

Bara J.P. 1977. *"Research on wetting collapsible foundation soils".* s.l. : Bureau of reclamation,U.S. department of interior,Report no.GR14-17, 1977.

Barden L. , Mc Gown A. and Collins K. 1973. *"The collapse mechanism in partly saturated soil".* s.l. : Engineering Geology, July, p:49-60, 1973.

Bayoglu and Esra. 1995. *Shear strenght and compressibility behaviour of sand-clay mixtures.* s.l. : Master thesis, Middle East Technical University, Turkey, 1995.

Beckwith G. 1979. *"Experience with collapsing soils in the Southwest".* s.l. : Paper presented to ASCE,Arizona Section,Spring Meeting,March, 1979.

Beckwith G.H. 1995. *"Foundation design practices for collapsible soils in the Western United States in Unsaturated Soils".* s.l. : In Proccedings of the First International Conference on Unsaturated Soils,E.EAlonso and P.Delage(eds) Vol.2 Paris,Sept.Balkema Rotterdam, 1995.

Bell F.G. and Bruyn I.A. 1997. *"Sensitive, expansive,dispersive and collapsible soils".* Paris : Bulletin of the International Association of Engineering Geology, 1997.

Benites L.A. 1968. *"Geotechnical Properties if the soils affected by piping near the Benson area.Cochise County,Arizona".* s.l. : M.S. Thesis,University of Arizona, 1968.

Burland J.B. 1965. *"Some aspects of the mechanical behaviour of partly saturated soils.* Butterworths,Sydney,Australia : In moisture equilibria and moisture schanges in soils beneath covered areas p:270-278, 1965.

Caquot A. and Kerisel J. 1948. *"Tables de poussees et butee".* Paris : Gauthier-Vallars, 1948.

Casagrande A. 1932. *"The structure of clay and its importance in foundations engineering".* s.l. : Journal of Boston Society of Civil Engineers,19,p:168-209, 1932.

Clemence S.P., Finbarr A.O. 1981. *"Design consideration for collapsible soils".* s.l. : Journal of Geotehnical Engineering ASCE107 (GT3), p:305-317, 1981.

Clevenger W.A. 1956. *"Experiences with loess as foundation material".* s.l. : Journal of the soil mechanics and foundation division,ASCE,32(3),p:1-26, 1956.

Clough G. and Duncan J. 1971. *"Finite element analysis of retaining wall behavoiur".* s.l. : Journal of geotechnical engineering,ASCE, Vol.97,p:1657-1673, 1971.

Collins K. 1978. *"A scanning electron microscopy study of natural engineering soils".* Glasgow,Scotland,U.K. : Ph.D Thesis, University of Strathclyde, 1978.

Coulomb C.A. 1776. *"Essai sur une application des Regles des maximis et minimis a quelque de statique".* Paris : Memoire Academie Royale des sciences,No.7, 1776.

Das B.M. 2008. *Fundamentals of Geotechnical Engineering. Third edition.* 2008.

Denisov N.Y. 1951. *"The engineering properties of loess and loess loams".* Gosstroiizdat,Moscow : s.n., 1951.

Derbyshire E., Dijkstra T. and Smally I. 1995. *"Genesis and proprties of collapsible soils".* The Netherlands : NATO ASI Series C:Mathematical and Physical Sciences 468,Kluwer Academic Publishers, p:375-382, 1995.

Dudley J.H. 1970. *Review of collapsing soils. Journal of the Soil Mechanics and Foundations Division,Proceedings of the American Society of Civil Engineers.* s.l. : p.925-947, 1970.

Fellenius W. 1927. *"Erdstatische Berechnungen mit Reigung and Koheasion und unter Annahme Kreiszylindrischer Gleitflaechen".* Berlin : Wilh.Ernst, 1927.

Franzius D. 1924. *"Versuche mit passivem Druck".* Berlin : Bauingencur.Ileft, 1924.

Freda J. 1964. *"Colloidal activity,shrinking and swelling of some clays".* s.l. : Proceedings of the soil mechanics seminar, p:531-546, 1964.

Gibbs H.J. and Bara J.P. 1962. *"Prediction surface subsidence from basic soil tests".* s.l. : ASTM-STP322. American society for testing and materials,p:231-247, 1962.

Gibbs H.J. and Holland W.Y. 1960. *"Petrografic and engineering properties of loess".* U.S. Bureau of reclamation,Denver : Engineer Monograph no.28, p"37, 1960.

Hanna A.M. and Ayadat T. 2009. *"Assesment of soil collapse prediction methods".* 2009.

Hansen Brinch J. 1953. *Earth pressure calculation.* Copenhagen : Danish technical press, 1953.

Holtz W.G and Hilf J.W. 1961. *"Settelment of soil foundations due to saturation".* Paris : Proceedings of the 5th International conference on soil mechanics and foundation engineering,p:673-679, 1961.

Holtz W.G. and Hilf J.W. 1961. *"Settelment of soil foundations due to saturation.* Paris : Proceedings of the 5th International Conference on Soil Mechanics and FOundation Engineering,p:673-679, 1961.

Houston S.L. and Houston W.N. 1977. *"Collapsible soils engineering".* Logan UT,USA : Unsaturated soil engineering practice,Geotechnical Special Publication,ASCE proceedings of the 1997 1st Geo Institute Conference,part 68,p:199-232, 1977.

James R.G. and Bransby P.L. 1970. *"Experimental and theoretical investigations of passive earth pressure problem".* s.l. : Geotechnique 20,No.1, p:17-37, 1970.

Janbu J. 1957. *"Earth pressure and Bearing capacity calculations by generalized procedure of slices".* s.l. : Proceedings of the fourth international conference on soil mechanics and foundation engineering. London, Vol.2 P:207-2012, 1957.

Jennings J.E. and Knight K. 1957. *"The additional settelment of foundations due to collapse of structure of sandy subsoils on wetting".* London : Proceedings of the 4th International Congress on Soil Mechanics and Foundation Engineering p:316-319, 1957.

Jennings J.E., and Knight K. 1975. *"A guide to construction on/or with materials exhibiting additional settelment due to "collapse" of grain structure".* s.l. : Proc.,6th Regional Conf. of Africa on SMFE, p:99-105, 1975.

Knight K. 1963. *"The origin and occurance of collapsing soils".* s.l. : Proc.,3rd Regional Conference of Africa on SMFE, p.127-130, 1963.

Knight K. 1960. *"The collapse os structures of sandy subsoils on wetting".* s.l. : Thesis,University of Witwatersrand, 1960.

Kumar J. and Subba Rao. 1997. *"Passive pressure coeficiients, critical failure surface and its kinematic admissibility".* s.l. : Geotechnique 47, No.1 p:185-192, 1997.

Lawton E.C., Fragaszy R.J. and Hetherington M.D. 1992. *"Review of wetting-induced collapse in compacted soil".* s.l. : Journal of geotechnical engineering 118 (9), p:1376-1394, 1992.

Markin B.P. 1969. *"Remarks on the article on standard criteria of sag in loess soils".* s.l. : By V.P.Aranev and Y.D.Gilman. Translated from russian by consulates bureau, SMFE.no.2, 1969.

Mashhour I. 2009. *"Negative skin friction on single piles in collapsible soil".* Montreal : Master's Thesis at Concordia University, 2009.

Milivic D., Stevanovic S. and Koprivica E. 1981. *"Settelments of high buildings founded on loess".* Stockholm : Proceedings of the tenth ICSMFE, vol.1 p:199-202, 1981.

Miller H., Hjeribib Y., Jeffreson I.F. and Smalley I.J. 1998. *"Modeling the collapse of metastable loess soils".* s.l. : Proceedings of the 3rd International Conference on Geo-Computaion, University of Bristol, United Kingdom, 1998.

Mitchell J.K. 1993. *"Fundamentals of soil behavior:.* New York : Jhon WIley and Sons,INc. N.Y. 2nd Edition, p:437, 1993.

Narain J., Saran S. and Nandakumaran P. 1969. *"Model study of passive pressure in sand".* s.l. : Journal of soil mechanics and foundations division proceeding of the ASCE, 1969.

Rahardjo H. and Al. 1984. *"General limit equilibrium method for lateral earth force".* s.l. : Canadian geotechnical journal,vol.21,p:166-175, 1984.

Rankine W.J.M. 1857. *"On the stability of loose earth".* s.l. : Trains Royal Soc. London,VOl.147, 1857.

Rendulic L. 1935. *"Ein Beitrag zur Bestimmung der Gleitsicherheit".* s.l. : Bauingenieur,Heft p:19/20, 1935.

Rowe P.W. 1963. *"Stress-Dilatancy,Earth Pressures, and slopes".* s.l. : Journal of soil mechanics and foundations, ASCE, VOl.89,No.3,pp:37-61, 1963.

Rowe P.W. and Peaker K. 1965. *"Passive earth pressure measurements".* s.l. : Geotechnique, Vol.15,No.1, 1965.

Sheeler J.B. 1968. *"Summarization and comparison of engineering properties of loess in the united states".* Washington DC : Conference on loess: Design and construction Highway research record 212 p:1-9, 1968.

Soliman S. 2010. *"Performance on reinforced collapsible soils".* Montreal : Doctorat Thesis at Concordia University, 2010.

Tadepalli R., Rahardjo H. and Fredlund D.G. 1992. *"Measurement of matric suction and volume changes during inundation of collapsible soils".* s.l. : Geotechnical Testing Journal 15,p:115-122, 1992.

Terzaghi K. 1948. *"Theoretical Soil Mechanics in Engineering Practices".* s.l. : Weiley, New York, 1948.

Terzaghi Karl. 1920. *"Old earth pressure theories and new test results".* s.l. : ENGR., vol85, no 14, pp.108-113, 1920.

Vitton S. J. 1997. *"Blast Damage Investigations of Foundations Constructed on Collapsible Soils".* s.l. : Journal of International Society of Explosive Engineers p291, 1997.

Zur A. and Wiseman G. 1973. *"A study of collapse phenomena of an undisturbed loess".* s.l. : Proceedings of the eighth international conference on soil mechanics and foundation engineering, vol.2,part2, 1973.